CORRECTION AND ENHANCEMENT OF LANDSAT DATA FOR HUDSON BAY LOWLANDS VEGETATION

by

© IAN LYLE JOHNSTON, B.Sc.

A Thesis

Submitted to the School of Graduate Studies

in Partial Fulfilment of the Requirements

for the Degree

Master of Science

McMaster University

September, 1980

CORRECTION AND ENHANCEMENT OF LANDSAT DATA FOR HUDSON BAY LOWLANDS VEGETATION

MASTER OF SCIENCE (1980)
(Geography)

McMASTER UNIVERSITY
Hamilton, Ontario

TITLE: Correction and Enhancement of Landsat Data for Hudson Bay Lowlands Vegetation

AUTHOR: Ian Lyle Johnston, B.Sc. (University of Toronto)

SUPERVISOR: Dr. P. J. Howarth

NUMBER OF PAGES: x, 179

ABSTRACT

The effects of solar and atmospheric corrections, and the linear contrast stretch, band ratioing and video filtering enhancements on Landsat data were studied for two areas of northern Canada. Studies were carried out using computer compatible tapes on an image analysis system and both numerical and visual evaluations were made. It was determined that solar and atmospheric corrections may not be sufficient to standardize Landsat data between different dates of imagery. In contrast, however, it was found that the linear contrast stretch and the band ratioing enhancements effectively emphasized the ground surface patterns. The video filtering enhancement was insufficient to enhance the image.

ACKNOWLEDGEMENTS

The author would like to express his sincere appreciation to Dr. P. J. Howarth for the advice and assistance given throughout the preparation of this thesis. In addition, the author would like to thank Dr. J. J. Drake, Mr. E. Boasson and Mr. R. Spitzer for their assistance during the final stages in this research.

This research would not have been possible without the assistance of Ms. Carolyn Goodfellow, Dr. Francis J. Ahern and Mr. Gunar Fesosejevs of the Canada Centre for Remote Sensing. I would like to thank Mr. G. M. Wickware of the Lands Directorate, Environment Canada and Dr. W. R. Rouse of McMaster University for permitting me to carry out field work in conjunction with their Hudson Bay Lowlands projects.

Financial support for the study was received in grants to Dr. Howarth from the Natural Sciences and Engineering Research Council of Canada (NSERC) and the McMaster University Presidential Committee on Northern Studies.

TABLE OF CONTENTS

LIST OF FIGURES

CHAPTER I

INTRODUCTION

1.1 Statement of the Problem

Since the first Landsat satellite was launched in 1972, remote sensing specialists have established the importance of the Landsat monitoring system. The first three Landsat satellites have a ground resolution of 60m by 80m in the visible and near infrared wavelengths of the electromagnetic spectrum (Simpson, 1978). These detailed spectral data have allowed significant advances in geology, geomorphology and forestry research, as well as expanding our knowledge of the earth's planimetry.

In this research, two distinctly different methods of data analysis have been developed, namely classification and enhancement. Classification in remote sensing is "computer techniques for mathematical manipulation, statistical sorting...of Landsat digital data using spectral information" (Simpson, 1978, p. 183). The sorted data are displayed as bold colours on a new image, and each colour represents a different spectral class, as illustrated in Figure 1.1. Researchers attempt to assign a surface cover class to each colour as Howarth (1976) has done.

The representation of these surface cover classes

Figure 1.1 Classification of the Hook Point Landsat data by the migrating means technique. The bold colours suggest different vegetation patterns in contrast to an enhanced image (Figure 5.8 for example).

as colours can be problematic because such classes are not always significant in the environment. Moreover, it is often difficult to determine the significance of these colours unless extensive field investigations are done.

Image enhancement, defined as"the use of computer techniques designed to increase image detail and allow more effective interpretation" (Simpson, 1978, p. 183), has been developed to maximize the usefulness of the image. Such methods enable the researcher, rather than the machine, to determine different spectral classes, provided of course, the different surface cover classes have unique spectral reflectances. In comparison with classification, image enhancement is a new field in which the most significant advances have been achieved during the last five years.

Unfortunately, most research in image enhancement has been directed to problems in geology and land use studies without regard to its potential for natural vegetation studies. Moreover, the importance of image corrections, especially solar and atmospheric corrections for both classification and enhancement have not been evaluated, although they are necessary for reducing the effects of atmospheric attenuation and for multi-date comparisons of imagery.

1.2 Aims of the Study

There are two goals in this research project. The

first goal is to evaluate the effectiveness of the Ahern solar and atmospheric corrections applied to the Landsat data. These corrections provide a standard solar illumination and remove the variations due to atmospheric attenuation. They are necessary so that the intrinsic reflectance properties of the target, and not the atmosphere, are enhanced. Moreover, they are necessary for comparisons of image data for the same area.

Once these corrections have been evaluated, the second goal is to investigate the capability of image enhancements to improve surface cover mapping using Landsat data. The contrast stretch, band ratioing and video filtering enhancements will be applied as they are the major ones described and used in the literature. One study site will be used to evaluate these corrections and enhancements. The same corrections and enhancements will then be applied to a second study site to test the repeatability of the procedures.

1.3 Research Sites

It was necessary to select two different study areas so that the Landsat enhanced imagery could be compared. Field investigations provided data from which ground cover maps were drawn for Hook Point, Ontario and Churchill, Manitoba. These research areas were selected because they

have common cover classes, and Landsat MSS data were available (see Chapter IV). In this section, a brief description of each study site has been presented.

1.3.1 Hook Point, Ontario

The Hook Point study site is located on the southern coast of Hudson Bay at latitude 54°50'N and longitude 82°15'W. It is situated entirely within the boundaries of Polar Bear Provincial Park, north of Attawapiskat and east of Winisk, as illustrated in Figure 1.2. The study site is part of the Hudson Bay Lowlands. The lowlands exhibit a uniform low slope extending 200 km inland over a distance of 1400 km parallel to the Hudson Bay and James Bay coasts (Cowell, 1968).

Unfortunately, very little climatic data are available for such a large area. The nearest weather station to the research area is Winisk, for which climatic data for all of Polar Bear Provincial Park are extrapolated. In summer, the moderating effects of Hudson Bay and James Bay determine the variations in local climate. The study area is cloud covered 75% of the year and low pressure cyclonic activity causes frequent frontal precipitation. The July mean daily temperature at Winisk rises to 11.7°C (Anon, 1977) but temperatures as high as 17°C have been reported (Neal and Kershaw, 1973). There is a paucity of additional climatic

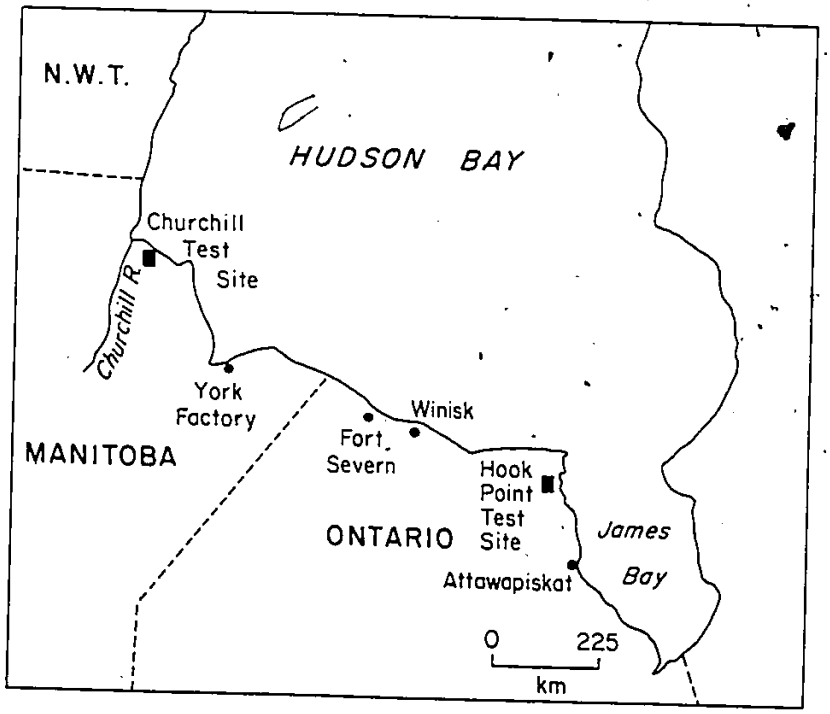

Figure 1.2 Location of the study sites.

data.

In contrast, more information is available about the geology. All of the research area is underlain by early Precambrian sediments. They have been intruded by granodiorites and granites to form the Archean basement complex. The Paleozoic strata are composed of limestones, dolomites and sandstones of Silurian and Devonian ages. Siltstones, shales, mudstones and sandstones are found near the study site. The only bedrock exposure is at Cape Henrietta - Maria, about 25 km to the north of the study site. Most surficial geology has been influenced by the Wisconsin glaciation, which is believed to have reached a maximum thickness over the area of 3000 meters, 20,000 B. P. (Anon., 1977). The ice mass retreated at approximately 7,500 B.P. and left a blanket of glacial debris deposited as blue-grey clay and dolomite silt (Webber et al., 1970). This has been subsequently reworked by the postglacial Tyrell sea.

Webber et al. (1970) have established a pattern of coastal emergence for which isostatic rebound has been calculated to be 1.2 meters a century. The pattern of coastal emergence has been linked with the formation of ancient beach ridges, the predominant feature of the region. Individual beach ridges range from one to several kilometers in length, a few hundred meters in width and from

one to three meters in height. They extend inland for approximately 240 km (Neal and Kershaw, 1973). They have been built by strong onshore winds producing high energy waves that carry materials onshore. The beaches at the study site have been formed within the last 1000 years (Anon., 1977).

Between these beach ridges, areas of lower elevation allow small lakes and drainage channels to form. The study site retains 75% of the total surface water collected from snow and rain in these small lake systems (Anon., 1977). Most lakes occupy shallow areas gouged out by glacial ice movement, but others form where beach ridges block the west to east flow of water. Most of the small lakes are less than 1 km in diameter (Anon., 1977). Streams conform to a parallel pattern, determined by the beach ridges. Topographically, the research area is a low, gently sloping plain with few variations in relief. There are no trees and the coastal zone is characterized by a gently sloping tidal mud flat and an adjacent salt marsh.

A lichen dominated vegetation system flourishes upon these ridges. Most of the flora is characterized as low or southern arctic vegetation, and the southerly extent of the treeline is maintained by cold onshore winds, fog and the absence of good drainage. Abrasion by blowing snow and the shallow active layer of the soils allows only a hardy vege-

tation to survive.

1.3.2 Churchill, Manitoba

Churchill, Manitoba is the second research area for this study. It is located 550 km northwest of the Hook Point site, at latitude 58°47'N, and longitude 94°11'W. The study site is located east of the Churchill River, as shown in Figure 1.2, within the westerly extent of the Hudson Bay Lowlands.

An Atmospheric Environment Service weather station is located at Churchill, and consequently, more weather data are available. Although farther north than Hook Point, both the average July (17°C) and January (-30°C) temperatures are warmer (Ritchie, 1960). The total precipitation is 40 mm per year (Ritchie, 1957). Hudson Bay acts as a moderating influence. The study site is cloud covered only about 40% of the year, so consequently, more Landsat data are available.

At Churchill, geologic structures similar to Hook Point underlie the sediments. The oldest rocks are of Archean age and are granitic in origin. Volcanic deposits are surrounded by greywacke and shale, which are thick bedded and dip to the north. Silurian sediments are mostly limestone and dolomite and are exposed at the surface along the coast. These outcrops are visible both on Landsat imagery and aerial photographs.

Beach ridges have formed parallel to the Hudson Bay coast. Although not as numerous, they are of similar dimensions to the ones located at Hook Point and have been built by strong onshore winds combined with coastal emergence. These beach ridges are probably the same age as the Hook Point ridges because their vegetation composition and their distance from the shoreline are both similar.

Between these beach ridges and rock outcrops, numerous small lakes have formed which vary in size. The larger lakes occupy alluvial flats between the uplifted coastal features. South of the coast, tamarac occur in the poorly drained areas with spruce on the better drained sites.

Lichen woodland areas are common in the Churchill area as they are supported in part by the warmer temperatures. Lichen heaths are found on the beach ridges close to the coast.

However, there has been urban settlement at Churchill which has altered the established vegetation patterns. Churchill was a strategic air base which in the past supported a large military and civilian population. A large airport, roads, buildings and several radio installations dominate the landscape along the coast and are visible on both aerial photographs and Landsat imagery.

CHAPTER II

REVIEW OF IMAGE CORRECTION AND ENHANCEMENT LITERATURE

2.1 Introduction

Image correction and enhancement literature is both diverse and recent. It has developed from studies of film chemistry, geology, land use studies and atmospheric physics in the late 1970's. Indeed, it is impossible as yet to establish an historical perspective to the literature. Due to the wide range of topics involved, only literature directly pertinent to the study under investigation will be described in this chapter.

2.2 Image Corrections

Radiometric and geometric corrections (described in Chapter III), are applied to all Landsat image data to form part of the record of the Computer Compatible Tape (CCT). A discussion of the tape format, together with a description of the radiometric and geometric corrections appears in Strome et al. (1975). Subsequent to this publication, several modifications to the radiometric corrections have been made which are described in Ahern and Murphy (1978).

In contrast to these corrections, atmospheric and solar corrections have not been applied to the CCT.

Researchers have investigated the use of these corrections on Landsat data. Turner et al. (1971) first discussed the problems associated with atmospheric attenuation in Landsat data and discussed how radiative transfer models could have been used to solve these problems. A numerical solution to the radiative transfer problem was derived by Turner and Spencer (1972). It had the advantage of rapid computation, although path radiance was underestimated in the model. The results of these studies and their application to satellite and aircraft data were discussed in the paper.

The Turner-Spencer equations and three other radiative transfer solutions were compared in O'Neill's (1977) publication. He found that an adjustment to the Turner-Spencer model was best for the estimation of path radiance. A summary paper by O'Neill et al. (1978) compared the Turner-Spencer and discrete ordinate techniques and suggested a new method to more accurately estimate atmospheric attenuation.

These results were used by Ahern et al. (1979) to correct Landsat data for atmospheric attenuation and also to change the illumination conditions by recalculating the solar zenith angle. Ahern et al. (1977) developed an interesting model for which the necessary input parameters were estimated by modelling path radiance over clear water bodies. Unfortunately, the model has not yet been evaluated with tests from different environments and latitudes.

2.3 Linear Contrast Stretch Enhancement

The linear contrast stretch enhancement changes the dynamic range of an individual band or a combination of bands of Landsat data displayed usually on a colour monitor, making full use of the display. Stretch limits on each band of data are defined so that data within these limits are enlarged to occupy the full dynamic range of the display using a linear formula. Data outside these limits are truncated. This enhancement is the most established in the literature.

The linear contrast stretch enhancement was an adaptation of the technique used to change the contrast curve of photographic film. Lockwood (1975) described the use of this technique with photographic film. He found that a particular range of wavelengths or a broadband could be emphasized within the film's total wavelength sensitivity range, by modifying the contrast curve. In effect, the data were stretched over the total range. Specific features imaged on the film were enhanced and hence more visible.

Moderate success was achieved by stretching Landsat colour composites, but it was realized that film grainyness was also increased. Therefore, digital methods of contrast stretching were developed that stretched the Landsat data before it was written onto film. There are many papers that discussed the digital contrast stretch methodology.

For example, Schwartz (1976) described the linear contrast stretch enhancements developed at the Jet Propulsion Laboratory. Formulae were presented with examples from Mariner 9 data of Mars. In addition, Soha et al. (1976) studied the linear contrast stretch with examples of Landsat data imaged over the Chilean-Bolivian border. The contrast stretch was investigated by Hummel (1977) as well as its implementation on an image analysis system. He found that the contrast stretch enhancement was inexpensively computed and easily programmed. In the paper, the interactive approach was discussed whereby the researcher has the ability to control the contrast stretch so that specific features can be enhanced.

The control of the contrast stretch was investigated by Lucas et al. (1977) using Landsat data from the south-central region of Iowa. The authors described the problem of data truncation, which occurred when Landsat data were not displayed because they were not within the stretch limits. Frequency histograms of the pre- and post-enhanced data were used to illustrate the problem. Sheffield (1976) further discussed the data truncation problem, although much of his work was repetitive of earlier work.

In contrast to the abundance of articles about the methodological and problematic aspects of the contrast stretch enhancement, relatively few have investigated possible

applications. Most studies have been for geological investigations.

Geological studies were conducted in Nevada, Alaska and Australia where authors have tried to correlate ground features with enhanced satellite data. Rowan et al. (1979) were the principle investigators at the Nevada study site, where widespread Tertiary volcanic and intrusive rocks covered 95% of the study site. An exposed section of Paleozoic mine tailings was present at the site. It was discovered that linear contrast stretch enhanced imagery had more scene contrast than the regular colour composites or non-linear stretched images and they provided slightly better discrimination of rock types. For example, basalt was distinguished from mafic intrusives, as were the mine tailings. In addition, Rowan et al. (1977) reported on developments at the Nevada study site using ground-based spectral reflectance data for different rock types. It was determined that the MSS scanner did not record in the wavelengths most suitable for distinguishing between the rock types in Nevada. They concluded that the linear contrast stretch was not very effective for exposed rock. As well, Simpson (1978) found little success in his Australian work. He reported that the linear contrast stretch appeared to work best in research areas where geologic structures were expressed as varied relief or in different vegetation zonations because they

were more easily interpreted. Similarly, a study by Smith and Baker (1975) in the Yuma area of Arizona, reported little success with linear contrast stretch enhancements for a 12 km^2 study site. Their study site contained faulted block mountains of Mesozoic crystalline and metamorphic intrusives. Smith and Baker (1975, p. 60) reported that "no dramatic increase in geologic information was achieved" with the linear contrast stretch enhancement compared to the unenhanced colour composite, although a few features were more visible on the enhancement.

A study by Myers et al. (1977) discussed the successful use of the enhancement in land use studies. They concluded that the enhancement could be used in vegetated areas.

2.4 Band Ratioing Enhancement

Band ratioing emphasizes the unique spectral characteristics of materials. Many different variations of band ratioing exist, but the most frequently discussed method in the literature is the ratio of a single MSS band to another (see Chapter III).

Santisteban (1976) has presented formulae used for many ratioing enhancements. Taranik (1978) has also discussed the band ratioing formulae together with examples and illustrations. However, Taranik's (1978) paper failed to discuss the effect of slopes, an important aspect of

band ratioing. A diagram of albedo values for slopes was given together with their ratioed values, but no explanation was provided. In contrast, Rowan et al. (1977) discussed the ratioing formula and the importance of slopes (see Chapter III). Moreover, they discussed the necessity of using the linear contrast stretch with the ratioed data because the dynamic range of the data was very small and difficult to display on a colour monitor.

Band ratioing has been applied with some success to geological investigations, particularly for rock identification. Rowan et al. (1979) showed that it separated subtle reflectance differences found in many geologic materials. The resulting enhancement was therefore, a visual display of differences between the digital values in different MSS bands. For example, playas were identified on the ratioed image, although discrimination of the mafic rocks was problematic when the same Band 4 to Band 5 ratios were used. A colour composite was produced from several single band ratios but its advantages over the single band ratioed images were minimal.

As well, experimentation by Rowan et al. (1977) using reflectance measurements of rock samples in MSS wavelengths showed that band ratioing was problematic because the reflectances were nearly equal in the MSS bands. Successful results were probably due to the presence of vegeta-

tion cover over rock. In contrast, Vincent (1977) had more success with laboratory reflectance studies, using minerals from several parts of the world (such as Hawaii, Canada, Tennesee and Oregon). He was able to show that some rocks could be characterized by their MSS ratios. However, Vincent overlooked the fact that many geologic formations are vegetation covered.

Smith and Baker (1975) evaluated previous results of band ratioing for their Arizona study site. Several combinations of bands were used but the single band ratios were best. Band 4 to Band 7 ratios were suited for differentiating between andesite, sandstone and shale. Merifield et al. (1976) experimented with band ratioing using Skylab S-192 scanner data obtained for the western Mojave Desert in California and found that vegetation was readily visible on ratioed imagery using bands that correspond to MSS Band 4 and Band 7. The near infrared was highly reflected by the xerophytic vegetation but not by geologic structures, except for some older alluvium present in the desert. Grasses and joshua trees were also enhanced, especially along the San Andreas fault, where a change in vegetation was apparent. Similarly, the Jet Propulsion Laboratory's (Anon., 1978) primer on image processing in geology contained Landsat imagery of Goldfield Nevada that was ratioed to show how vegetation was enhanced along linear features,

a discussion of which, appeared in Simpson's (1978) article.

Some researchers have investigated band ratioing for land use studies. For example, Chavez et al. (1977) used colour ratio composites for a land use study of Phoenix Arizona. They found that ratioing Band 4 to Band 7 or Band 5 to Band 7 was particularly useful for interpreting agricultural land use because different crops had unique ratioed values. They found that any combination of bands was useful for interpreting changes from urban to rural land use. In a similar study, Todd (1977) discussed the use of band ratioing for a land use study of Atlanta, Georgia. Marrs (1975) used band ratioing for a land use survey of Beaver Creek, Wyoming. He determined that Band 4 to Band 7 ratios were best for his study.

The discovery that band ratioing could illustrate unique ratioed digital values for vegetation was a significant contribution. A study by Tucker (1978) showed how MSS Band 7 correlated with the chlorophyll content of healthy green trees. As well, Thomas (1979) discussed plant physiology and the theoretical basis for relating MSS data to plant vigor or change in plant cover. He found that the ratio of MSS Band 4 to Band 7 clearly illustrated the changes in plant cover in Australia. Turner (1973) studied phreatophytes in Tucson, Arizona and showed that desert plant communities had characteristic near infrared to visible

MSS band ratios. These plants could be separated from grasslands because their ratioed coefficients were different. Moreover, Rao et al. (1978) discussed how crops could be distinguished when no reflectance from bare soil was present. Vlcek (1974) found that there were great difficulties in defining characteristic spectral curves for trees from spectral radiometer work. His results differed from work by Kalensky and Wilson (1975) who suggested that Landsat data could be useful in mapping natural vegetation.

2.5 Video Filtering Enhancement

The video filtering enhancement removes anomalies in an image through an application of spatial statistics, so that the interpreter can more easily recognize patterns in the imagery. As well, linear features are enhanced. It can be applied to corrected or classified Landsat data.

Unfortunately, the enhancement has not been well documented. A few papers have been written about the implementation of the video filtering enhancement. For example, Wallis (1976) described a filtering formulae with two examples. Taranik (1978) presented a discussion of a possible method of selecting filter sizes and strengths.

As well, there have been a few papers that have illustrated the uses and effects of video filtering enhancements. For example, Soha et al. (1976) explored the effects

of video filtering on Landsat data imaged over China and they showed how linear features were enhanced by the 3 by 3 filter. Chavez et al. (1977) enhanced linears in southwest Jordan and discovered that filter size and strength were critical for the enhancement. They found that the use of a 3 by 3 filter at a strength of .5 caused a loss of image detail. However, it permitted linear features to be enhanced. An unidentified section of Landsat data was used by Vanderbrug (1977) to examine the effect of changing filter size. A larger filter caused defocusing in the image. Simpson (1978) used different filters to enhance the structural detail of the Kombolgie Formation in Milingimbi, Australia. He discovered that a 3 pixel by 3 pixel size filter was useful for enhancing vegetation patterns and drainage features, but several unwanted artifacts in the enhanced image were produced that could not be correlated with known ground features.

2.6 Conclusions

This chapter has presented virtually all of the relevant literature on the correction and enhancement of Landsat data. It is apparent from previous studies that the Ahern atmospheric corrections have not been evaluated. In contrast, the linear contrast stretch and band ratioing enhancements have been studied for geology and land use applications. Researchers have had limited success with

these enhancements. A few papers have been written about video filtering, but not enough work has been done to assess its merits.

CHAPTER III

LANDSAT DATA CORRECTIONS AND ENHANCEMENT

3.1 Introduction

It is important to understand the methods by which Landsat data are received, corrected and enhanced. This aids the analyst in his interpretation of Landsat imagery. In addition, a knowledge of the various steps in image processing permits the identification of potential sources of error that might create anomalies in the imagery.

In this chapter, Landsat data acquisition will be briefly discussed, as this topic is frequently presented in the Landsat literature. In contrast, image correction and enhancement will be more fully considered, with specific reference to the algorithms for the image analysis system used in this study.

3.2 Landsat Data Acquisition

The Landsat 1 and Landsat 2 satellites contained within their payload two separate sensor systems, the Multispectral Scanner and the Return Beam Vidicon. For this project, only data generated from the Multispectral Scanner (MSS) were used because data from this system were

most suited to digital analysis and enhancement.

The MSS is a four channel sensor that detects electromagnetic radiation in the visible and near infrared regions of the electromagnetic spectrum. The specific broadbands are .5 μm to .6 μm (Band 4), .6 μm to .7 μm (Band 5), .7 μm to .8 μm (Band 6), .8 μm to 1.1 μm (Band 7) (Vishnubhatla, 1977). For each sensor channel or band, there are six individual optic fibers that receive light reflected through a telescopic optical chain from a first surface scanning mirror. Each of these six fibers is connected to a band-dependant filter. The optic fibers and filters radiate onto photomultiplier tube detectors for the Landsat MSS Band 4, Band 5 and Band 6. Silicon photodiode detectors are used for Band 7.

As the scanning mirror rotates, reflected radiation from a fixed swath width of the earth is flashed across the optic fibers, and a continuous voltage stream is generated from the detectors. The scanning arrangement of the MSS is illustrated in Figure 3.1. Each swath contains six scan lines - one scan line for each detector (Figure 3.2).

The continuous voltage output associated with these ground swaths is sampled by an electronic crystal clock every 9.95 usec (Simpson, 1978). The signal is, therefore, broken into discrete components, whose length is determined by the swath width, and whose width is determined by the

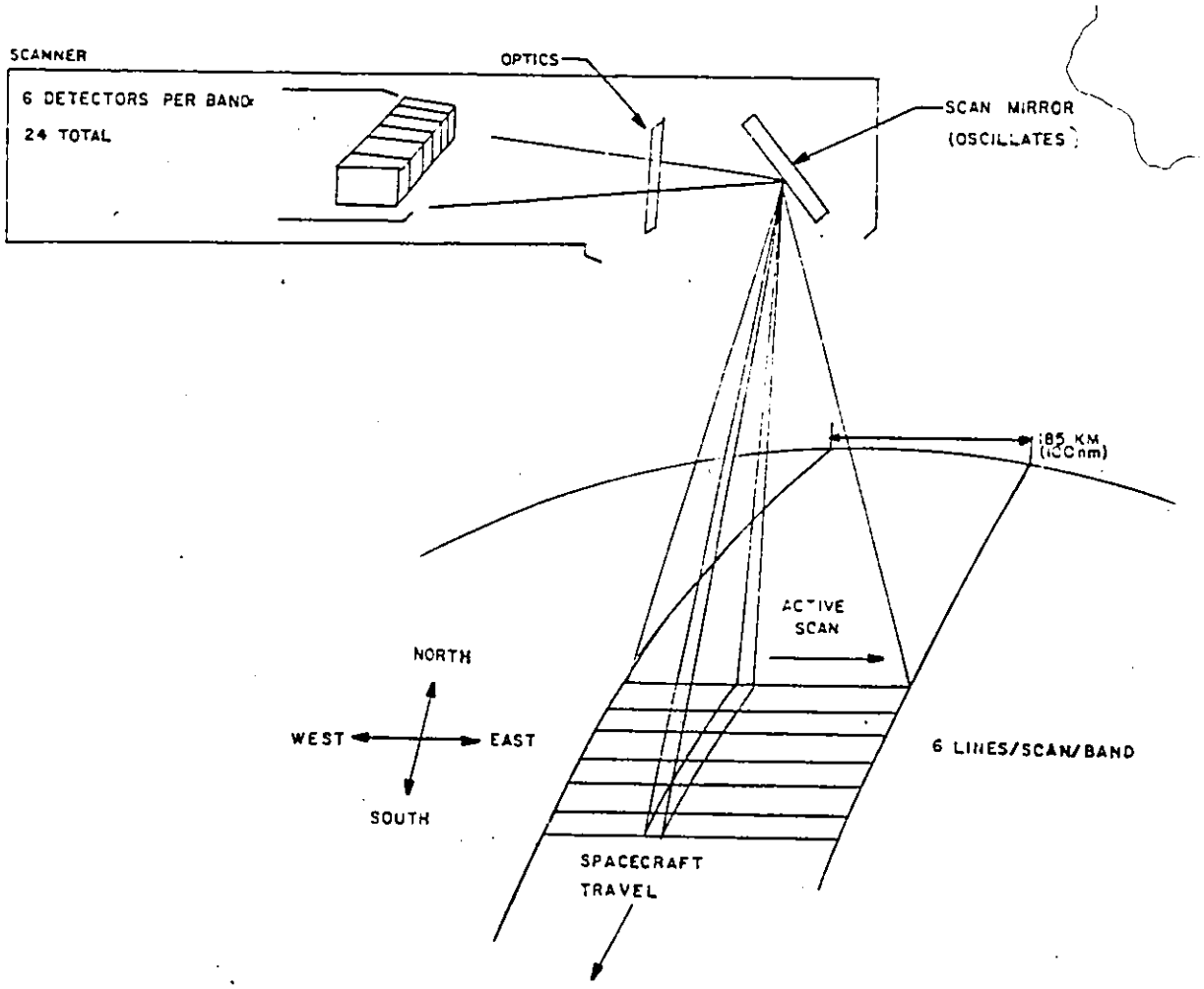

Figure 3.1 The MSS scanning geometry. The row of six detectors receive reflected radiation from six scan lines.
(Source: Strome et al., 1975)

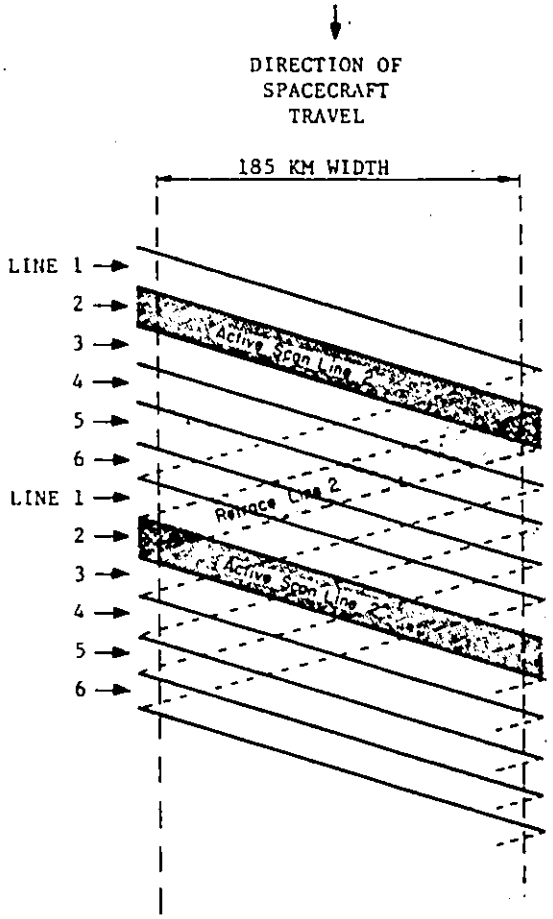

Figure 3.2 The ground scan pattern for a single MSS band. (Source: Strome et al., 1975)

crystal clock sampling rate. This creates a rectangular picture element called a pixel, which is about 60 m by 80 m on the ground. The scanning mirror rotates through an arc of 5.08° (Strome et al., 1975). Therefore, from an altitude of 915 km, the scan lines are about 185 km long and a single Landsat image or scene is about 185 km by 185 km.

The scan line information is logarithmically compressed for Band 4, Band 5 and Band 6 and combined with the already compressed Band 7 before transmission to receiving stations at Prince Albert, Saskatchewan and Shoe Cove, Newfoundland. At receiving stations, raw data are compiled onto high density magnetic tapes. These tapes are processed for radiometric and geometric corrections and reformated into a Computer Compatible Tape (CCT). The pixel data are divided into 256 discrete radiance levels or digital values in the linear mode (used for the computer processing in this project) or 64 digital values used in the compressed mode (used for special reproductions).

3.3 Radiometric, Geometric, Solar and Atmospheric Corrections

For this project, three sets of corrections were applied to the raw Landsat data before they were enhanced. First, radiometric corrections were applied to equalize the

systematic radiometric errors present in the data. These are due to changes in sensor response, changes in electronics and changes in the throughput of the MSS optics that have occurred since the satellites were launched. Second, geometric corrections were applied to give visual sensibility to the data because the uncorrected MSS bands are offset, and the uncorrected imagery is highly skewed. Finally, solar and atmospheric corrections were applied so that Landsat imagery from different dates could be compared by reducing the intervening effects of atmospheric attenuation and changing solar altitude.

3.3.1 Radiometric Corrections

During the retrace cycle of the MSS scanning mirror, a shutter wheel closes off the view of the earth and a calibration lamp is permitted to radiate onto the optic fibers. The calibration lamp contains a variable density filter that changes from 1% to 100% light transmission rapidly and then to 1% slowly, thereby creating a calibration wedge. The voltage output from the detectors is sampled starting from the midpoint of the on ramp of the calibration wedge. The wedge data is transmitted together with the earth view data.

The ground base calibration of the detectors proceeds in two phases. First, the absolute calibration of one stable detector is calculated. The method undertaken assumes that

the voltage output and scene radiance are linearly related as demonstrated by pre-launch MSS tests. In addition, it assumes that a detector can be used that is stable and reliable. Certain detectors are used that are both stable and reliable and are listed in Ahern and Murphy (1978). Finally, it is assumed that the calibration lamp is both stable and reliable, which is tested in two ways. First, lamp radiance is measured against solar radiance once every orbit. Second, a change in lamp current is measured and transmitted to earth. These methods did not detect changes in the calibration lamp.

The absolute calibration is

$$V'_{ref} = \frac{1}{a}(V_{ref} - b) \qquad 3.1$$

where V'_{ref} is the calibrated digital value for the reference detector on a scale of 0 to 255, V_{ref} is the calibrated radiance and a and b are the gain and offset respectively (Ahern and Murphy, 1978). The gain and offset are calculated from six samples of each wedge as follows:

$$a = \sum_{j=1}^{6} C\ V_{cal}, \qquad b = \sum_{j=1}^{6} D\ V_{cal} \qquad 3.2$$

where C and D are coefficients calculated from the prelaunch data and V_{cal} is the decompressed digital value for the reference detector from six calibration wedge samples (Ahern

and Murphy, 1978). Six samples from each of nine wedges are used in the calibration procedure.

In the second phase of the calibration, the other detectors are calibrated relative to the reference detector. This has the effect of removing stripes in the imagery. Relative calibration is better than absolute calibration of all detectors because the calibration source uses data from within the scene, rather than the redder spectrum of the calibration lamp. It can be appreciated that if the broad-band detectors are equalized for radiance in one spectrum, they may not be equalized in another.

Because of the large number of pixels in a scene, it can be assumed that the statistical distributions of scene radiances are normal (Strome et al., 1975). Therefore, differences between the detectors in any band can be expressed as differences in the mean and variance. Linear equations can be solved that relate each detector to the reference detector in any band. Once the gain and offset have been calculated for each detector, then scene data can be radiometrically corrected. If necessary, each of these new digital values can be converted to scene radiance (mW/cm^2 - sr) by a linear function described in Ahern and Murphy (1978).

3.3.2 Geometric Corrections

The MSS mirror oscillation relative to the detectors

plus the satellite's motion relative to the surface of the earth make it necessary to apply geometric corrections to Landsat data to provide a planimetrically correct image. There are two geometric corrections applied and they change the relative positions of existing pixel elements.

The first geometric correction is the scan line registration transformation. The MSS is sampled sequentially by an internal crystal clock. As a result, the detectors within and between each band are not sampled simultaneously for the same ground field of view. This creates a mis-registration of the scan lines. The offset effect is corrected by the addition of null radiance values (zero digital values) to the left positions of each scan line as illustrated in Figure 3.3. This correction is applied individually within and between each Landsat image.

In addition, the earth rotation correction is applied to the Landsat data, for which an understanding of space-craft travel geometry is necessary. The satellite travels in a circumpolar orbit and crosses the equator at the same time every day. During its north to south travel, the earth rotates in an easterly direction as shown in Figure 3.4. This results in skewing of the data. An algorithm based on the latitude of the earth is used to correct this effect.

In addition to these corrections, there are optional

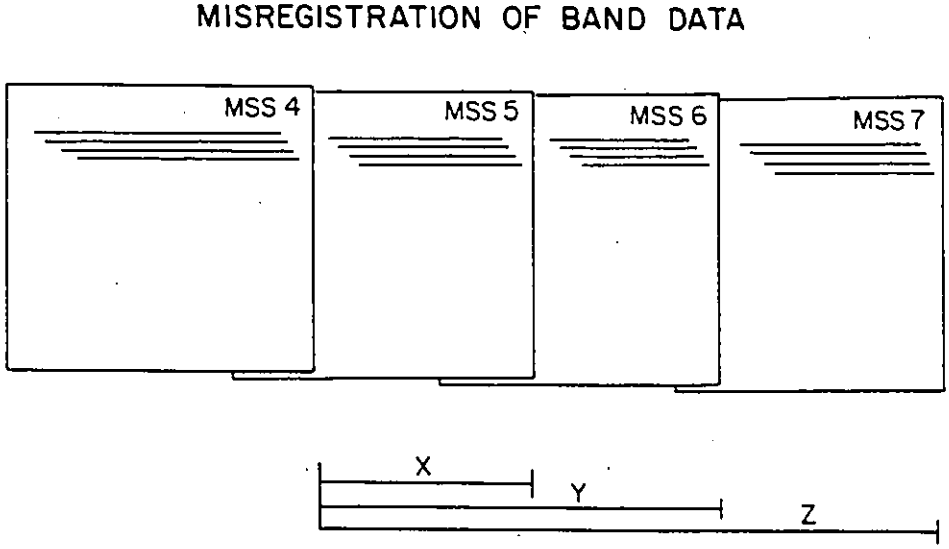

Figure 3.3 Misregistration of the scan lines. The Landsat data are normally misregistered in the uncorrected data. They are corrected by adding null digital radiance values to the scan lines within each band and by shifting the bands by amounts x, y and z.

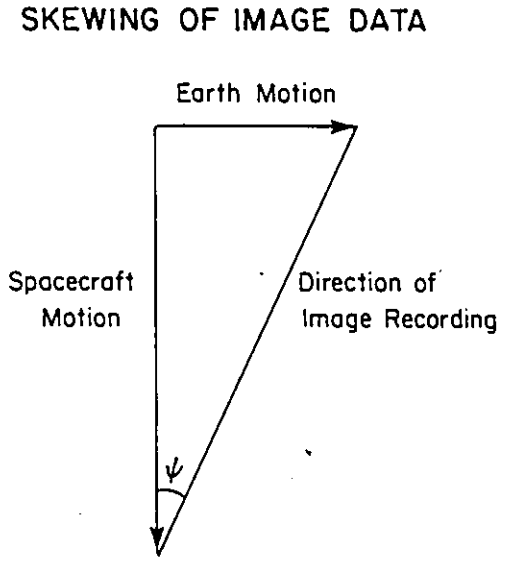

Figure 3.4 Skewing of the Landsat data. The data are skewed by an amount ψ due to the motion of the earth and the velocity of the spacecraft. An algorithm shifts the data to remove angle ψ.

geometric corrections for variations in mirror scan velocity and scan line length. However, these corrections have not been applied to the data because they require the addition of synthetic pixels and the reformatting of pixels which would reduce the representativeness of the pixel data.

3.3.3 Solar and Atmospheric Corrections

The purpose of these corrections is to reduce variations in observed radiance due to changes in solar elevation, and changes in optical thickness and composition of the atmosphere. In this section, the Ahern solar and atmospheric corrections are described. They are applied to data from the CCT. These are not part of the standard corrections applied to the Landsat data.

The radiance observed by a satellite can be expressed as:

$$L_{sat} = H_{tot} \frac{\rho}{\pi} T + L_p \qquad 3.3$$

where L_{sat} is the radiance observed by the satellite in a spectral band, H_{tot} is the total direct and diffuse downwelling irradiance at the target of interest, ρ is the intrinsic reflectance of the target of interest, T is the transmission of the atmosphere and L_p is the path radiance observed by the satellite from the atmosphere (Ahern et al., 1977b). From this equation, it is evident that the measured

radiance by the satellite is linearly related to the intrinsic radiance ($H_{tot} \frac{\rho}{\pi}$) of the target of interest.

If the intrinsic reflectance of the target is needed, then equation 2.3 can be solved for ρ. However, the earth's atmosphere varies in both time and space. Precise atmospheric data are required to solve for ρ. A smaller correction is required (and hence smaller errors remain) if the observed radiance is recalculated to a radiance observed under conditions of standard illumination (H'_{tot}), (T') and path radiance (L'_p). Therefore, the corrected radiance can be expressed as:

$$L'_{sat} = \frac{H'_{tot}\, T'}{H_{tot}\, T} (L_{sat} - L_p) + L'_p \qquad 3.4$$

where the primed quantities refer to standard conditions (Ahern et al., 1977b).

The solution to the above equation requires a knowledge of the unknown quantities. If assumptions are made about the earth's atmosphere, then the Turner and Spencer (1972) equations for L_p, $H_{tot} \frac{\rho}{\pi}$ and T can be used. The assumptions are that no diffuse radiation enters the earth's atmosphere from above the satellite, the terrain is Lambertian, there is no absorption within the region where scattering occurs, there are no clouds present, and that the particle size and distribution of aerosols are constant. The equations have a solution for each unknown quantity provided that the following parameters are known:

(a) average background albedo,

(b) solar-satellite geometry,

(c) atmospheric extinction coefficient.

The average background albedo is derived as a quotient of the average Landsat scene digital value and the total downwelling irradiance. The solar-satellite geometry is obtained from a CCT record of location, time and date of imagery or from user selected solar elevations. The extinction coefficient can be derived from the Ahern et al. (1977a) clear lakes method.

Ahern et al. (1977a) have determined the contribution of atmospheric path radiance to Landsat data using oligotropic lakes as standard targets. The radiance received by a satellite over these targets is the sum of radiances contributed by light scattered below the water surface (L_{vol}), by diffuse light reflected from the water surface (L_{surf}), by light from the surface due to specularly reflected sunlight (L_{glint}) and by path radiance as illustrated in Figure 3.5. From radiance measurements for nine clear lakes from northern Quebec, Ahern et al. (1977a) determined the contribution of lake radiance in each Landsat MSS band for these clear water bodies (Figure 3.6). These values can be used to find the path radiance for any Landsat scene with clear lakes present. Once path radiance is known, the Turner-Spencer equation for path radiance can be used to estimate

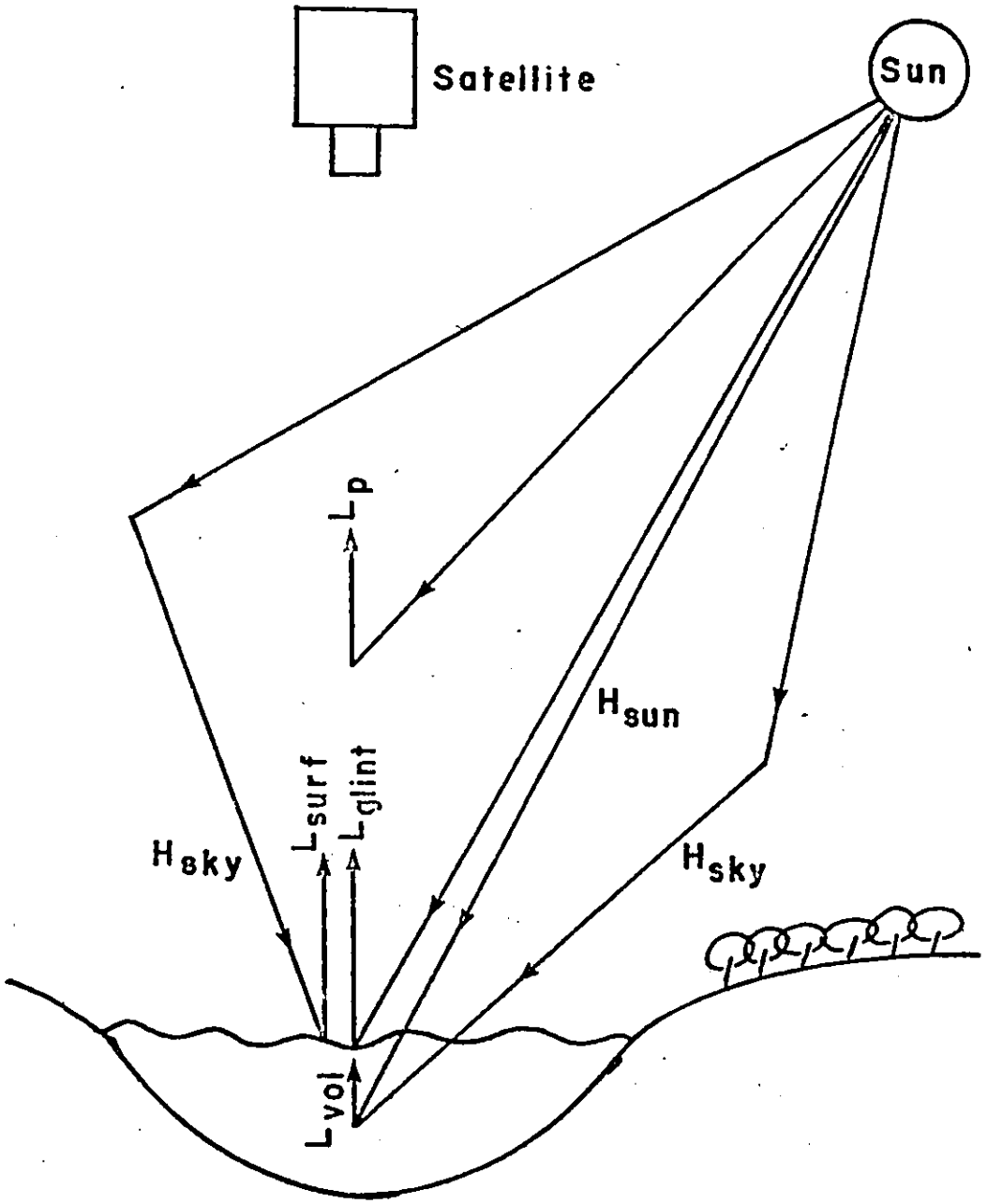

Figure 3.5 Schematic diagram of radiation processes over a lake. Sunlight illuminates the lake (diffusely (H_{sky}) or directly (H_{sun})) or the atmosphere and is scattered back to a satellite as path radiance (L_p). The radiance measured by a satellite (L_{sat}) is $(L_{vol} + L_{surf} + L_{glint})\,T + L_p$ where T is the atmospheric transmission. (Source: Ahern et al., 1977a)

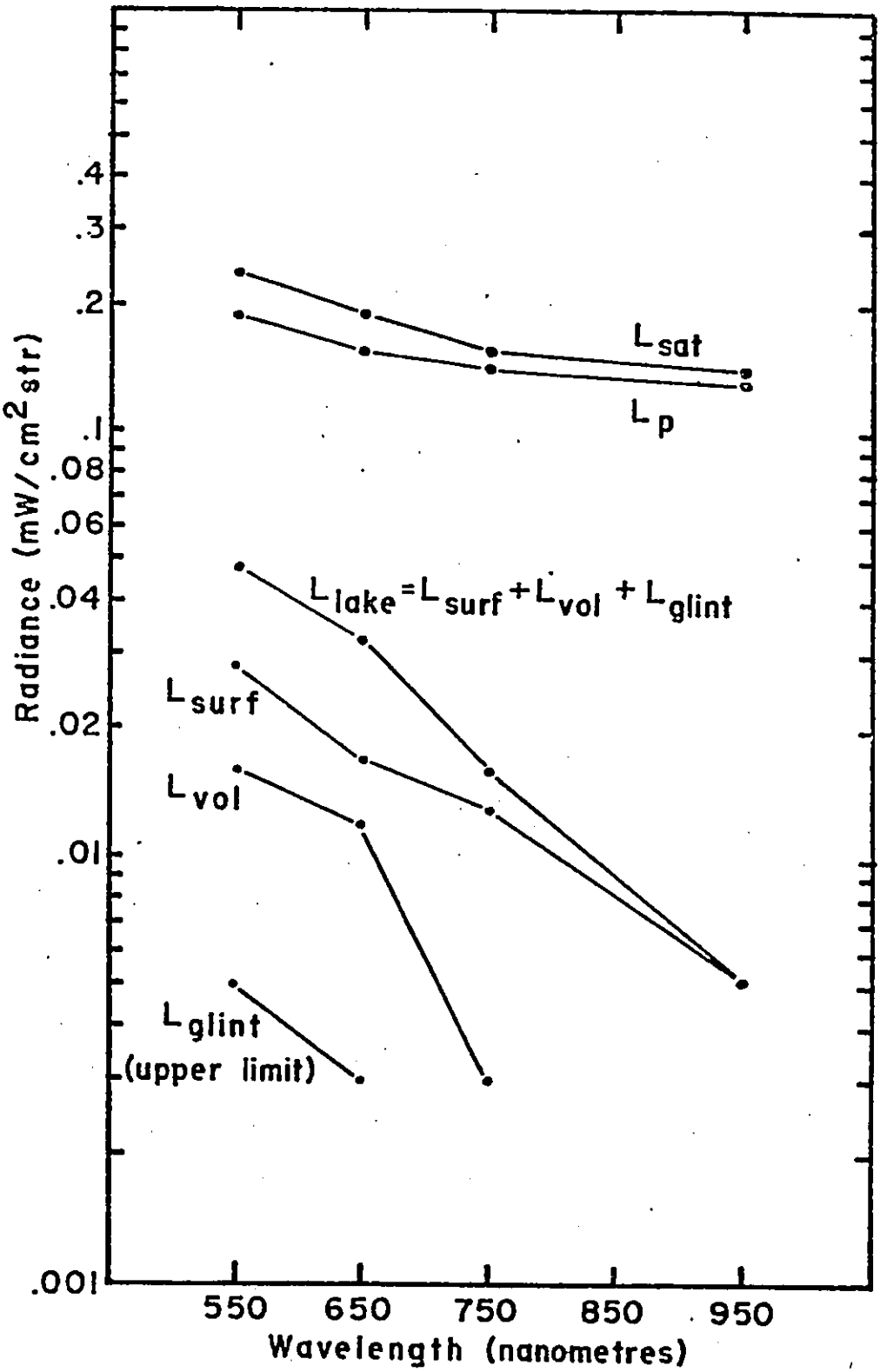

Figure 3.6 Relative magnitudes of the contributors to the radiance observed by a satellite as measured by Ahern et al. (1977a).
(Source: Ahern et al., 1977a)

the extinction coefficient.

However, the path radiance varies in the Landsat scene because the atmosphere varies. Therefore, the path radiance must be modelled for the Landsat image by the following method. Digital value histograms are used to display each band of image data. In Band 7, clear water has low digital values because infrared radiation is absorbed. In Band 4, turbid water has high digital values so that these must be excluded. Wider limits are set on Band 5 and Band 6 so that all of the clear water pixels defined in Band 4 and Band 7 are included and possible false data are excluded. This procedure identifies all of the clear water pixels in the Landsat image. The image is then partitioned into 2 to 64 equal size rectangles in the horizontal and vertical dimensions so that clear water pixels are present in each one. The mean intensity, standard deviation and geometric centroid of the clear water pixels in each rectangle is calculated and a constant, linear or quadratic function is selected to fit a clear water pixel surface on the image. The lake radiance value is subtracted from the surface to find path radiance.

As mentioned, these data are used in the Turner-Spencer equations. Unfortunately, it has been determined by O'Neill et al. (1978) that the equations overestimate the extinction coefficient. Therefore, a correction has been introduced

based on results from the more accurate discrete ordinate approach to adjust calculated values of the extinction coefficient. The results are used in the equations for each Landsat band and new digital values are calculated for each pixel. A small correction is included for the view angle effect in the images due to the MSS viewing geometry.

There are several problems associated with the use of the equations. First, the equations depend on the calibration accuracy of the detectors, which are subject to systematic errors. Second, the atmospheric equations cannot correct for the conditions which invalidate the assumptions. Third, the method for calculating path radiance is inaccurate, and can lead to large errors. Fourth, the equations do not account for variations in shadowed and sunlit slopes.

3.4 Image Enhancements

Corrected Landsat data can be enhanced to display MSS data in the best possible way. In this section, three different enhancements are discussed.

3.4.1 Linear Contrast Stretch

The purpose of the linear contrast stretch is to enhance particular ground surface features, such as water bodies or vegetation cover, so that there is greater contrast between a few features at the expense of reduced

contrast in others. To accomplish this task, the range of available output digital values on the display device must be increased for these features. For example, vegetation reflects strongly and water absorbs strongly in the near infrared. Therefore, gain and bias values can be selected so that radiance data for vegetation in Band 6 and Band 7 are displayed for an increased range of digital values.

A simple linear equation defines the linear contrast stretch:

$$g = af + b \qquad 3.5$$

where f is the digital value for a MSS band, a and b are the gain and offset respectively, and g is the new digital value. As illustrated in Figure 3.7, the relationships between the data are not changed. All Landsat bands are stretched individually, so that different gain and bias values are needed for each band, and every pixel in each band is stretched.

There are two problems with this enhancement. First, the selection of gain and bias values is arbitrary. Therefore, the analyst cannot specify the best gain and bias values. Second, some data is truncated. Radiance data whose stretched quantity is greater than 255th digital value is set to 255th digital value. Similarly, values less than zero digital values are set to zero. These data appear light or dark in the display but they are not easily identified. Therefore, line prints of digital data must be consulted in

conjunction with the stretched imagery (see Chapter IV).

3.4.2 Band Ratioing

The band ratioing enhancement displays differences in the digital value data between bands. Band ratioing is achieved by displaying the quotient of two bands of Landsat data on a pixel by pixel basis. The display intensity of each new digital value depends on the calculated ratio. For example, if a feature's reflected spectral curve is uniformly horizontal across all bands as illustrated in Figure 3.8, then the ratioed value will equal one, whereas if the spectral curve is not horizontal, a value different from one will be displayed.

The band ratioing formula (usually) has gain and offset factors because the resultant ratios usually produce an image with little scene contrast. Therefore, the band ratioing formula has the following form:

$$g = a(x/y) + b \qquad 3.6$$

where x and y are the pixel digital values for MSS band x and band y, a and b are the gain and offset selected to display the ratioed values, and g is the output digital value. On some systems a value of 1 is added to y to prevent the zero over zero case, but it is not present in the algorithm used for this study.

As with the linear contrast stretch, constraints are

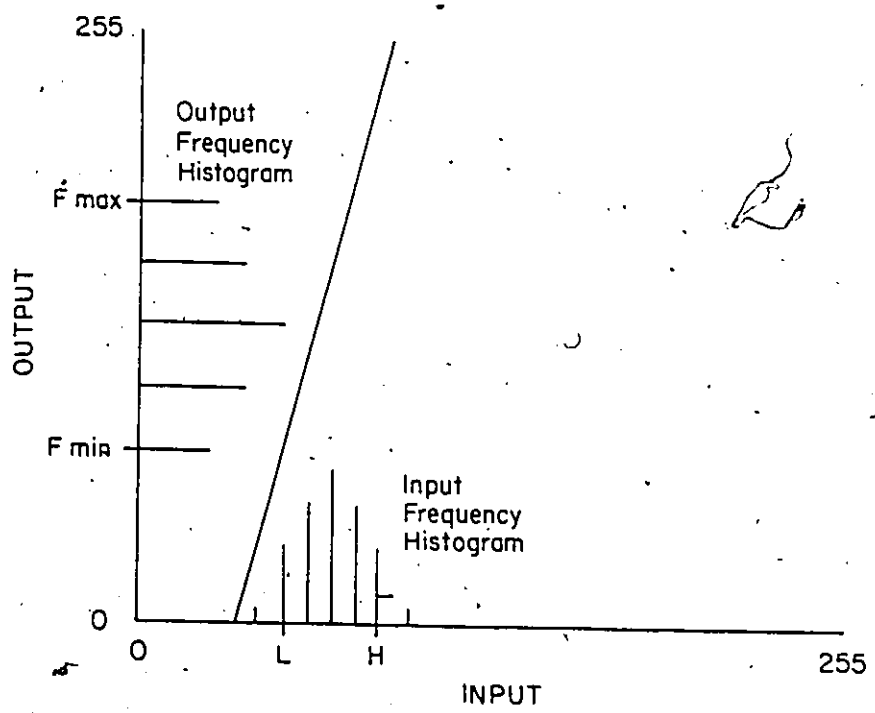

Figure 3.7 An example of the linear contrast stretch. The values L and H are points within which data are to be stretched. The relationship between the radiance data are not changed.

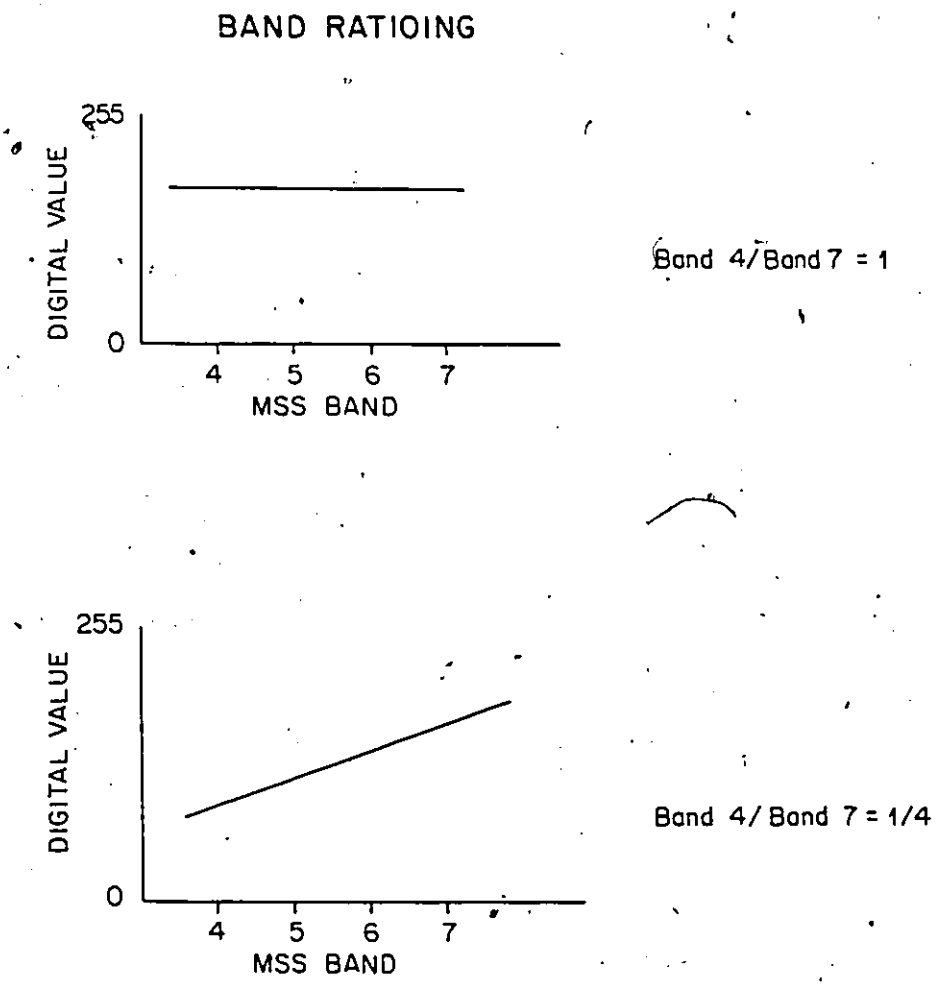

Figure 3.8 Two examples of band ratioing are illustrated with their calculated results.

imposed on the gain and offset calculations to set data greater than 255 digital values at 255 digital values and to set data less than zero digital values to zero. The truncated data cannot be seen in the display. Therefore, line prints of digital values must be consulted in conjunction with the ratioed imagery (see Chapter IV).

Band ratioing has two important effects on Landsat data. Brightness variations, caused by differences in slope, are reduced because the ratioed digital values are independent of solar illumination. In addition, atmospheric effects are reduced because the attenuation in one band is partially cancelled by the attenuation in another. The magnitude of attenuation in each band is different so that attenuation is not removed.

3.4.3 Video Filtering

Video filtering differs from the linear contrast stretch and band ratioing enhancements because only certain pixel digital values may be changed. The result is an image with more pattern uniformity and linear features, such as roads and lineaments have a greater contrast with their surroundings.

Video filtering has many names (such as boxcar, spatial and frequency filtering), and many formulae. However, in this application, one filter strength and size

is selected for study that has been described in the literature. The dimensions of this filter are 3 pixels by 3 pixels and the strength is .5.

The video filter for a single MSS band is:

$$g = aA + b \qquad 3.7$$

The gain and offset are a and b respectively, and they are selected to compensate for a possible loss in dynamic range. The filter function (A) for a strength of .5 is:

$$A = .5(f - (\varepsilon x/9)) + .5f \qquad 3.8$$

where f is the digital value of the center pixel in the 3 by 3 pixel matrix and εx is the sum of all nine pixel values (Taylor, 1978). From equations 3.7 and 3.8 it follows that:

$$g = af - a(\varepsilon x/18) + b \qquad 3.9$$

The new digital value (g) is set to 255 whenever it is greater than 255 digital values and it is replaced by zero whenever it is less than zero digital values. Each pixel is sampled sequentially, starting with the second line and second pixel.

There are problems with the video filtering enhancement. The video filter reduces the complexity of spatial patterns present in the image and as a result, pixels are created which are not true representations of the ground. Furthermore, radiometric errors that may be present in the

image are often enhanced.

3.5 Conclusions

In this chapter, Landsat data acquisition, and the methodology for correcting and enhancing that data were presented. A few problems associated with these methods were discussed.

The next two chapters will consider the methods by which data are displayed, recorded and analyzed.

CHAPTER IV

FIELD AND SATELLITE DATA USED FOR ANALYSIS

4.1 Introduction

A discussion of how the data have been obtained for this study is presented in this chapter. The data have been obtained from two sources: from field investigations during July and August of 1979, and from satellite data recorded during the summers of 1975, 1976 and 1977.

4.2 Field Data

The field data were collected from two study sites, the Hook Point site and the Churchill site (see Chapter I for site locations and descriptions).

The Hook Point study site was used for several reasons. The broad surface cover patterns were discernible on Landsat imagery. In addition, the low vegetation mat facilitated mapping of the surface cover in the field. The low topographic relief of the study site minimized the complicated relationship between shadows and brightness response in the imagery. Moreover, a few cloud-free images or scenes of Landsat data were available for the area.

At the Hook Point study site, two types of field data were collected for comparison with the satellite data.

First, the surface cover was mapped onto panchromatic enlargements of air photos. Second, radiometer measurements were taken over some surfaces so that surface cover reflectances could be derived.

It had been hoped that the author would be in the field when the Landsat satellite passed overhead so that an extinction coefficient could be calculated using both satellite and radiometer data. This would have been useful input data for the atmospheric corrections described in Chapter III. However, cloudy weather obscured the earth from the view of the satellite. Therefore, older cloud-free imagery had to be used. Nevertheless, the radiometer data provided some information about the ground characteristics.

Radiometer measurements were not available for the Churchill study site, although a ground cover map was produced. This study site was selected because it had a surface cover which differed somewhat from the Hook Point site. It provided a second study site for which to test the procedures for enhancing imagery that were developed at the Hook Point site.

4.2.1 Surface Cover Maps

A surface cover map was necessary as a reference with which to compare the corrected and enhanced Landsat imagery. Unfortunately, a surface cover map was not available for

either the Hook Point or Churchill study sites. Therefore, it was necessary to produce these maps from field investigations. Suitable surface cover classes were identified and mapped onto 1 to 6,000 scale panchromatic air photo enlargements for the Hook Point study site, (or onto 1 to 7,000 scale panchromatic air photo enlargements for the Churchill study site). Subsequently, the surface cover classes were transferred onto standard size panchromatic air photos and labelled.

The surface cover classes represented the apparent surface patterns visible at the study site. A more detailed classification scheme could have been used, but smaller features would not have been viewed by the MSS. The entire research area was not mapped in detail because only small areas of the site were used for the study, as discussed in section 4.3.3.

In July 1979, a surface cover map for the Hook Point study site was produced, as illustrated in Figure 4.1. Five major cover classes could be identified:

(a) Alluvial Thickets (A). This class has many wetland species such as Carex aquilitus, partially submerged in water, as illustrated in Figure 4.2a.

(b) Low Shrub Fen (F). This class has shrubs such as Betula glandulosa and Salix spp. The cover class is located adjacent to stream banks and within the area between the

Figure 4.1 Surface cover map for the Hook Point study site. The alluvial thicket (A), low shrub fen (F), tidal flats (T), lichen heaths (L) and open water (W) surface cover classes used for the study are indicated.

(1:40,000 approx.)


T
L
T
James
Bay
A24484 — 62

4.2a Alluvial Thicket

Figure 4.2 Ground level views of each surface cover class for the Hook Point study site.

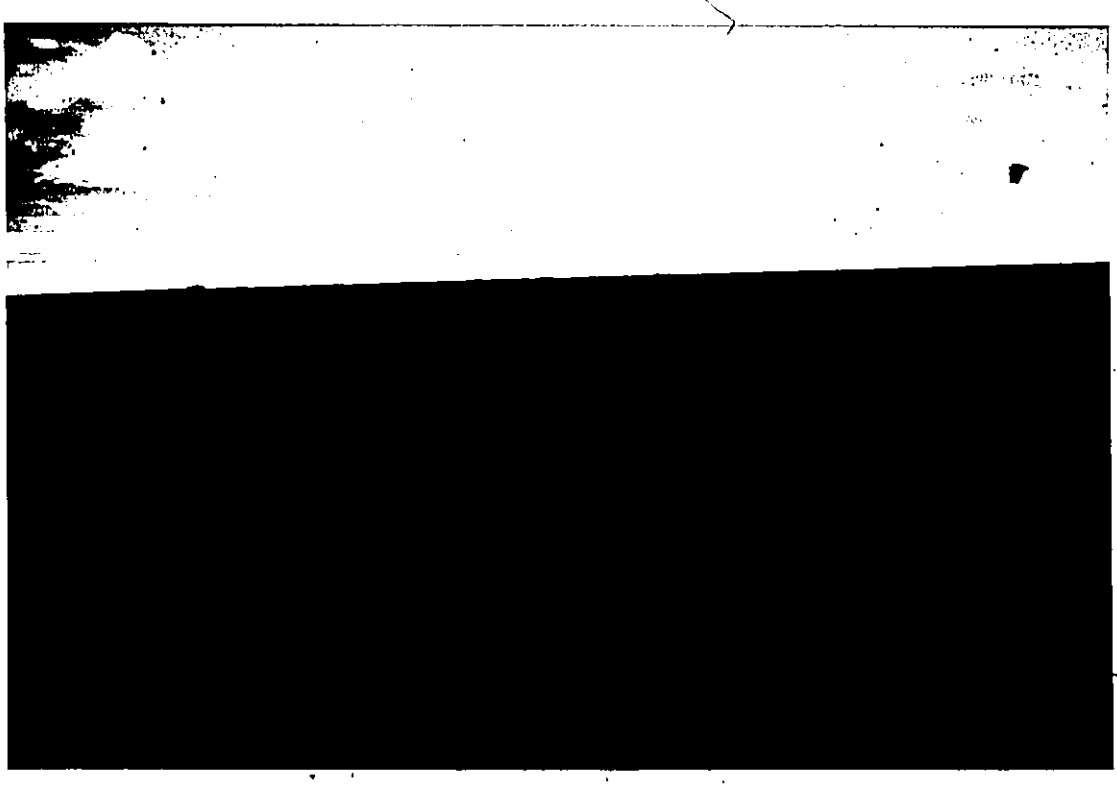

4.2b Low Shrub Fen

4.2c Tidal Flats

4.2d. Lichen Heath

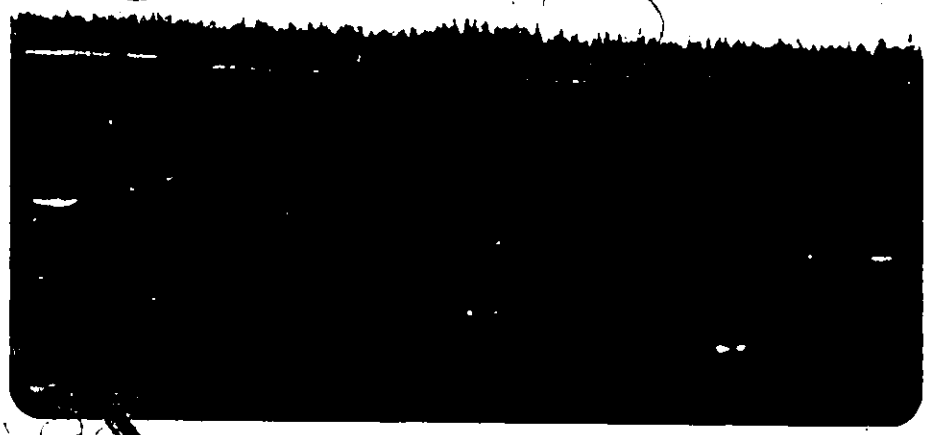

4.2e Open Water

alluvial thickets and lichen heaths (Figure 4.2b).

(c) Tidal Flats (T) are visible in both the air photos and the satellite imagery, although their size varies due to tidal conditions (Figure 4.2c).

(d) Lichen Heaths (L) are located on the crests of beach ridges and have common arctic plants such as Dryas integrifolia and Hedysarum Mackenzii (Figure 4.2d).

(e) Open Water (W). This class contains the clear water bodies (Figure 4.2e). Some of the clear water bodies are used for the solar and atmospheric corrections described in the third chapter.

In addition to the alluvial thickets (A), lichen heaths (L) and open water (W) surface cover classes, the Churchill study site has three other major cover classes that are illustrated in Figure 4.3. The three classes are described below:

(a) Bare Rock Outcrops (R) occur along the shoreline as pictured in Figure 4.4a.

(b) Urban Settlement (U) which is due to the settlement history of Churchill (Figure 4.4b).

(c) Spruce-Lichen Woodlands (I). This class is located in the south portion of the study area, and black spruce and many heath species are common. They are illustrated in Figure 4.4c.

Figure 4.3 Surface cover map for the Churchill study site. The alluvial thicket (A), lichen heath (L), open water (W), bare rock outcrop (R), urban settlement (U) and spruce lichen woodland (I) cover classes used for the study are indicated.

(1:106,000 approx.)


Churchill
River

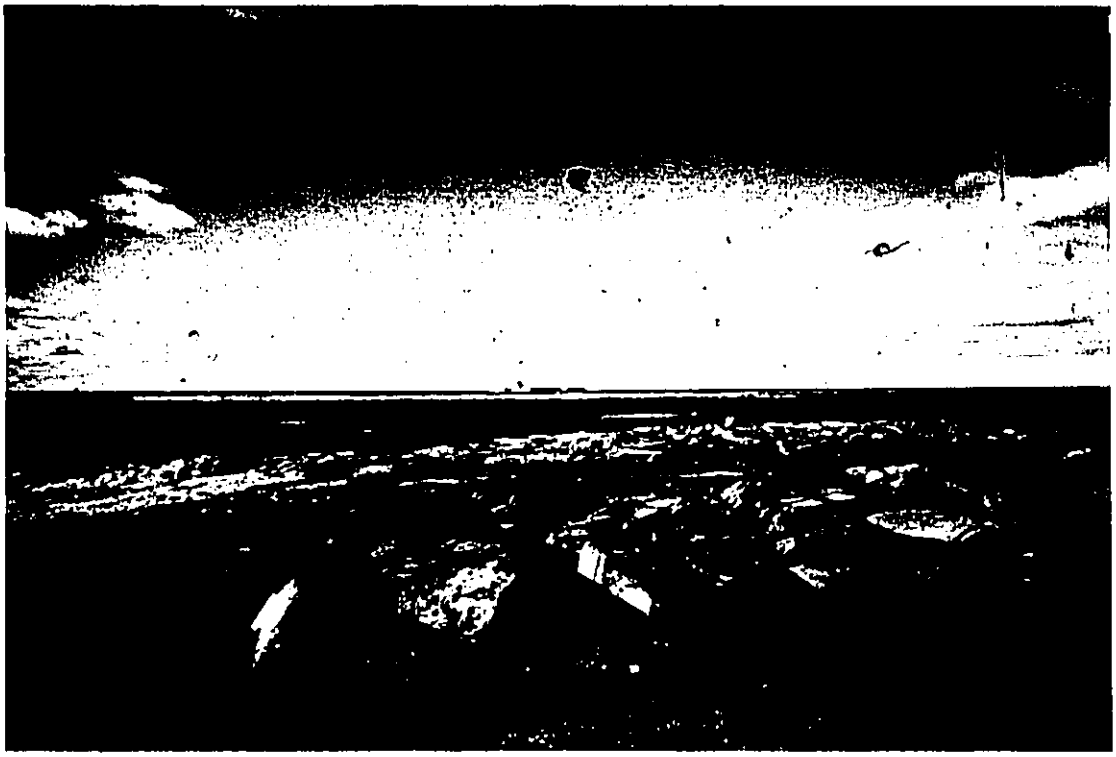

4.4a Bare Rock Outcrop

Figure 4.4 Ground level views of the different cover classes for the Churchill study site.

4.4b Urban Settlement

4.4c Spruce-Lichen Woodland

4.2.2 Surface Reflection Measurements

As an aid to comparing reflectance values from the different surfaces defined in section 4.2.1, an Exotech ERTS model 100A radiometer has been used in this study to measure upwelling and downwelling shortwave radiation for which reflectance can be calculated. This radiometer is calibrated to the four Landsat MSS bands. As illustrated in Figure 4.5, there are four individual sensors, and each one is calibrated to one MSS band. A set of four viewing heads screws into the sensors, and in the figure, the 2π steradians viewing heads are shown. As well, Figure 4.5 illustrates a side view of the radiometer and the instrument support stand. The radiation flux readings are recorded in millivolts from an indicator or a digital analog recorder. Appendix A contains the instrument specifications provided by the manufacturer.

The millivolt output is calibrated in units of milliwatts per square centimeter for all viewing heads. If one accepts the stability and calibration of the radiometer, a measure of reflectance can be obtained by deriving the quotient of reflected (upwelling) to incoming (downwelling) radiation. The downwelling radiation is measured by the sum of direct and diffuse solar radiation for each band, using the 2π steradian viewing heads. For the upwelling radiation, one must be careful to exclude the radiation reflected from the legs of the instrument support stand.

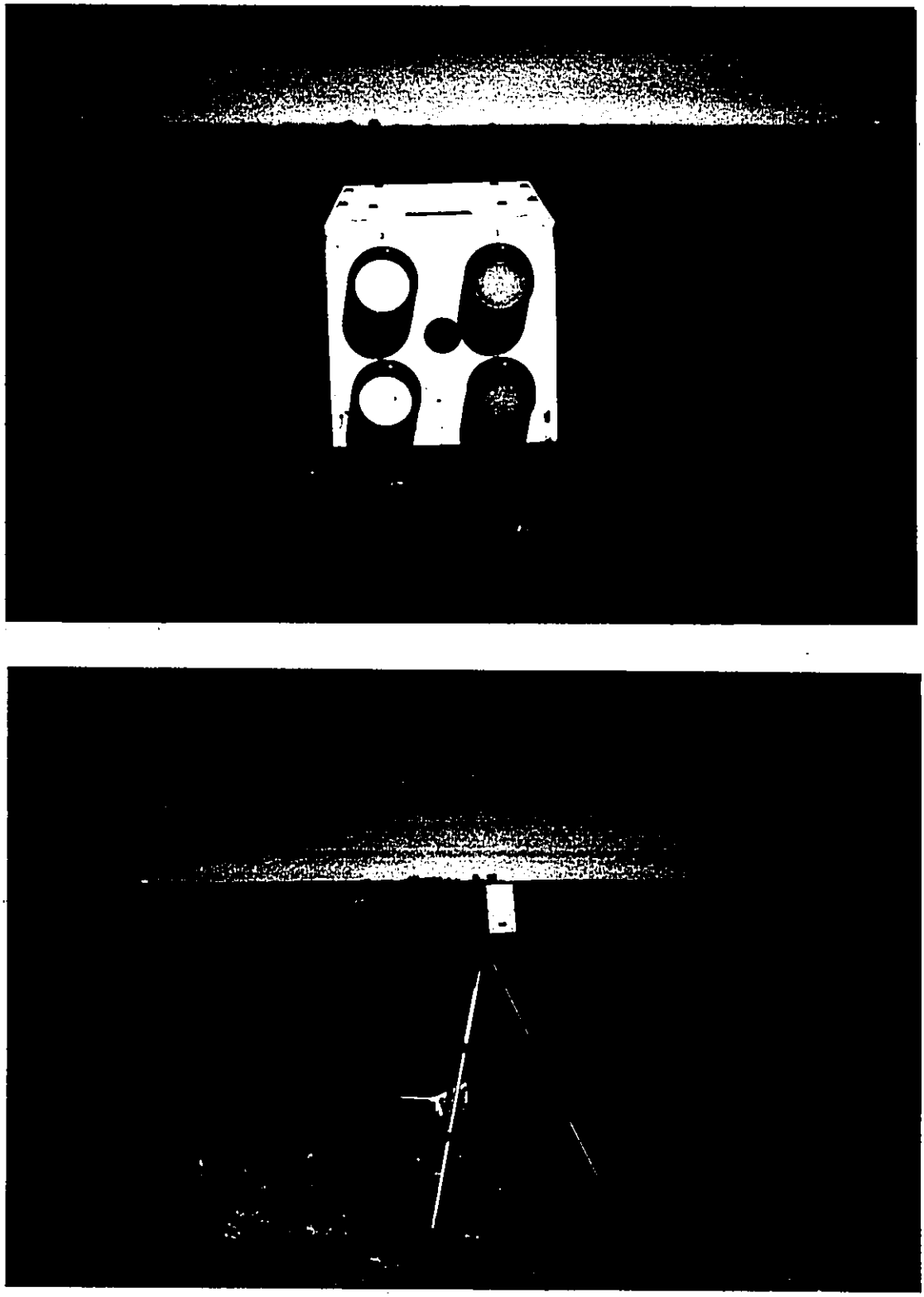

Figure 4.5 The ERTS 100A radiometer. The top picture shows the instrument viewing heads. The bottom picture shows the instrument on its support stand.

Therefore, the fifteen degree field of view viewing heads were used.

4.3 Satellite Data

4.3.1 Selection of Satellite Data

As described in Chapter I, the study sites are cloud covered most of the year, creating a paucity of cloud-free Landsat data. For the Hook Point test site, fourteen images are cloud-free for Landsat 1 and Landsat 2 but only three can be selected from these that are both snow and ice-free. These scenes are listed in Table 4.1. Table 4.1 also lists the Landsat image selected for the Churchill study site that is without clouds, snow and ice.

4.3.2 Image Analysis System

The Landsat imagery has been solar and atmospherically corrected, and enhanced by the various methods described in Chapter III on the image analysis system at the Canada Centre for Remote Sensing. It is a dedicated PDP11/70 computer, connected to a modified General Electric Image 100 which is used as an image display mechanism. Landsat CCT's are read on tape drives and image data are written onto quick retrieval disc packs and displayed on the Image 100 screen. Enhancement and correction programmes are also stored on disc. All control functions are performed through a Tekronix inter-

Table 4.1

Hook Point Test Site Imagery

Date of Recording	Frame Number	Landsat Number
June 9, 1975	20138-15492	2
July 22, 1977	20912-15265	2
Sept. 10, 1976	11510-15082	1

Churchill Test Site Imagery

Date of Recording	Frame Number	Landsat Number
June 29, 1975	11071-16395	1

active display terminal.

Each Landsat image is displayed on the Image 100 colour monitor, shown in Figure 4.6. The monitor has controls, also shown in Figure 4.6, which adjust the brightness and saturation of each colour on the display and control a movable cursored area displayed on the screen. The size of the cursored area can be specified by the terminal, and the centre control (illustrated) determines the location of the cursored area on the screen. In this project, the cursored area is used to select subscene areas from the whole Landsat image (see section 4.3.3). Extreme care is exercised so that the colour monitor controls are not adjusted because the images are photographed by a 35 mm camera from the monitor, and changing these controls introduces colour variability that cannot be compensated for when photographic prints are produced.

The colour monitor displays CCT data, or corrected and enhanced data after programme algorithms act on the data. There are four methods to obtain this data from the colour monitor. First of all, the display can be photographed and the prints produced can be documented and analyzed. Second, the digital values producing the display can be written directly onto colour film by the Electron Beam Image Recorder (EBIR), but this procedure is very costly and was, therefore, not used in this study. Third, line printers are connected to

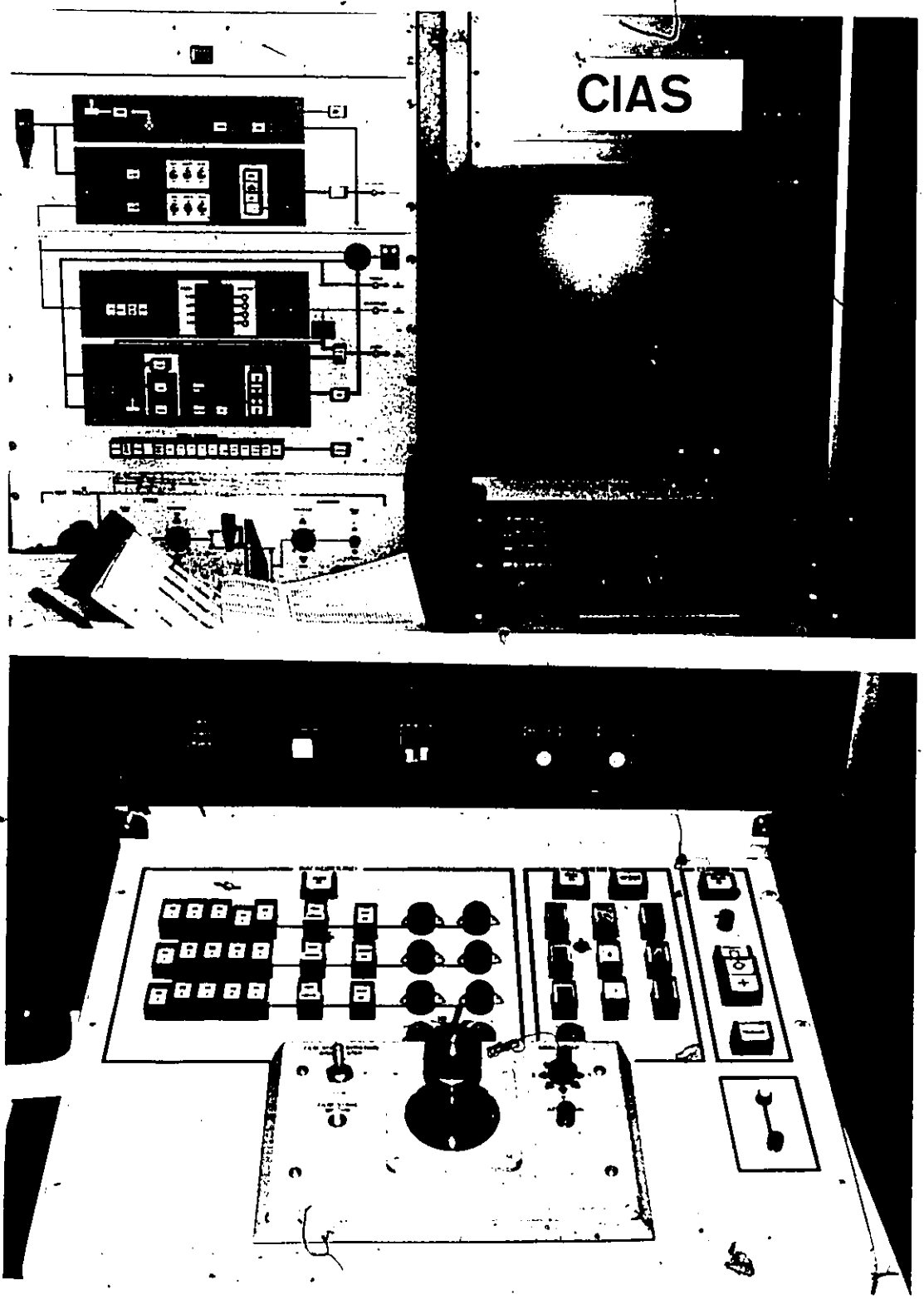

Figure 4.6 The image analysis system display monitor. The top picture shows the display screen, and the bottom picture shows the screen controls. The cursored area control is indicated.

the analysis system so that digital values from any MSS band of data can be obtained. Finally, grey level video plots (each grey level representing a range of digital values), can be printed on a line printer for any band of MSS data at any desired scale. A more detailed discussion of system hardware can be found in Goodenough (1979).

4.3.3 Colour Monitor Display Considerations

There are several considerations with each data output. For example, as described in Chapter III, the whole Landsat scene is 185 km square, but this area is too large to study in detail. Therefore, a subscene can be selected that contains the study site.

For both sites, subscenes were selected that were 512 pixels by 512 pixels in size, or about 35 km by 40 km. These subscenes were not square because the pixels are rectangular. This subscene size was selected because it corresponded to a 1 to 1 resolution of pixels to the display resolution on the colour monitor. An advantage of this size of area is that the pixels were small enough to produce an image with spatial continuity, both on the display monitor and the photographic reproductions. In all corrected and enhanced imagery, MSS Band 4 was reproduced as blue on the colour monitor, Band 5 as green and Band 7 as red. Band 6 was not displayed on the colour monitor.

Several problems were associated with the photographic reproduction of images displayed by this method. For this project, the colour display was photographed with Kodacolour outdoor emulsion 100 ASA 35 mm film. The outdoor emulsion may not have accurately reproduced the colours displayed on the monitor. As well, there may not have been any stability in the film processing, which was done at different times. Moreover, it was necessary to perform these enhancements at different times during the analysis period, so that colour intensity controls on the display monitor were probably changed.

The 512 pixel by 512 pixel area subscene was too large for output on the line printer. Indeed, the large number of digital values for each band would be difficult to analyze. Therefore, small subscenes were defined within the large subscene that were 30 pixels by 50 pixels, or 2.5 km by 4 km in size. These dimensions correspond to a single page output on a line printer and in addition, corresponded to the areas selected for detailed study at the test sites. The locations of these smaller subscenes are illustrated in Figure 4.7.

For each of these small subscenes, the following data were obtained:

(a) A 16-tone video plot of each MSS band at 1 to 50,000 scale. The plots were maps that help locate the digital value in (b). Each tone represents 16 digital values.

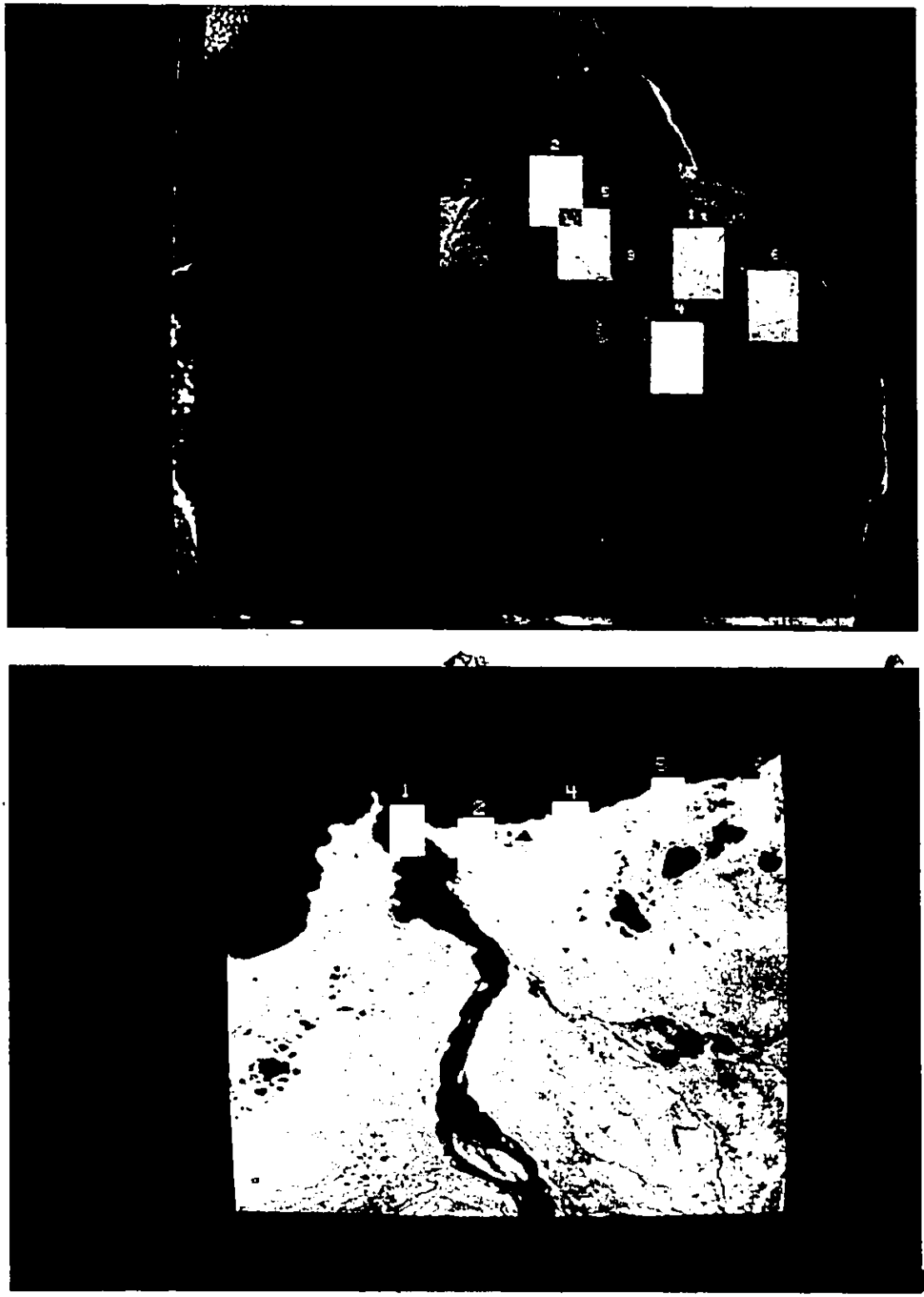

Figure 4.7 The smaller subscenes within each 512 pixel by 512 pixel area are illustrated. The top picture shows the Hook Point test site and the bottom picture shows the Churchill test site.

(b) Line prints of digital values for each MSS band.

4.3.4 Geometric Registration of the Hook Point Landsat Data

It was necessary to undertake geometric registration of the three dates of Hook Point Landsat data. If not done, the coordinates of the line prints of the 30 pixel by 50 pixel subscenes could not be matched because each 512 pixel by 512 pixel subscene is from a different section (and hence a different viewing geometry) of each CCT.

The procedure for geometric registration was performed as follows. First, the two different dates of imagery were displayed simultaneously on the colour monitor as indicated in Figure 4.8. Coordinates for common points were selected and matched by a surface fitting function. Following this, the pixels for one image were then adjusted to fit the other. This procedure was repeated because there were three images. The trend surface fitting function, used both for atmospheric corrections and geometric registration, had RMS errors less than 2 digital values.

4.3.5 Method of Analysis of Satellite Data

It is possible to show the sequence in which the satellite data were obtained. The sequence of steps in data aquisition has been outlined by a flow chart illustrated in Figure 4.9. First of all, the data for one CCT, for example, the July Hook Point image, were displayed and a 512 pixel by 512

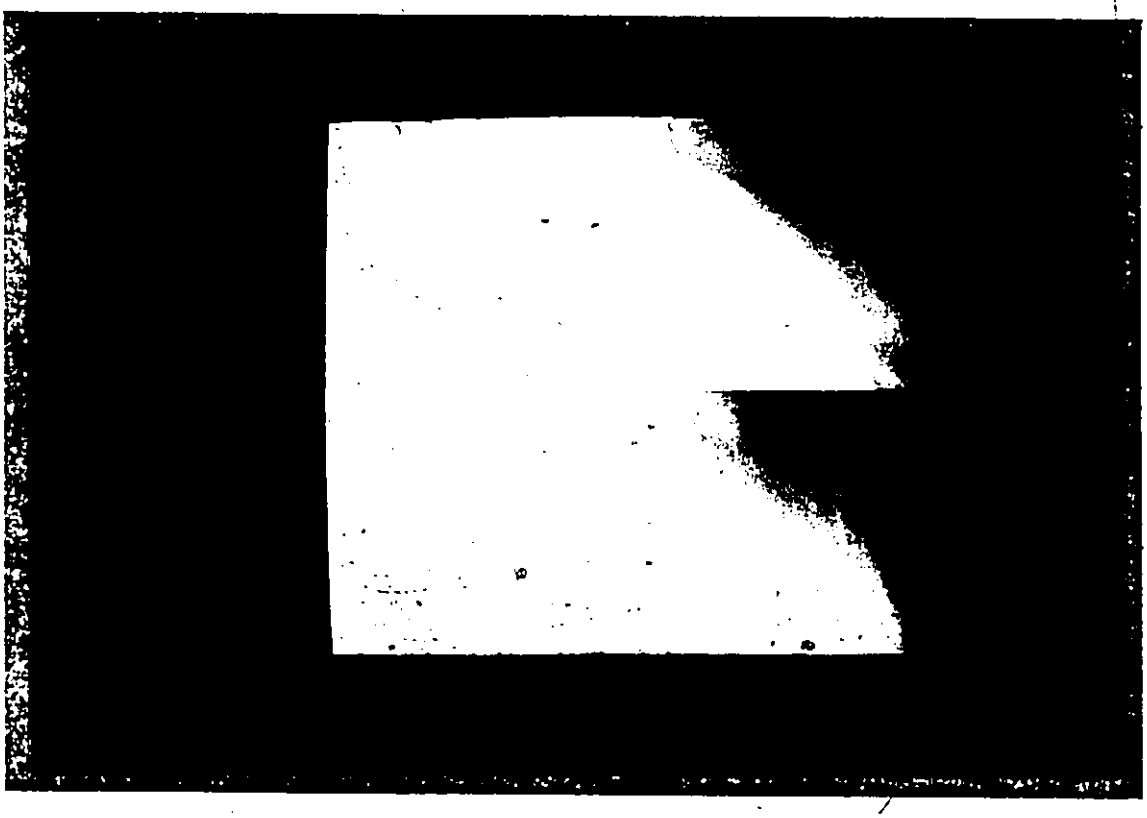

Figure 4.8 A display of the top halves of two 512 pixel by 512 pixel areas for geometric registration. Common points are selected and used for the registration so that the 30 pixel by 50 pixel areas (Figure 4.7) will match.

1. CCT Read on Image Analysis System and Whole Image Displayed (start with Hook Point)
2. 512 Pixel by 512 Pixel Subscene Selected by Use of Cursor
3. 30 Pixel by 50 Pixel Subscene Selected by Use of Cursor
4. If Hook Point Data, Another CCT Read and Whole Image Displayed, if Churchill Data - Step 8
5. 512 Pixel by 512 Pixel Subscene Selected by Use of Cursor
6. Both 512 Pixel by 512 Pixel Subscenes Geometrically Registered
7. Repeat Step 1 to Step 6
8. 512 Pixel by 512 Pixel Subscene on Colour Monitor Photographed and Line Prints and 16-Tone Video Plots Obtained for 30 Pixel by 50 Pixel Subscenes
9. Solar and Atmospheric Corrections on 512 Pixel by 512 Pixel Subscene
10. Repeat Step 8 to Obtain Corrected Landsat Data
11. Linear Constrast Stretch on 512 Pixel by 512 Pixel Subscene
12. Repeat Step 8 to Obtain Enhanced Landsat Data
13. Band Ratioing Enhancement on 512 Pixel by 512 Pixel Subscene
14. Repeat Step 8 to Obtain Enhanced Landsat Data
15. Video Filtering Enhancement of 512 Pixel by 512 Pixel Subscene
16. Repeat Step 8 to Obtain Enhanced Landsat Data
17. End of Procedure

Figure 4.9 Flow chart of steps for obtaining Landsat Data for detailed study.

pixel subscene was selected. Smaller 30 pixel by 50 pixel subscenes were also selected and the coordinates were recorded. Following this, the data from another Hook Point scene were displayed and a 512 pixel by 512 pixel subscene was geometrically registered to the July subscene by the method described in section 4.3.4.

At this point, the "raw" Landsat data have not been solar or atmospherically corrected or enhanced. Data were then obtained for the raw data: photographs of the 512 pixel by 512 pixel areas, and line prints and 16-tone video plots of the 30 pixel by 50 pixel subscenes.

After the raw data for the subscenes were obtained, solar and atmospheric corrections were applied to each of the Hook Point subscenes in turn, by the methods described in the third chapter. This produced corrected subscenes for which corrected data were obtained for the same pixel areas outlined above.

Each of the three enhancements were performed on one corrected Hook Point 512 pixel by 512 pixel subscene (see Chapter V). Photographs were obtained for this subscene and line prints and 16-tone video plots were obtained for the 30 pixel by 50 pixel size subscenes after each enhancement.

The same data were created for the Churchill study site, but only one date of imagery was used. Thus geometric registration, described in section 4.3.4, was not required.

4.4 Conclusions

This chapter has described the methods employed for obtaining ground and satellite data so that the two can be compared. A flow chart of logical steps in data collection was presented and discussed.

The next chapter will present the analysis and discussion of the study.

CHAPTER V

ANALYSIS AND DISCUSSION

5.1 Introduction

The results from the analysis of the data will be presented in this chapter. First, the solar and atmospheric corrections from the Hook Point study site will be analyzed; both numerical and visual assessments will be presented. A similar approach will then be used to evaluate the cover classes from Hook Point and the three enhancements will also be analyzed. Finally, solar and atmospheric corrections, cover classes and the three enhancements from the Churchill site will be assessed, again using both numerical and visual approaches.

5.2 Application of the Solar and Atmospheric Corrections to the Hook Point Subscenes

5.2.1 Assumptions Necessary for the Evaluation

Before an analysis of the solar and atmospheric corrections could proceed, it was necessary to select a standard reflector for which MSS data could be compared between subscenes. Oligotrophic lakes can be used as a standard reflector because their albedos have been studied and are similar. At the Hook Point site, there are many oligotrophic

lakes and they could be easily identified in each subscene.

Two important assumptions had to be made before these lakes were used. The first assumption was that it was necessary to assume that the suspended sediment concentration did not change from 1975 to 1979. If the sediment concentration changed, so would the reflectance of the lake, as Ahern et al. (1977a) have discussed. This assumption was accepted because the Band 4 and Band 5 open water class frequency histograms did not have high digital values, suggesting that no sediments were present. Some surface ice was present in the June subscene, partly obscuring the water beneath.

The second assumption was that these lakes did not change their surface dimensions, otherwise digital data could have been misread on the line prints. This assumption was acceptable for two reasons. First, climatic data from the Winisk meteorological station showed that approximately the same rainfall occurred each year. Therefore, the same area of water could have been present on the ground surface each year. Second, no changes in lake dimensions were detected between the 1976 air photos and the 1979 field investigations.

5.2.2 Open Water Class Digital Values

Having defined the standard reflector, the subsequent

task was to record sufficient digital values for each band from both the raw and corrected Hook Point subscenes. Open water class pixels from the lakes were easily identified on the Band 7 16-tone video plots because they appeared black, as illustrated in Figure 5.1. The coordinates for each water pixel were identified and recorded. Following this, the corresponding digital values from the line prints were obtained. It was possible to record 42 open water class pixels for each subscene, and they have been listed in Appendix B.1 and B.2.

5.2.3 Analysis of the Digital Values from the Hook Point Subscenes for the Open Water Class

The data will be compared between the raw and corrected subscenes so that the solar and atmospheric corrections can be investigated. The mean digital values for the water pixel data appear in Figure 5.2. Several important details about the data can be noted. The raw subscenes have higher mean digital values than the corrected Band 4, Band 5 and Band 6 subscenes. This is expected because the corrected solar elevation is 50^{o}, which is smaller than the uncorrected solar angle. However, the magnitude of the difference is too large to be explained by this alone. The corrections are still in the experimental stage, and the systematic errors in the calculation of the extinction coefficient have not been

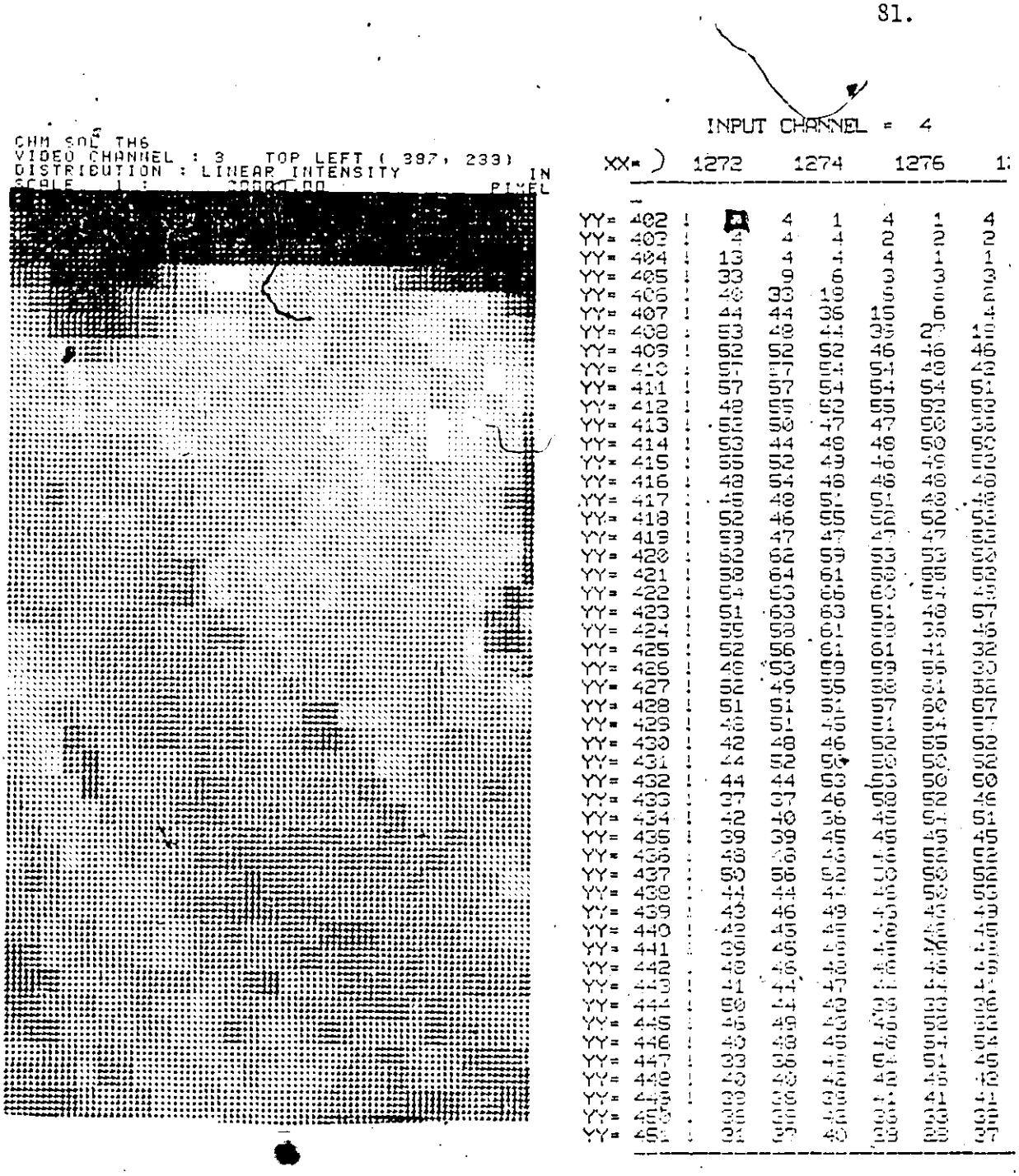

Figure 5.1 An example of water pixel identification. Each water pixel is identified on the 16-tone video plot (left) and the coordinates are noted. Following this, the digital value for the same water pixel is determined from the line print (right).

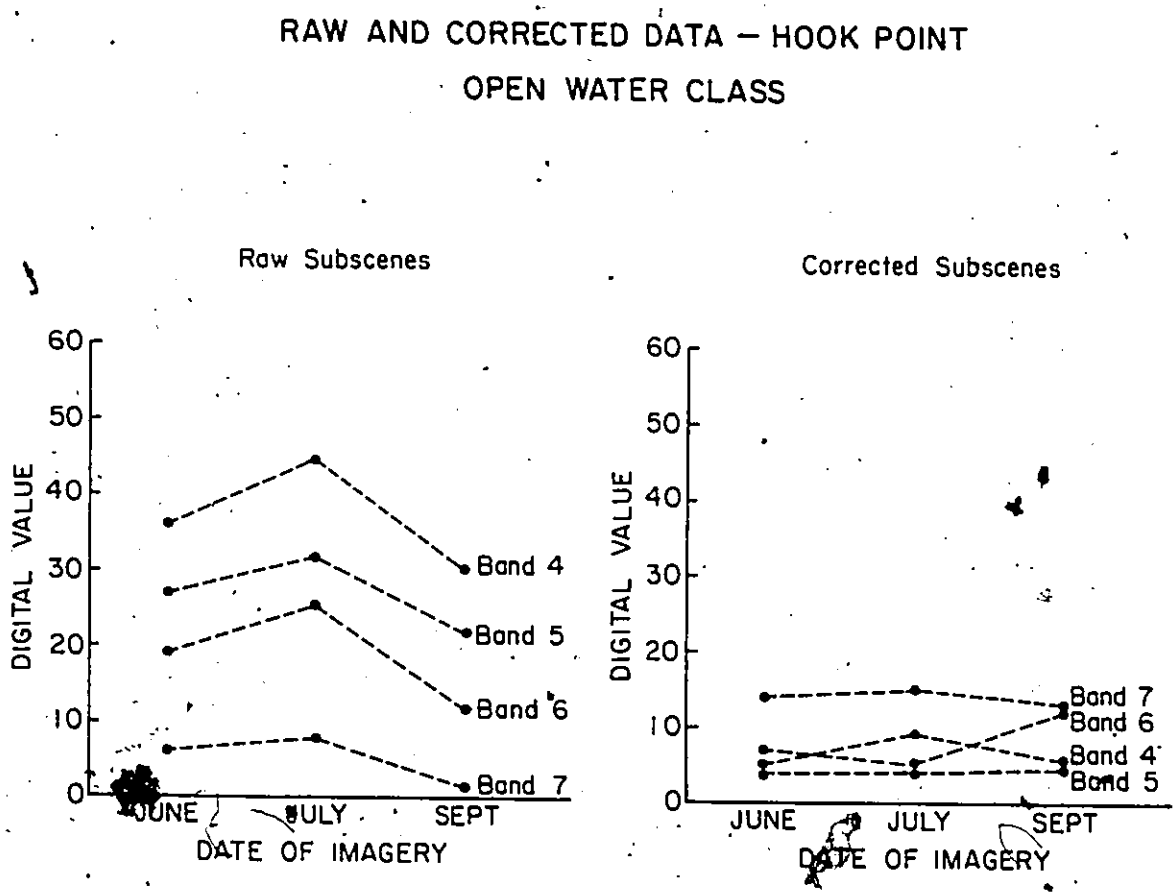

Figure 5.2 The unweighted mean digital values are plotted for the raw and corrected Hook Point Landsat data. The raw data have higher digital values than the corrected data and the raw data have more variability.

eliminated (Ahern, Canada Centre for Remote Sensing, Ottawa, pers. comm.).

The systematic errors account for the increased Band 7 digital values after corrections have been applied. With corrections to a lower solar elevation, the Band 7 digital values should be decreased. In comparison to the other MSS bands, the extinction coefficient is consistently underestimated. Therefore, larger values for Band 7 may be produced after corrections (Ahern, pers. comm.).

The importance of these corrections is exemplified by a consideration of the reduced variation in the mean open water class pixels within each band after corrections. The differences between the mean digital values in any band are less after corrections are applied.

To determine if differences existed in the digital values between image dates within each band, the open water class data were tested in pairs for each of three combinations of image dates. This resulted in twelve paired tests for either the raw or corrected subscenes. The Kolmogorov-Smirnov two sample one-tailed test was selected because it has a high power and some of the data were not normal, requiring the use of non-parametric statistics. The test determined if there was a significant difference between the distributions and it is sensitive to differences in central tendancy. The results have been summarized in

Appendix B.1. The accepted probability of a Type I error was .1, because small sample statistical tables by Conover (1971) used elsewhere in this study had test statistics calculated at the .1 level, rather than the conventional .05 level..

The results show that for all raw data, the probability that any pair of different subscene date samples are drawn from the same population is less than .001. This result is expected because atmospheric conditions and solar illumination vary greatly between subscene dates. For all but two pairs of the corrected data, the probability that both of open water class samples are drawn from the same population is less than .05. This result is not expected because the open water class mean digital values should be equal after corrections have been applied.

There are several possible explanations for this problem. First, the assumptions for the use of the Turner-Spencer equations may be incorrect and as a result, the radiative transfer solutions cannot be used in real atmospheres. Second, the statistical test is sensitive not only to central tendancy, but to the whole distribution. The distribution can vary in dispersion due to variations in the geometric corrections or geometric registration. As well the use of clear lakes as a standard reflector may not be suitable for such accurate assessments because the

dispersion in reflectance from water is not constant over time. Moreover, there are other untested factors, such as the presence of shadows from scrub vegetation, very high sun glint conditions or pixels that represent the open water class and other classes.

Nevertheless, the probability that two samples are drawn from the same population of water pixels has increased by a factor of 50. As well, the Band 5 June and July, and the Band 7 June and July samples have probabilities that exceed the .1 test statistic. Therefore, it may be concluded that the data are more standardized, but that complete standardization may yet be possible with current techniques because there are several untested factors.

5.2.4 Analysis of the Visual Display of Corrected Data

As illustrated in Figure 5.3a, 5.3b and 5.3c, the raw subscenes have different colour tones in contrast to the more uniform red tones and the greater clarity of the corrected subscenes, presented in Figures 5.4a, 5.4b and 5.4c. However, there are two problems with these displays. First, there are colour variations due to changes in the colour monitor controls and instability in the film processing (as discussed in Chapter IV). Second, the Band 7 corrected data is inaccurate, as discussed in Section 5.2.3. As a result, there are stronger red tones in the corrected

Figure 5.3a June Hook Point raw subscene. The raw subscenes have varying amounts of atmospheric haze, which contrasts to the clarity of the corrected subscenes (Figure 5.4).

Figure 5.3b July Hook Point raw subscene.

Figure 5.3c September Hook Point raw subscene.

Figure 5.4a June Hook Point corrected subscene.

Figure 5.4b July Hook Point corrected subscene. The change in red tone compared to the other corrected subscenes is probably due to changes in the colour monitor controls. Cloud cover is present in the south portion of the image. Changes in the red tone correspond to changes in vegetation cover.

Figure 5.4c September Hook Point corrected subscene.

subscenes.

There is one noteworthy feature of the corrected imagery. The July subscene has cloud cover present in the south quarter of the image (Figure 5.3b). The cloud cover remains in the corrected subscene (Figure 5.4b) obscurring the ground view beneath, because the Turner-Spencer equations do not correct for cloud cover. However, the haze in the July raw subscene is reduced by the corrections to standard conditions because variations within (as well as between) subscenes are reduced.

The corrected subscenes appear clearer and are more standardized. Therefore, they have been used to test the enhancements.

5.3 Evaluation of the Surface Cover Classes for the Corrected Hook Point July Subscene

5.3.1 Assumptions Necessary for the Evaluation

In this section, the cover classes from one corrected subscene have been analyzed for each band of data. They will eventually be compared with enhanced data. The July corrected subscene has been selected because it is the most recent and can be compared to field data.

There is another reason for selecting the July corrected subscene. Previously, lakes have been selected as a standard reflector based on assumptions of constancy in size

and sediment concentration. Similar assumptions can be applied to subartic vegetation cover, although their albedos have not been as well studied. For example, over a short period of time, the vegetation cover (and hence the albedo) probably does not change. Field investigations did not reveal a change in ground cover when present ground conditions were compared with the 1976 air photos. However, legumes such as Hedysarum Mackenzii flower during July and August colouring the lichen heaths red. This flowering period may not have extended to June and September, and as a result it cannot be assumed to be present in the June or September Hook Point subscenes. Therefore, satellite and radiometer data can be more confidently compared with the July subscene.

5.3.2 Cover Class Digital Values and Reflectance Measurements

The cover class digital values were selected by the same method outlined in section 5.2.2. Cover classes were identified on the Band 7 16-tone video plots for which a corrected Landsat subscene photograph and the ground cover map were used to help identify the classes (Figure 5.5). The coordinates of the pixels were recorded and used to identify the corresponding digital values. A total of 169 pixels could be identified for all of the cover classes

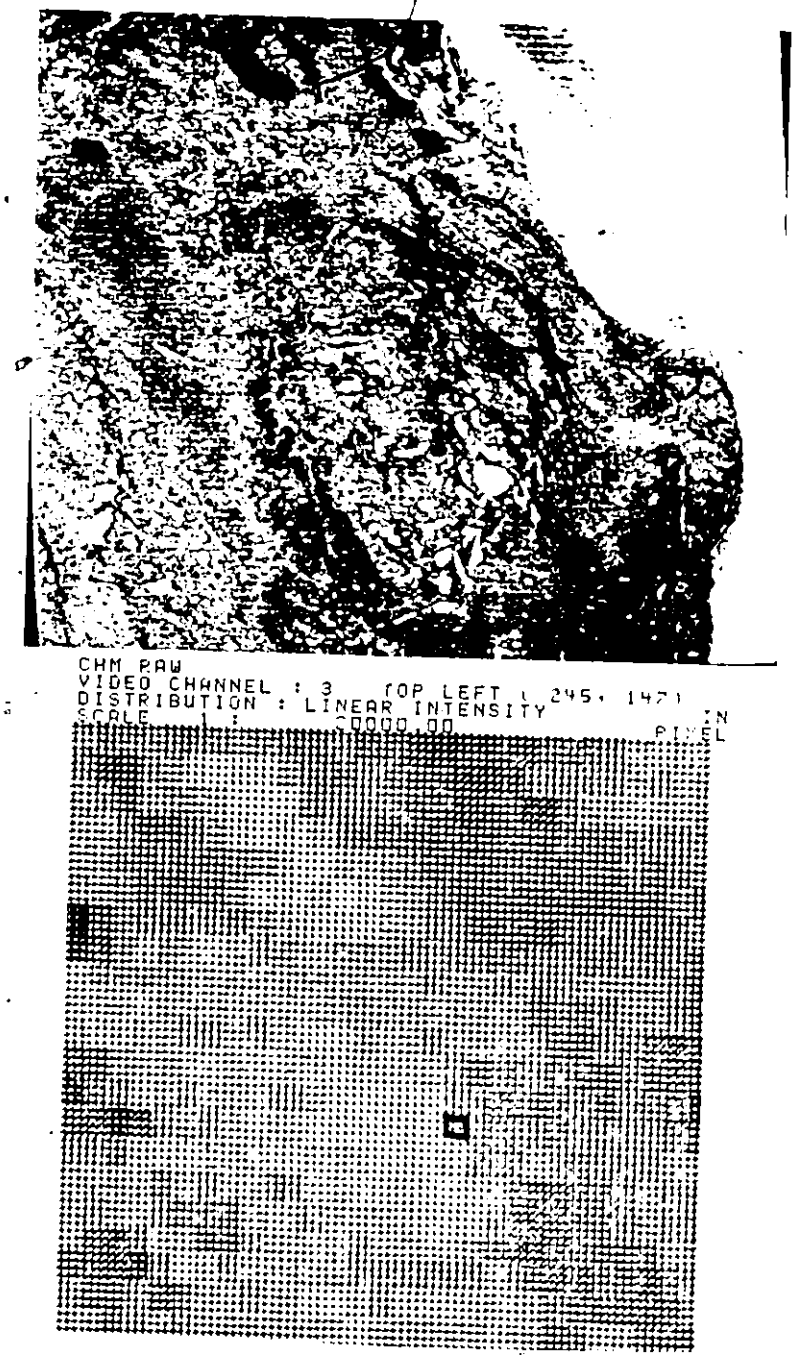

Figure 5.5 An example of cover class pixel identification. Each cover class is identified on the 16-tone video plot and the corrected image (left) and the coordinates noted. Following this, the digital value for the same pixel is determined from the line print (right).

(42 pixels were from the open water class used previously) and they have been listed in Appendix B.3. A plot of mean digital value for each band of each cover class has been illustrated in Figure 5.6.

In contrast, only sixteen measurements were obtained from the ground based radiometer due to inclement weather (Appendix B.4). Reflectance (in percent) was calculated by determining the quotient of upwelling to downwelling radiation for each band (see section 4.2.2). The measurements were taken at random points along transects within each defined 30 pixel by 50 pixel area described in Chapter IV. The mean reflectance values have been presented in Figure 5.6. A change of 1% reflectance is approximately equivalent to 2.5 digital values. Measurements were not obtained for the open water class. Measurements were not used for MSS Band 7 because the radiometer was not functioning for this band.

5.3.3 Analysis of Digital Values and Reflectance Data for the July Hook Point Cover Classes

The cover classes have been tested by the same method outlined in section 5.2.3. The hypothesis under study tests if all classes are from different pixel populations. If this is true, then the choice of cover classes is appropriate. Furthermore, they can be separated through

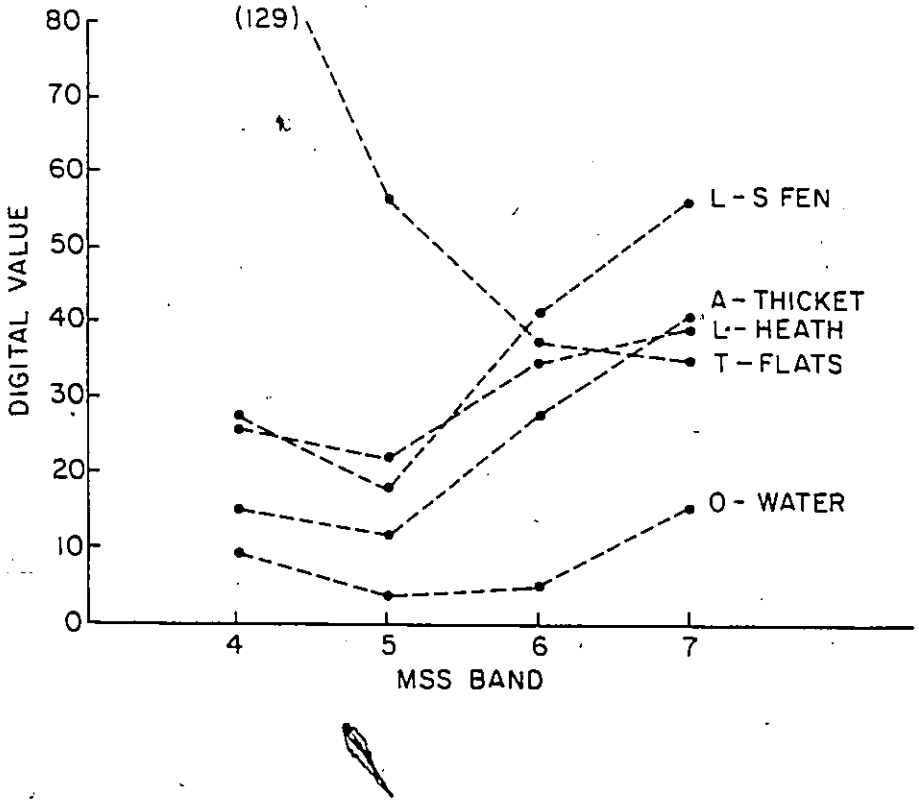

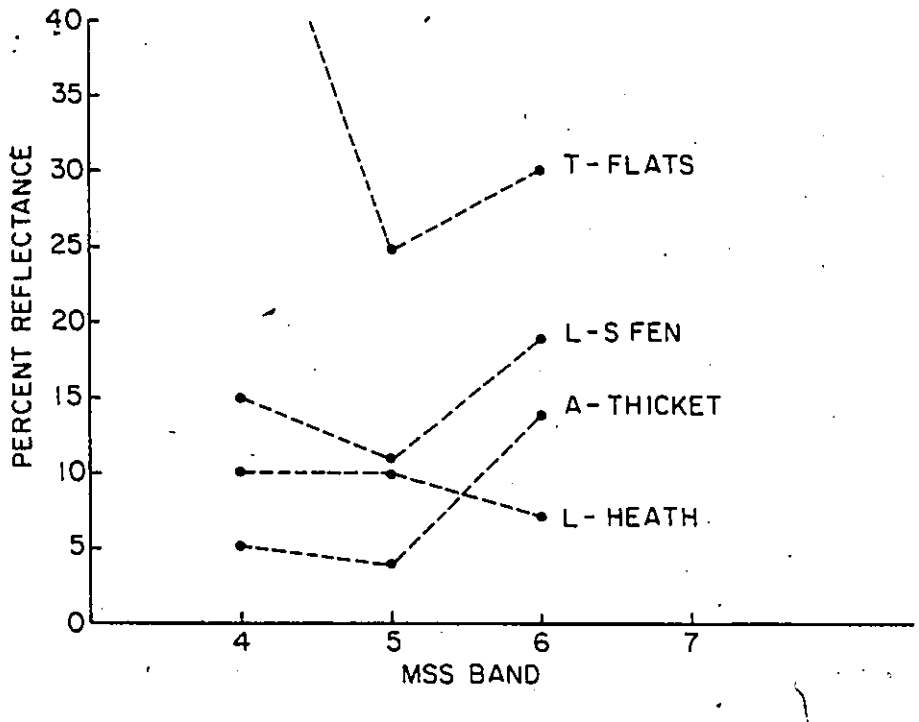

Figure 5.6 The plotted cover class data (Hook Point). The Landsat digital data (top) and the radiometer data (bottom) can be compared (2 1/2 digital values is about 1 percent reflectance)

the use of MSS data.

It was necessary to test the classes in pairs between each class within each MSS band using the Kolmogorov-Smirnov two sample one-tailed test. The test was done on each of ten possible combinations of class data for each MSS band for a total of 40 tests (Appendix B.3). For 38 pairs, the probability that samples of two different classes were drawn from the same population was less than .05. This attested to the suitability of these classes. The remaining two pairs were the lichen heath and low shrub fen in Band 4 and the alluvial thicket and lichen heath in Band 7 for which the probabilities that the two classes were drawn from the same population were between .2 and .3, and .2 and .3 respectively.

A probable explanation for this discrepancy was the loss of some contrast in the data because atmospheric attenuation was present despite corrections to standard conditions. The explanation has been verified with a consideration of the radiometer data. Because only sixteen measurements were taken from the radiometer, the Kolmogorov-Smirnov test results were determined from the small sample tables in Conover (1971). There were 20 possible pair combinations. Each pair of samples was from significantly different populations at the .1 probability level. This included the Band 4 class samples that were not significant

at the .1 probability level for the Landsat data. The results from these tests have been summarized in Appendix B.3.

It is important to compare the mean digital values plotted graphically in Figure 5.6. Mean values for the various cover classes are linked with dashed lines to suggest a possible spectral curve for each class. Unfortunately, the actual spectral curve may look quite different because the plotted data only represent the average of broadband sensor data.

From the graph, the vegetation classes mean digital values agree with studies of reflection in green vegetation. Vegetation reflects in the visible green (Band 4), absorbs in the visible red (Band 5) and reflects highly in the near infrared (Band 6 and Band 7). The same results are observed with field reflectance data, except that the Band 6 reflectance of the lichen heath class is different.

As well, the Band 6 reflectance of the tidal flat class also differs from satellite measurements. The field of view of the radiometer is small in comparison to the field of view of the satellite. Therefore, it is possible that more water was viewed by the radiometer during field measurements of lichen heaths, and that less water was viewed by the radiometer during field measurements of tidal flats compared to what was viewed by the Landsat MSS.

The difference in field of view, as well as possible differences in ground conditions at the time of measurement,

probably account for differences between the satellite and radiometer mean data. When the subscene data is changed to standard solar and atmospheric conditions, less contrast in the satellite data will be observed because the atmospheric effects are not removed, and the class digital values appear closer together. However, the radiometer measurements were obtained during periods of variable cloudiness. As well, the radiometer may not measure radiance accurately because the instrument calibration changes with temperature and battery current. Therefore, a comparison between satellite and radiometer data is meaningless.

5.3.4 Analysis of the Visual Display of Cover Classes

The cover classes have different digital values so that they should be distinguishable on the raw (Figure 5.3b) and corrected (Figure 5.4b) subscenes. Indeed, the cover classes appear as different red tones. The corrected subscene appears less hazy. It would probably be better for mapping these classes because there is more contrast between the classes.

It is difficult to estimate the value of these corrections for interpretation of surface cover because there are several untested variables. As previously mentioned, the colour monitor controls and the film processing are difficult to stabilize. Moreover, it is impossible to

quantify the skill, experience and visual acuity of the interpreter. Therefore, it must be realized that conclusions drawn from such visual assessments may not apply elsewhere.

5.4 Evaluation of the Image Enhancements for the Hook Point July Subscene

5.4.1 Linear Contrast Stretch Enhancement

The vegetation classes were emphasized in this enhancement. Unfortunately, there was no objective method for selecting the stretch limits. The limits were selected, therefore, on the basis of reflectance theory for vegetation. Band 6 and Band 7 were useful because vegetation reflected highly in the near infrared. In contrast, water absorbed strongly in these bands. This produced a bimodal frequency histogram for the 512 pixel by 512 pixel subscene. Other bands failed to show this pattern. As a result, the selection of the gain and bias values were more subjective in Band 4 and Band 5.

The gain was calculated as the quotient of the total range of 255 digital values of output and the range of 64 digital values of vegetation class data identified for Band 7. An offset of 24 was selected to maintain positive digital values. The gain and bias values selected for the other bands have been listed in Figure 5.7 together with graphic plots of the resulting mean digital value. Line prints were

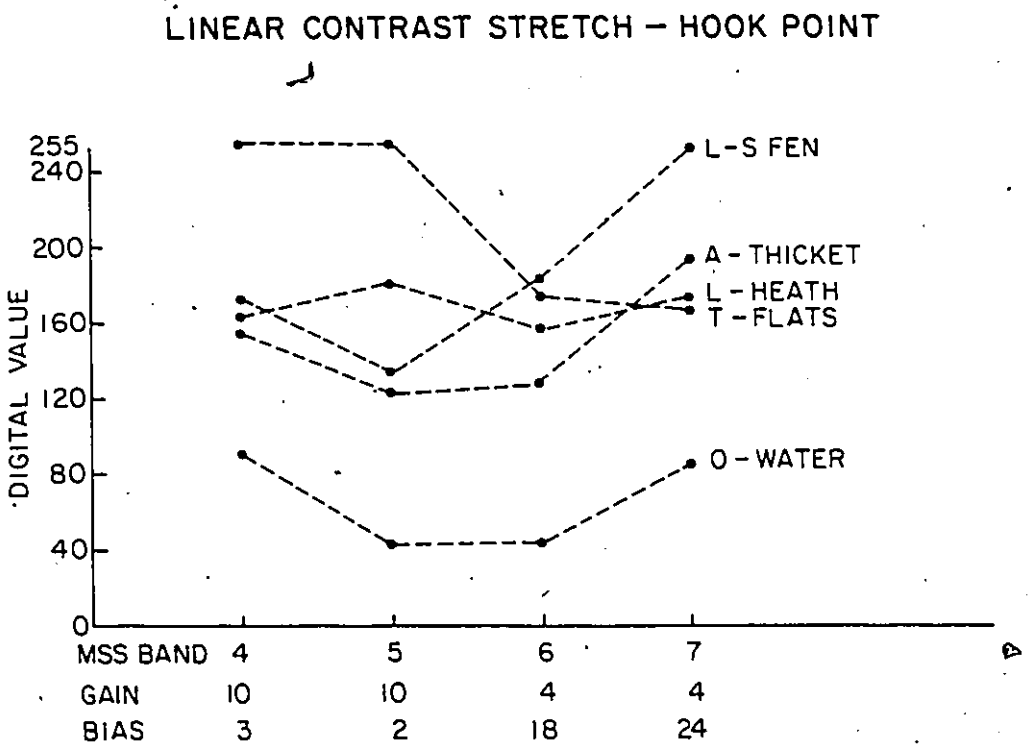

Figure 5.7 The plotted mean digital values for the linear contrast stretch. The gain and bias values for each band are listed. These are for the July Hook Point subscene.

used to record enhanced pixel digital values for the same class pixels.

Because different gain and bias values were selected for each band, the mean digital values were all different. The differences between the digital values were emphasized in each band. The enhanced mean digital values were all different compared to the pre-enhanced or corrected values (Figure 5.6). Therefore, a comparison was meaningless.

The enhancement changes the appearance of the image. The tidal flat class was truncated at the 255th digital value in Band 4 and Band 5, compared to 124th and 60th digital value respectively for the corrected class. Therefore, this class appears bright blue and green (Figure 5.8). In contrast the open water class appears dark because all of the mean digital values are lower in the enhanced data. The blue tone is due to the relatively higher Band 4 values. The enhanced vegetation classes appear as mixed shades of blue, green and red because the digital values are different compared to the unenhanced digital values. For example, the low shrub fen appears bright red in the subscene because its Band 7 mean digital value is higher after enhancement.

The linear contrast stretch enhancement is effective for the display of natural vegetation because the mean digital value for each band of each vegetation class is

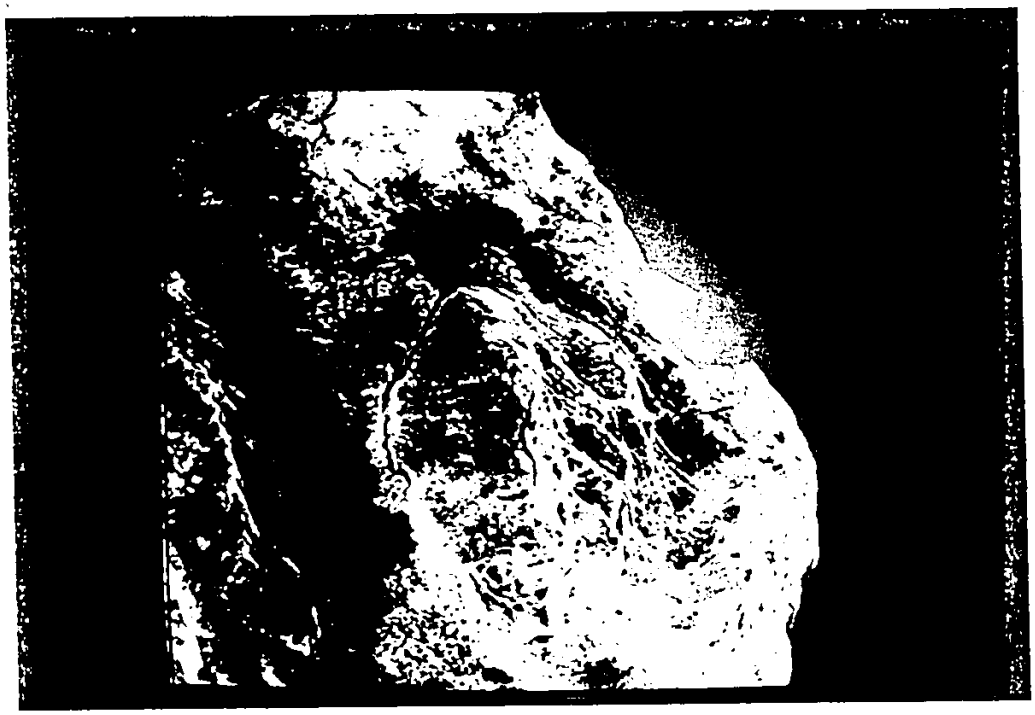

Figure 5.8 The linear contrast stretch enhancement of the July Hook Point subscene. Note the white tones of the lichen heaths, the blue tones of the alluvial thickets and the red tones of the low shrub fens.

different. This contrasts with the studies of the linear contrast stretch in geologic applications described in Chapter II.

5.4.2 Band Ratioing Enhancement

Band ratioing can also be used to emphasize differences in vegetation cover. Previous works by Thomas (1979) and others have reported that the infrared response in vegetation is related to a change in plant vigor or a change in plant type. The visible reflection is not as well correlated with vegetation.

The ratio of Band 4 to Band 7 was tested in the study. The same pixels used in section 5.3.2 were used after enhancement to find the mean digital value (Figure 5.9). They have been presented so that they can be compared with previously plotted data. The enhanced subscene has been presented in Figure 5.10. Because only one digital value was produced in this enhancement, only one colour was needed for the display.

The wide range of mean digital values attested to the differences between each cover class. The lichen heath and alluvial thicket cover classes were clearly displayed as different tones on the image because their ratioed values were very different. The low shrub fen was displayed as a light tone similar to the lichen heaths. The tidal flat

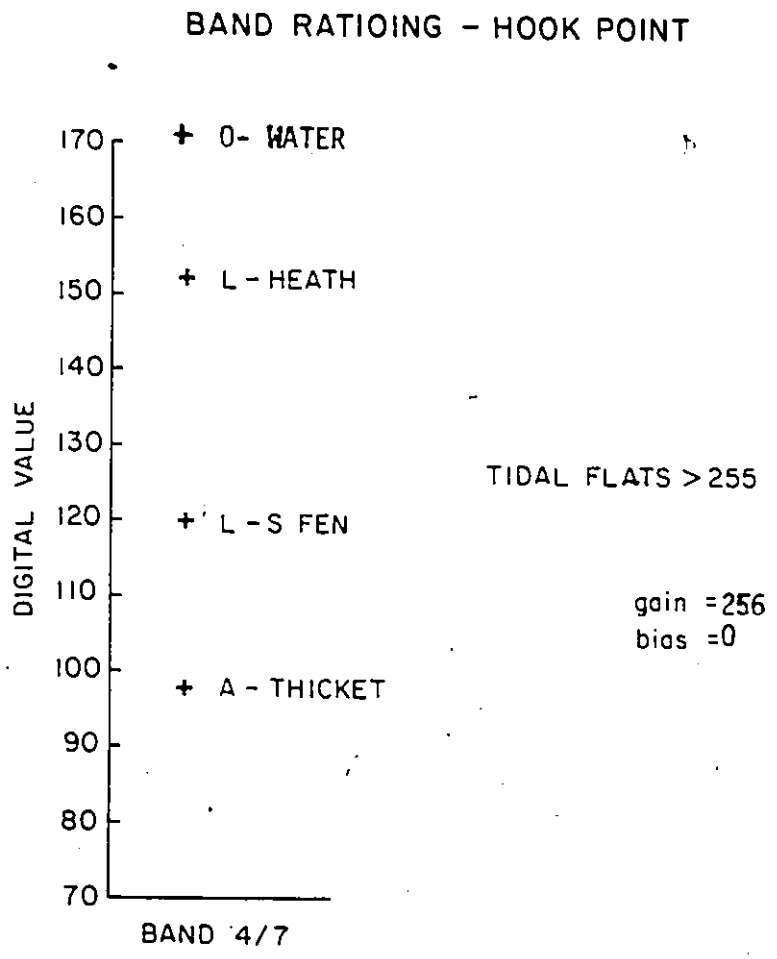

Figure 5.9 The mean digital values for the band ratioing enhancement (Hook Point July subscene).

Figure 5.10 The band ratioing enhancement for the July-Hook Point subscene. The cloud cover is reduced in the image.

cover class data were set to the 255th digital value by the contrast stretch selected for the display. The cloud cover was reduced because its effect was partially divided out. Radiometric striping has been enhanced because the radiometric errors have not been eliminated.

Unlike the linear contrast stretch enhancement, it was impossible to predict if the digital values would remain significantly different between classes, because more than one variable was included in the equation. Therefore, another series of Kolmogorov-Smirnov two sample one-tailed tests was used on six possible paired samples of the four enhanced vegatation classes (excluding the tidal flat class). The results showed that for all pairs, the probability that the two class samples were drawn from the same population was less than .001 (Appendix B.5). This included the alluvial thicket and open water pair for which the calcuated probability was less than .001.

There is one reason for the lower calculated probability (.001) for all of the six sample pairs for the enhanced compared to the pre-enhanced classes. The band ratioing enhancement uses more of the spectral information to calculate a unique number. This number is dependent on the displacement on the digital value scale. It has a different meaning than a single MSS digital value and different results would be expected.

The alluvial thicket and open water classes have different ratios because the alluvial thicket has little water present. The broadband spectral curves are similar.

Again, these results do not agree with the geological investigations described in the second chapter. The ratioed values for Hook Point vegetation cover are unique, whereas they are similar for different types of exposed rock. Therefore, the band ratioing enhancement can be used more successfully for this application.

5.4.3 Video Filtering Enhancement

The video filtering enhancement was achieved through the use of equation 3.9. The gain and bias values were selected to increase scene contrast when necessary, and they have been listed together with the mean digital values of the enhanced cover classes in Figure 5.11. The enhanced 512 pixel by 512 pixel subscene has been illustrated in Figure 5.12.

A series of statistical tests were applied to a possible 10 paired samples of classes within each band for a total of 40 tests. The Kolmogorov-Smirnov two sample one-tailed test was used and the results have been summarized in Appendix B.6. The data for the test were randomly selected because the enhancement depends on selecting adjacent pixels. Random number tables were used to select coor-

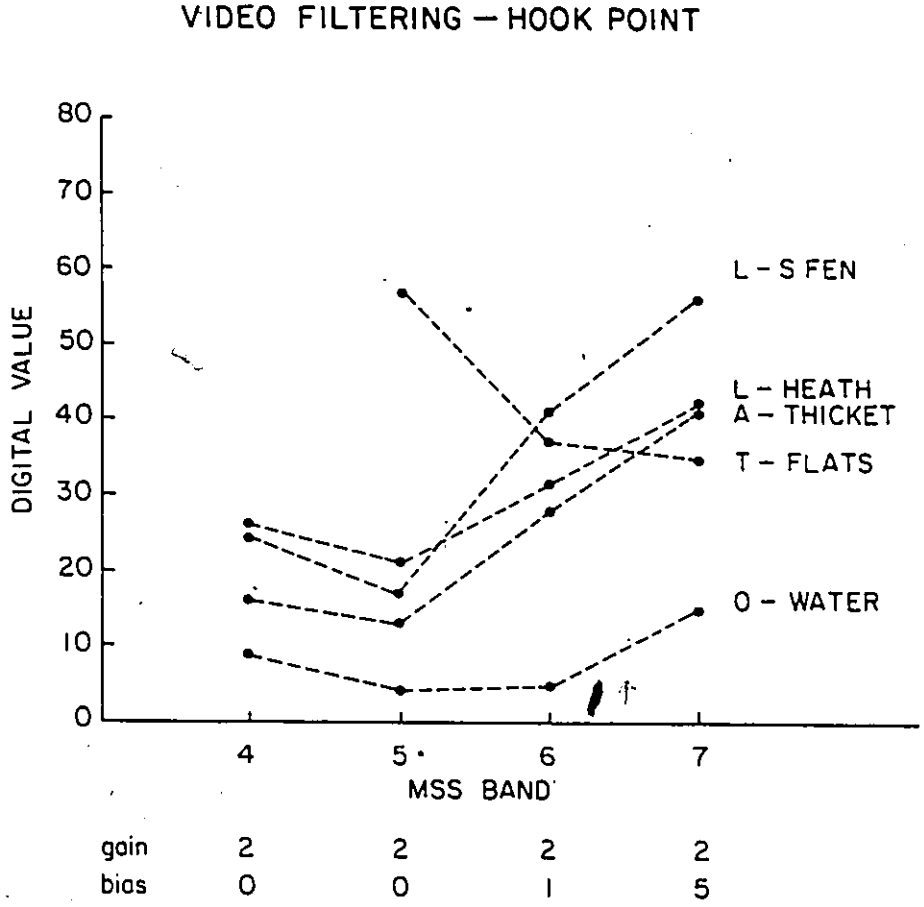

Figure 5.11 The plotted mean digital values for the video filtering enhancement (Hook Point-July subscene).

Figure 5.12 The video filtering enhancement for the July Hook Point subscene (3 pixel by 3 pixel filter at .5 strength).

dinates from within the 30 pixel by 50 pixel subscenes and they have been listed in Appendix B.6. Small samples were selected.

The results show that for 39 pairs, the probability that the two samples were drawn from the same population was less than .1. The lichen heath and alluvial thicket Band 7 samples were not from different populations at the .1 probability level.

The results were different from the results for the pre-enhanced Hook Point cover classes. For example, both the lichen heath and low shrub fen in Band 4, and the alluvial thicket and lichen heath in Band 7 were from significantly different populations with the enhancement. The results are explained with the enhancement formula. The enhanced digital values may be more representative of each class because the mean of a group of digital values from each class has been used in calculations of the new result. Conversely, the lichen heath class is not enhanced. The mean digital value is calculated from the alluvial thicket class, because the lichen heaths are small features surrounded by the alluvial thickets. The lichen heath enhanced values are closer to the alluvial thicket digital values in all bands, and especially in Band 7.

There is little difference between the pre-enhanced (Figure 5.6 top) and enhanced mean digital values. The

mean digital value was calculated from randomly selected pixels. The scene contrast was not increased with the gain and bias values selected because the available brightness values were sufficient to display all of the data. There were two major changes. First, the Band 7 alluvial thicket and lichen heath mean digital values were nearly equal, for reasons discussed above. Second, the enhanced tidal flat class mean digital value for Band 4 was not displayed because an error in the line print coordinates made it difficult to locate the tidal flat enhanced pixels.

The results of this investigation concur with previous studies. The enhancement has limited use. The author cannot detect increased contrast between classes or with linear features on the enhanced subscene in the visual display. The MSS radiometric calibration errors are not enhanced.

5.5 Application of the Result to the Churchill Subscene

The Churchill study site has several cover classes in common with the Hook Point site. Therefore, the Churchill site is a suitable area for which the results of the Hook Point investigation can be tested. The Churchill data will be analyzed using the same techniques.

For the Churchill study site, Band 7 16-tone video plots and line prints were used to identify cover class

pixels and their corresponding digital values. Plots of mean digital value were produced and appear throughout this section. Where appropriate, Kolmogorov-Smirnov two sample one-tailed tests have been used.

5.5.1 Atmospheric Corrections Applied

The raw and corrected subscenes for the Churchill study site are presented in Figure 5.13. A total of 37 open water class pixels have been identified (Appendix B.7). They have been used to find the mean digital values, graphically displayed in Figure 5.14. As can be seen, the corrected mean digital values are much lower than the uncorrected values. The solar elevation has been lowered to 50^{o}, but the low digital values are also explained by systematic errors in estimating the extinction coefficient (Ahern, pers. comm.). The systematic errors in Band 7 have been corrected. Compared to the Hook Point open water class data (Figure 5.6) the mean digital value differs slightly in Band 4, Band 5 and Band 7. The water pixels selected from the Churchill subscene are from small lakes that frequently fluctuate in water levels. Therefore, reflection from lake bottoms may influence the water albedos that may not have been a factor at the Hook Point study site.

The corrected subscenes appear more red than the raw subscenes because the Band 7 digital values are relatively

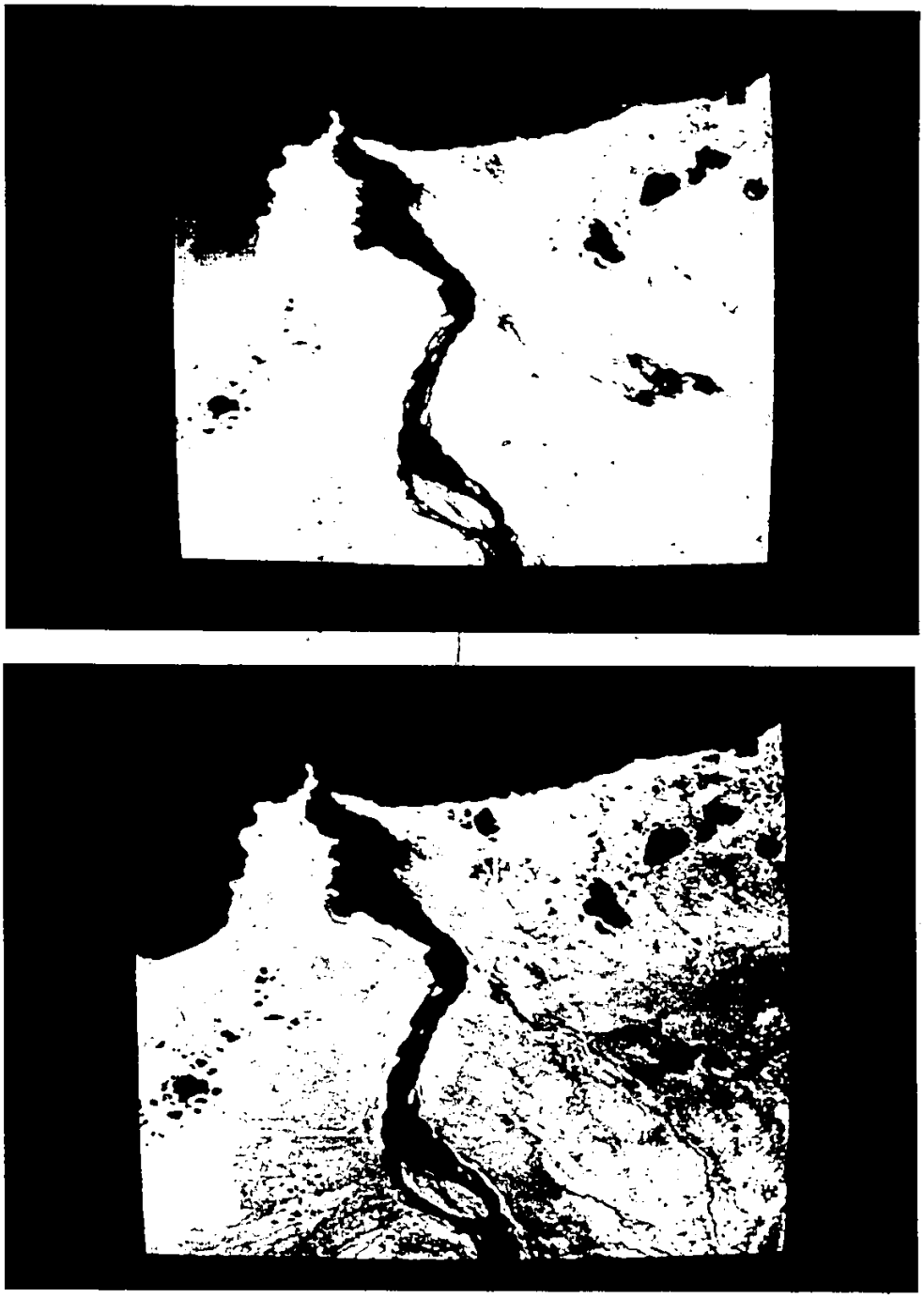

Figure 5.13 The Churchill study site raw (top) and corrected (bottom) subscenes. The corrected subscene appears clearer, as seen by the absence of haze over the delta of the Churchill River. The bare rock outcrop and urban settlement classes cannot be distinguished.

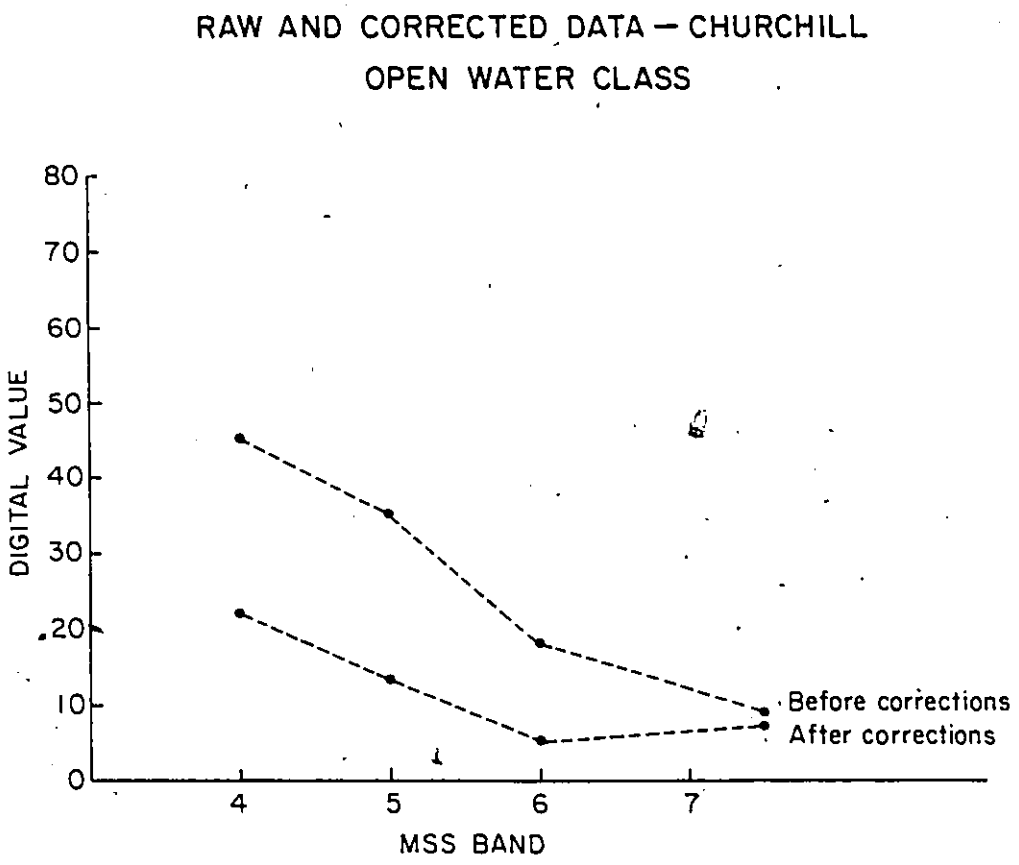

Figure 5.14 Raw and corrected Churchill subscene (open water class).

higher. As well, the corrected subscene is clearer than the raw subscene because much of the visible haze has been removed.

5.5.2 Surface Cover Class Data Analysis

The same assumptions in the analysis of the Hook Point cover classes were applied to the Churchill data with one exception. The urban settlement class has recently changed due to rapid depopulation. Several buildings present in the 1972 air photographs have been removed. As a result, it was necessary to select pixels from features that remained unchanged, such as airport runways.

The pixels were selected by the same method outlined in section 5.3.2. Cover class data were identified on the Band 7 16-tone video plot with the aid of field information and the Landsat corrected subscene. The corresponding digital value was extracted from the line prints. A total of 158 pixels were identified for the six classes (Appendix B.7).

A graphic plot of mean digital values for each cover class has been presented in Figure 5.15. Once again, there was greater infrared absorption by the open water class in contrast to the high infrared reflectance of vegetation. The rock outcrop and urban settlement classes had nearly equal mean digital values throughout.

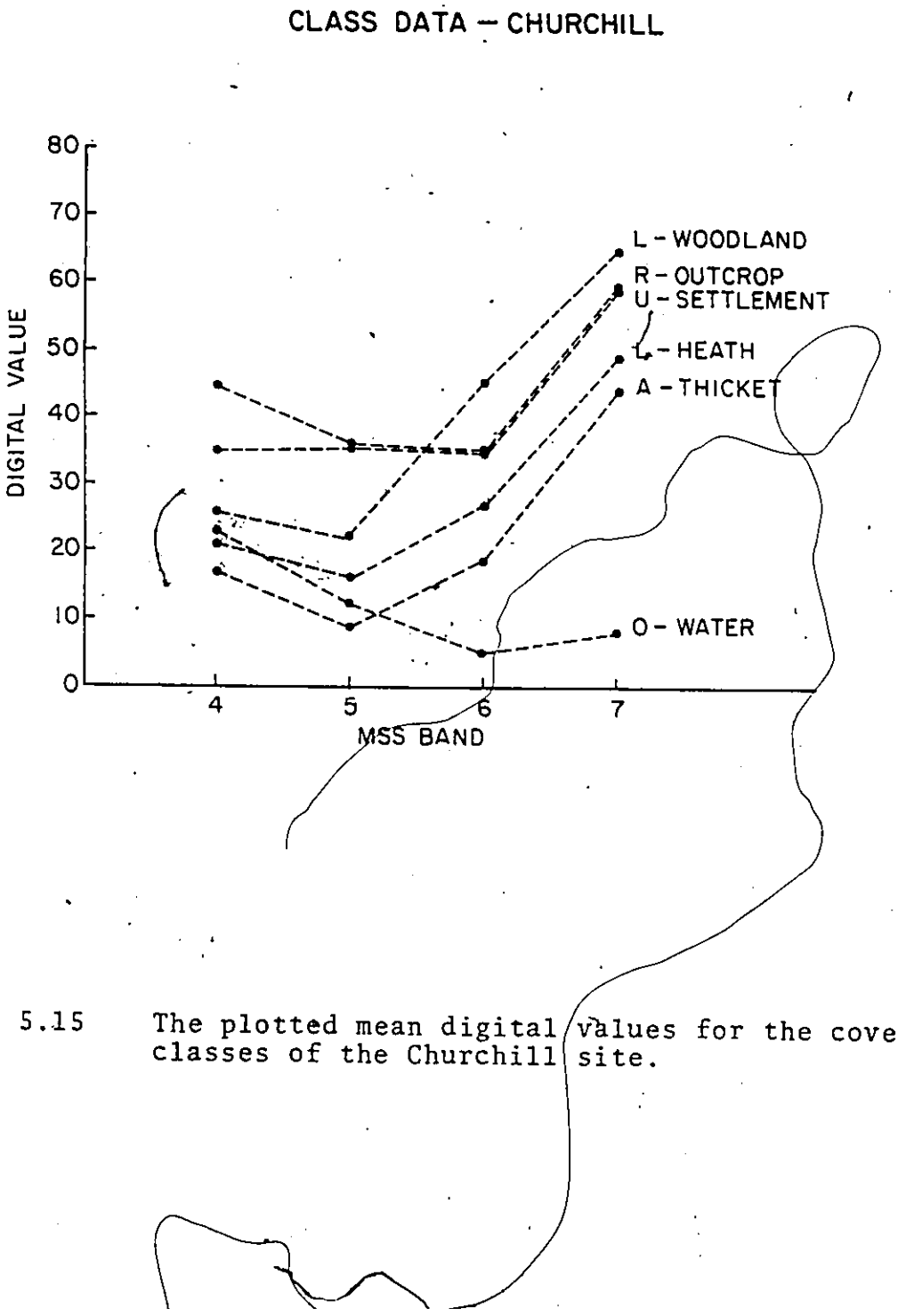

Figure 5.15 The plotted mean digital values for the cover classes of the Churchill site.

The digital values were tested using the Kolmogorov-Smirnov two sample one-tailed test. The tests were performed on class sample pairs within each band of corrected data. There were 15 possible paired combinations within each band for a total of 60 tests. The results show that for 55 pairs, the probability that each sample was drawn from the same population was less than .05. The MSS digital data is suitable for separating these cover classes.

The same conclusion was not reached for the rock outcrop and urban settlement classes. All four MSS bands had probabilities that class samples were drawn from the same population that exceeded the .1 criterion level. This was explained by a consideration of the classes themselves. Much of the exposed rock at Churchill has been quarried for the runways, roads and other services. Therefore, both classes were similar. The remaining pair was the open water and lichen heath Band 4 data for which the probability of being drawn from the same population also exceeded the .1 criterion level. An examination of the graphic plots (Figure 5.15) revealed that all Band 4 mean digital values had a narrow dynamic range. A reduction in contrast, due to attenuation in the atmosphere, probably accounts for the higher probability.

The alluvial thicket and lichen heath cover classes have slightly different MSS mean digital values compared to

the Hook Point mean digital values. Ground conditions were probably different for the dates and locations of Landsat data so that small differences were produced.

5.5.3 Evaluation of the Image Enhancements for the Churchill Subscene

(A) Linear Contrast Stretch Enhancement

The vegetation classes were emphasized in this enhancement. The stretch limits were selected on the basis of reflectance theory for vegetation. Band 7 was displayed in frequency histogram form, and the range of vegetation digital values noted. The gain was calculated as the total range of 255 digital values to the range of 64 for vegetation, and an offset of 8 digital values was used to maintain positive digital values. The enhancement is illustrated in Figure 5.16.

The same pixels selected for the previous section were used to calculate the mean digital value that is graphically displayed as Figure 5.17. As can be seen, different gain and bias values were selected for each band, and as a result, the mean digital values were stretched in each band. The lichen woodland appeared as shades of bright red because its high infrared reflectance produced high Band 7 digital values. The lichen heath ridges had lower Band 7 values so they appeared more blue and green. The open water class appeared blue and green because its Band 4 and Band 5 digi-

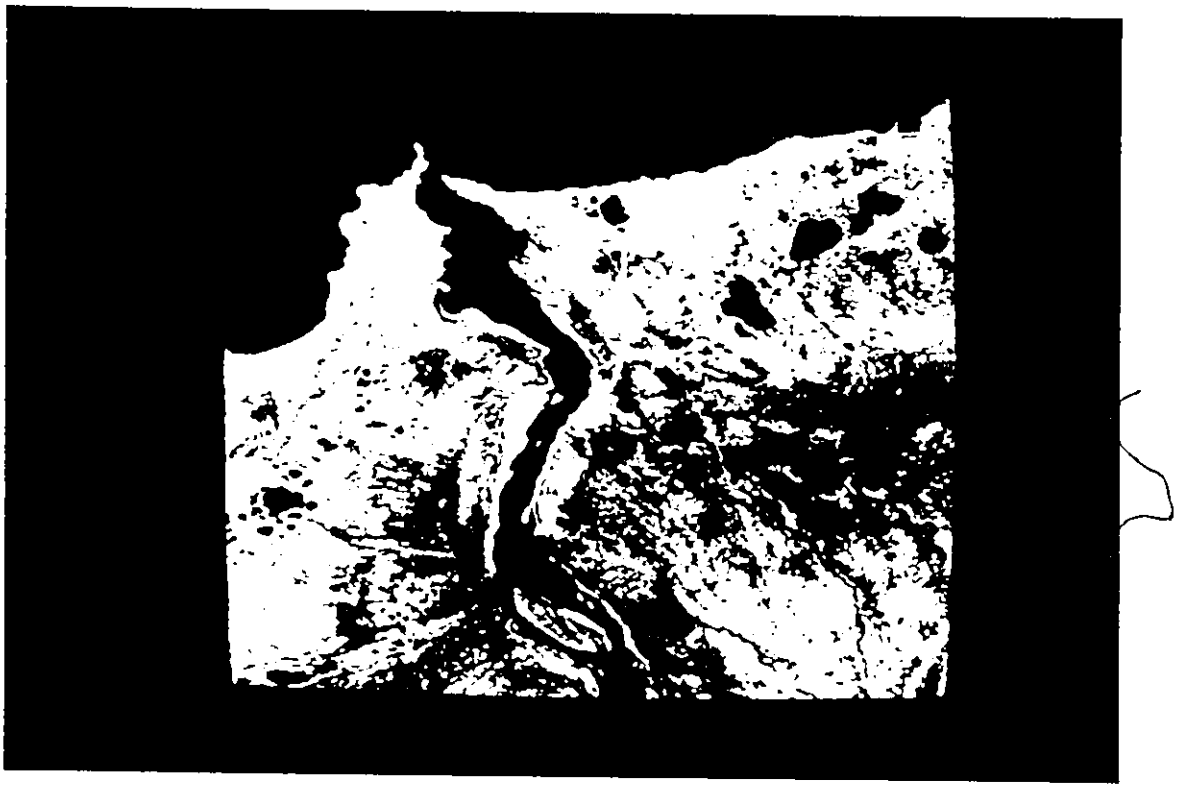

Figure 5.16 The linear contrast stretch enhancement of the Churchill site. The vegetation classes can be clearly distinguished, in contrast to the urban settlement and rock outcrop class.

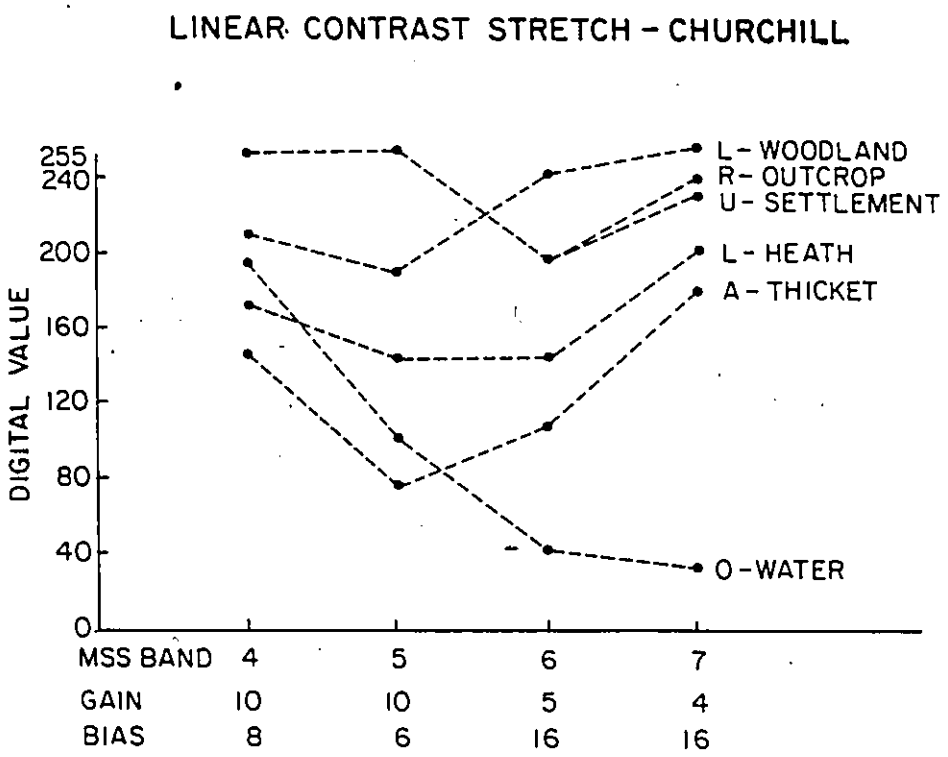

Figure 5.17 The plotted mean digital values of the linear contrast stretch of the Churchill cover classes.

tal values were high.

Because the rock outcrop and urban settlement classes had nearly equal values, they were poorly separated by this enhancement. For these classes, both the Band 4 and Band 5 digital values were truncated at 255.

The enhancement is, therefore, suitable for emphasizing vegetation. The same result has been determined for the Hook Point investigation. In agreement with the previous studies, the geologic materials which have similar albedos cannot be differentiated by this enhancement.

(B) Band Ratioing Enhancement

The band ratioing enhancement (Figure 5.18) was studied for the Band 4 to Band 7 ratio. Once again, the same cover class pixels were selected to calculate the mean digital value (Figure 5.19). The gain and bias were selected to best display the ratioed subscene data.

Fortunately, the gain and bias values selected for analysis were similar to the Hook Point enhancement. The Churchill 512 pixel by 512 pixel subscene had less contrast and hence, less dynamic range for the whole scene. As a result, a different gain and offset was needed so that the colour monitor could display the ratioed subscene.

The 10 possible combinations (without the open water class tuncated at the 255th digital level) of classes were tested using the Kolmogorov-Smirnov two sample one-tailed

Figure 5.18 The band ratioing enhancement of the Churchill site. The vegetation patterns can be distinguished on the image. The open water class appears white because its stretched value exceeded 255.

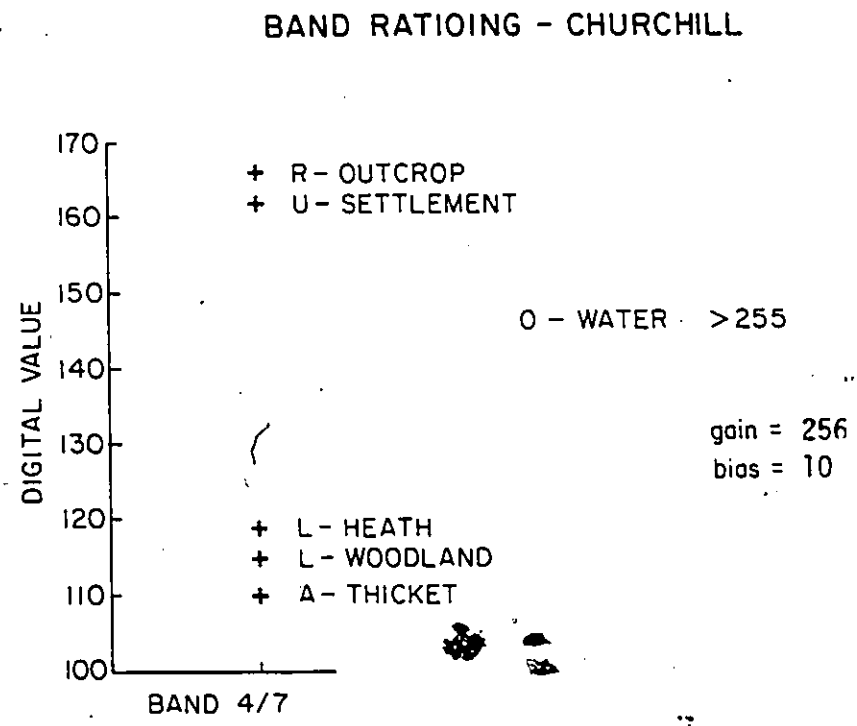

Figure 5.19 The mean digital values for the band ratioing enhancement of the Churchill cover class data.

test (Appendix B.8). For two pairs, the probability that samples of two classes were drawn from the same population exceeded the .1 criterion level. One pair was the rock outcrop and urban settlement classes. As previously described, the two classes cannot be separated because their MSS values were virtually equal. The lichen woodland and alluvial thicket classes also exceeded the critical level. Unique ratios were not produced for these classes. This contradicts the results for the Hook Point study. Therefore, unique ratios for vegetation, as Thomas (1979) has found, may not always exist.

The enhanced subscene appears clear and most of the surface cover can be mapped. As found with the Hook Point investigation, the radiometric errors are enhanced. They are displayed as horizontal stripes in the subscene.

(C) Video Filtering Enhancement

The video filtering enhancement was tested for the same size and strength of filter used in the Hook Point study. Once again, it was necessary to select 60 pixels randomly, using random number tables to select coordinates. The coordinates have been listed with the digital values in Appendix B.9.

The mean digital value has been derived from the random pixels and is graphically displayed in Figure 5.20. The gain and bias values were selected so that the dynamic

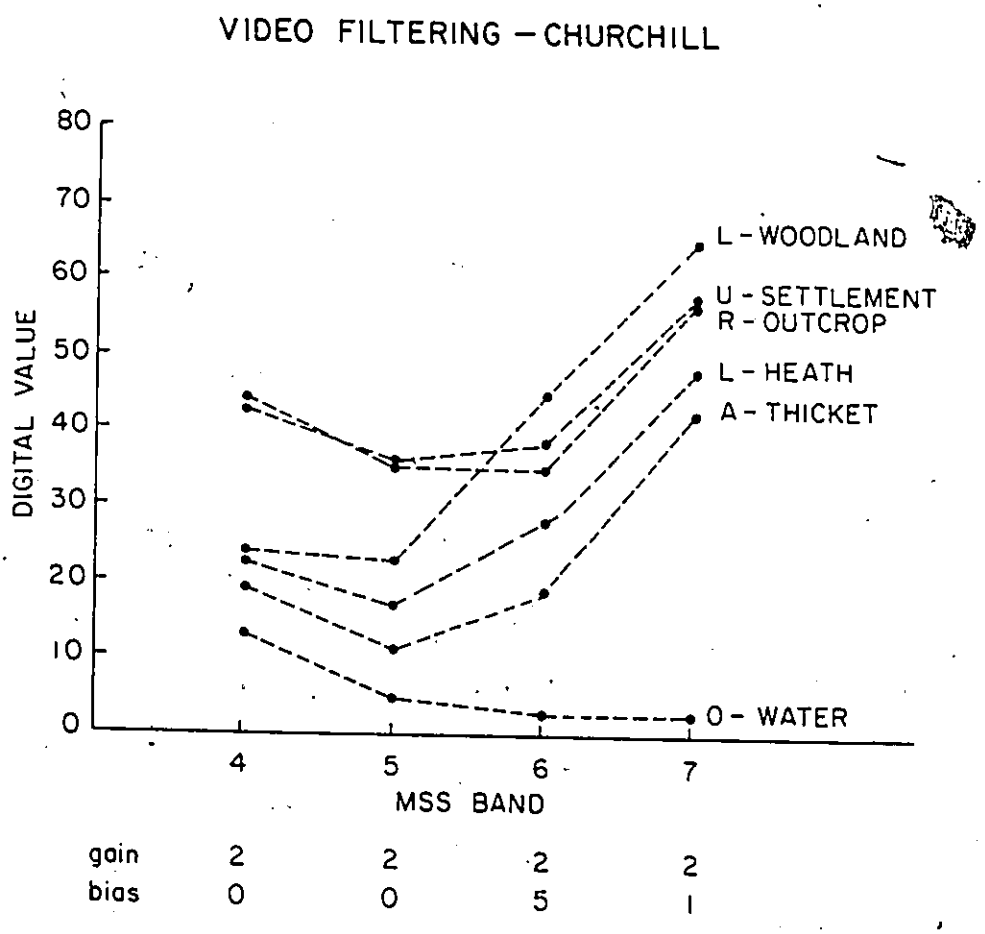

Figure 5.20 The plotted mean digital values for the video filtering enhancement of the Churchill cover classes. (3 pixel by 3 pixel at .5 strength).

range was not increased. The enhanced mean digital values are similar to the pre-enhanced digital values (Figure 5.15) except for two cases. First, the Band 7 open water class digital value is lower in the enhancement. Second, in all bands, the rock outcrop and urban settlement classes are slightly different in the enhancement.

A series of Kolmogorov-Smirnov two sample one-tailed tests were applied to each of the 15 possible combinations of classes within each band, for a total of 60 tests (Appendix B.9). For 59 tests, the probability that any pair was drawn from the same population did not exceed the .1 probability level. Only the Band 4 rock outcrop and urban settlement classes could have been drawn from the same population.

The results contradict the results of the pre-enhanced cover classes. The classes had probabilities of being drawn from the same population that exceeded the .1 criterion level. As described in the Hook Point investigation, the average of several pixels has been used in the enhancement. The rock outcrop and urban settlement classes are small surface cover features. Therefore, the enhancement averages other cover classes to derive the new value, so that the two classes become dissimilar. The enhancement may not be considered useful if precise detail is necessary.

Indeed, the video filtering enhancement appears

similar to the corrected (pre-enhanced) subscene (Figure 5.21). Radiometric errors were not enhanced. The cover classes do not appear clearer and they cannot be easily mapped.

5.6 Conclusions

The analysis and results of the application of corrections and enhancements to the Hook Point and Churchill subscenes have been presented in this chapter. The study has shown that atmospheric and solar corrections may not be enough to standardize Landsat data from different dates, but several factors have not been examined in this study. The images appeared clearer after corrections were applied. The cover classes were analyzed before and after enhancement and the linear contrast stretch and band ratioing enhancements were suitable for differentiating vegetation cover classes. Video filtering was not very effective.

Chapter 6 will discuss the implications and recommendations from this study and summarize the most important points.

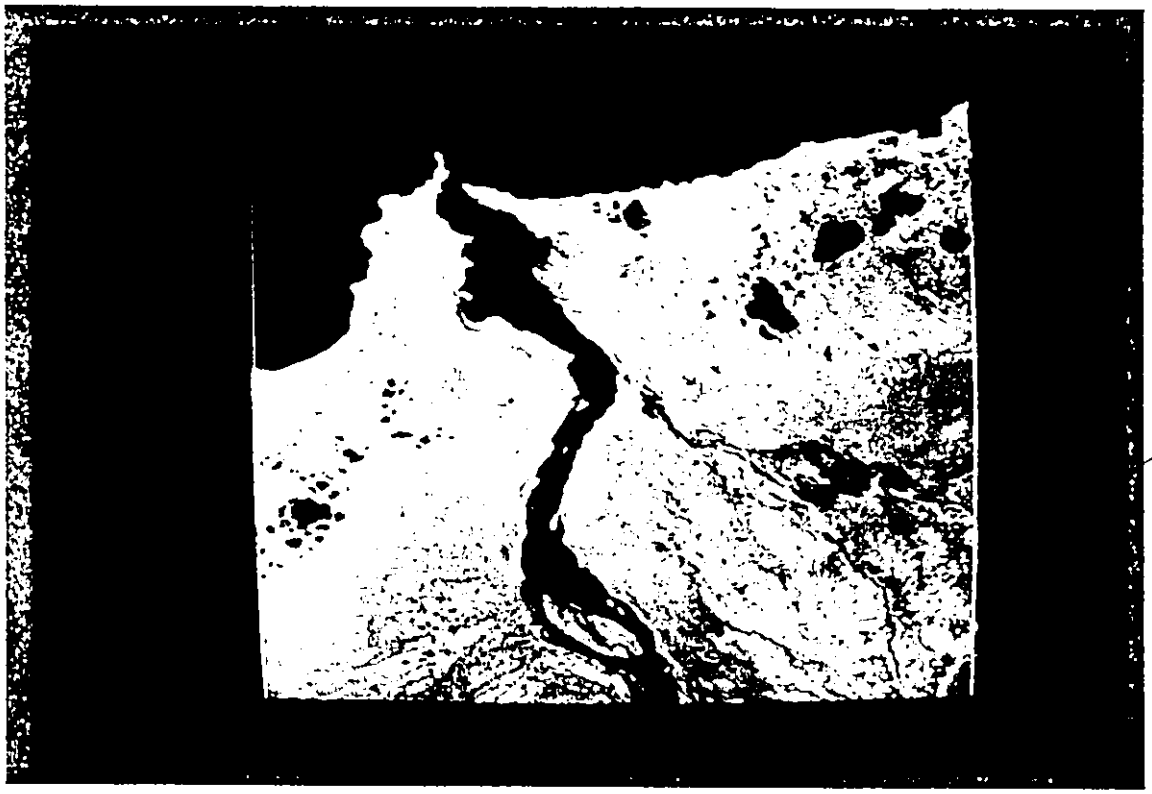

Figure 5.21 The video filtering enhancement for the Churchill study site. The level of detail is similar to the corrected subscene (Figure 5.13). The orange colour of the subscene is probably due to changes in colour monitor controls.

CHAPTER VI

CONCLUSIONS AND RECOMMENDATIONS

6.1 Conclusions

The effects of solar and atmospheric corrections, the linear contrast stretch, band ratioing and video filtering enhancements were examined for two study sites in northern Canada. For the first test site, the solar and atmospheric corrections did not standardize digital values between different dates of imagery, but the digital values were closer to equality after the corrections were applied. The linear contrast stretch and band ratioing enhancements were effective for emphasizing differences in vegetation, but the video filtering enhancement failed to do so. Similar results were found for the second test site.

Several conclusions may be derived from this study: (1) There are several limitations to the use of the Ahern solar and atmospheric corrections which partially account for the discrepancies with these corrections. First, the corrections assume Lambertian ground reflectance, but many ground targets probably reflect directionally. Second, the corrections are ineffective for cloud cover and non-homogenous atmospheres. Third, the corrections depend on input parameters that are inaccurately calculated.

In addition to the above, there are several untested sources of error which have affected the evaluation of these corrections. The assumptions about the use of clear water for comparison of digital values may be incorrect. Second, the clear water pixels may not represent only clear water. As well, factors such as unusually high sun glint may affect the digital value response. Finally, there is always sampling error, due to possible variations in the geometric corrections or geometric registration. Therefore, one cannot conclude that these corrections are ineffective.

(2) Although there are many sources of error, there are many advantages for the use of these corrections. In particular, they help standardize the data that have atmospheric effects present. They enhance the appearance of the visual display. Moreover, corrections by the Ahern method circumvent the use of field data. It can be applied to any Landsat scene where clear lakes are present. In classification, corrected data may then be separated into classes that represent ground variations and not ground plus atmospheric variations in radiance. For enhancements, the intrinsic radiance of the ground will be enhanced.

(3) Although the corrections described are necessary for all Landsat data, more corrections are needed for areas of variable relief. In these areas, the application of digital terrain models is a necessity.

(4) For the Hook Point study site, almost all the cover classes studied had unique albedos. Not all of the radiance values received by the MSS were unique because contrast is lost as a result of intervening effects in the atmosphere. The mean digital values and the radiometer measurements agree with established remote sensing literature about reflectance of green vegetation. It must be realized that the satellite and radiometer data have been obtained on different dates, and that the radiometer may not measure reflectance accurately. Furthermore, inclement weather prevented obtaining better measurments. Therefore, direct comparisons of satellite and radiometer data are questionable.

(5) In this study, the linear contrast stretch was effective for enhancing differences between vegetation. Some other data were stretched to the 255th digital value and, therefore, were not meaningfully displayed. The results differ from the geological studies described in Chapter II, which reported little success with this enhancement.

(6) The band ratioing enhancement emphasized the vegetation patterns described in this study because unique ratioed values were produced. For the Churchill study site, two classes with similar MSS digital values were not enhanced. The results support the geological studies described in the second chapter because unique ratioed values for exposed rock were not produced.

(7) The specific video filtering enhancement did not enhance the cover classes in this study. In a few cases, the enhancement was detrimental. The enhancement has a term which calculates the average of a number of pixels. However, for classes that are small in size, the average value may not be representative of the class itself. The results of this study supports the results of other studies described in the second chapter.

6.2 Recommendations

The scarcity of studies applying image corrections and enhancements to Landsat data indicates a need for more research. From this study, the following future research goals can be suggested:

(1) To investigate the use of a large and stable reflector which can be used to properly evaluate the Ahern solar and atmospheric corrections.

(2) To test other radiative transfer solutions on the Landsat data to determine if a more accurate result can be found other than the solution tested in this study.

(3) To determine what is the critical amount of relief for the use of digital terrain models in addition to the corrections described in this study.

(4) To examine the effects of the linear contrast stretch enhancement when different portions of MSS band data are

stretched, and to compare the results to this investigation.

(5) To test all of the different band ratios to determine their effects on the same cover classes described in this study. Alternatively, the same band ratio used in this study can be used to enhance cover classes from different environments.

(6) To study different video filter strengths and sizes on the same subscene so that its effectiveness can be more completely evaluated. Alternatively, the same size and strength of video filter used in this study can be used to enhance cover classes from different environments.

(7) To determine if a method can be developed that quantifies the colour monitor control variations and stabilizes the film reproduction techniques so that variability between each image is reduced.

GLOSSARY

16 Tone Video Plot	A map of grey tones for any MSS band. Each grey tone is 16 digital values.
Broadband	A range of frequencies or wavelengths in the electromagnetic spectrum that a detector is sensitive to.
Computer Compatible Tape (CCT)	A 1600 B.P.I. magnetic tape that contains a Landsat image and library information.
Colour Monitor	A colour picture tube that displays remote sensing data. It is a part of the image analysis system.
Digital Values	A range of unitless radiance levels on a scale of 0 to 256 or 0 to 64.
Line Prints	A document that contains the digital values for a portion of one MSS band.
Pixel	An image element that defines the apparent ground resolution of a remote sensing system.
Subscene	A portion of the scene or image contained on the CCT.

REFERENCES

Ahern, F. J. D. G. Goodenough, I. C. Jain, V. R. Rao and G. Rachon, 1977a. Use of clear lakes as standard reflectors for atmospheric measurements. Proc. 11th Int. Symp. Rem. Sens. Env. Ann Arbor, MI. pp. 731 -

_____, 1977b. Landsat atmospheric corrections at CCRS. Proc. 3rd Can. Sym. Rem. Sens. Edmonton, Abta. pp. 583 - 595.

Ahern, F. J. and J. Murphy, 1978. Radiometric Calibration and Correction of Landsat 1, 2 and 3 MSS Data. Research Rpt. 78-4. Canada Centre for Remote Sensing, Ottawa, Ont., 23 pp.

Ahern, F. J., P. M. Teillet and D. G. Goodenough, 1979. Transformation of atmospheric and solar illumination conditions on the CCRS image analysis system. Proc. 5th Mach. Process. Rem. Sens. Data Symp., Layfayette, ID, pp. 34 - 52.

Anon., 1974. Erts 100A Radiometer. Exotech. Inc. Gaithersburg, MD. 18 pp.

_____, 1977. Polar Bear Provincial Park Background Information Report. Ontario Ministry of Natural Resources. Toronto. 54 pp.

_____, 1978. Computer Image Processing - Geologic Applications. Research Rpt. 78 - 34. National Aeronautics and Space Administration Jet Propulsion Laboratory. Pasadena, CA. 29 pp.

Chavez, P. S. Jr., G. L. Berlin and W. B. Mitchell, 1977. Computer enhancement techniques of Landsat MSS digital images for land use/land cover assessments. Proc. 6th Ann. Conf. Rem. Sens. Earth Res. Tullahoma, TN. pp. 259 - 276.

Conover, W. J., 1971. Practical Nonparametric Statistics. John Wiley and Sons Inc., Toronto, Ont. 462 pp.

Cowell, F. N., 1968. Polar Bear Provincial Park Investigational Survey. Ontario Department of Lands and Forests. Toronto. 37 pp.

Goodenough, D. G., 1979. The image analysis system (CIAS) at the Canada Centre for Remote Sensing. Can. Jour. Rem. Sens. 5:3-17.

Howarth, P. J., 1976. An Evaluation of Landsat Imagery for Land Classification on Eastern Melville Island, N.W.T. Canada. Environment Canada. Ottawa, Ont. 158 pp.

Hummel, R., 1977. Image enhancement by histogram transformation. Computer Graphics and Image Processing. 6: 184-195.

Kalensky, Z. and D. A. Wilson, 1975. Spectral signatures of forest trees. Proc. 3rd Can. Symp. Rem. Sens. Quebec City, Que. pp. 151 - 171.

Lockwood, H. E., 1975. Photographic image enhancement and processing. Proc. 5th Wkshop. Colour Aerial Photog. Souix Falls, SD. pp. 24-43.

Lucas, J. R., J. V. Taranik and F. C. Billingsley, 1977. Land Classification of South-Central Iowa from Computer Enhanced Images. Contract Rpt. Iowa Geological Survey Remote Sensing Lab. Des Mones, 10. 228 pp.

Marrs, R. W., 1975. Preliminary Analysis of the Beaver Creek and Ninemile Hills Areas, Wind River Basin, Wyoming using Image Ratios and Thematic Classification. Special Rpt. University of Wyoming Remote Sensing Laboratory. Laramie, WY. 28 pp.

Merifield, P. M., D. L. Lamar and J. V. Lamar, 1976. Analysis of S-192 Imagery of the Western Mojave Desert, California. Tech. Rept. 76 - 1. California Earth Science Corp. Santa Monica, CA. 22 pp.

Myers, V. I., K. J. Dalsted, R. G. Best, J. R. Smith, J. C. Eidershink, F. A. Schner, A. S. Andrarvis and P. H. Rahn, 1977. Application of Remote Sensing in South Dakota to Provide Accurate Assessment of Agricultural Crops, Enhance Contrast in Photographic Products, Monitor Rangeland Habitat Loss, Map Aspen and Prepare Hydrologic Surveys. Ann. Progress Rpt. Remote Sensing Institute of South Dakota. Brookings, S.D. 99 pp.

Neal, M. W. and K. A. Kershaw, 1973. Studies on lichen dominated systems. III. Phytosociology of a raised beach system near Cape Henrietta Maria, Ontario. Can. Jour. Bot. 55: 1115-1125.

O'Neill, N. T., 1977. Radiative Transfer Modelling Applied

to Ground-Based and Satellite Optical Data. York University Centre for Research in Experimental Space Science. Toronto, Ont. 115 pp.

O'Neill, N. T., J. R. Miller and F. J. Ahern, 1978. Radiative transfer calculations for remote sensing applications. Proc. 5th Can. Symp. Rem. Sens. Victoria, B.C., pp. 572 - 578.

Rao, V. R., E. J. Brack and A. R. Mack, 1978. Crop discrimination in the visible and near infrared regions. Photo. Eng. Rem. Sens., 44:1179-1184.

Ritchie, J. C., 1957. The vegetation of northern Manitoba. II. A prisiere on the Hudson Bay Lowlands. Ecology. 38: 429-435.

Ritchie, J. C., 1960. The vegetation of northern Manitoba. V. Establishing the Major Zonation. Arctic, 13:210-219.

Rowan, L. C., A. F. H. Goetz and R. P. Ashley, 1977. Discrimination of hydrothermally altered and unaltered rocks in visible and near infrared multispectral images. Geophysics. 42: 522-535.

Rowan, L. C., P. H. Wetlanfer, A. F. H. Goetz, F. C. Billingsley and J. H. Stewart, 1979. Discrimination of Rock Types and Detection of Hydro-thermally Altered Areas in South-Central Nevada by the Use of Computer - Enhanced ERTS Images. Professional Paper 883. United States Geological Survey. Reston, VA. 41 pp.

Santisteban, A., 1976. The band ratioing technique applied to Landsat MSS images. Thematic Mapping, Land Use, Geological Structures and Water Resources in Central Spain. Inst. Geogradico Y. Catastral. Madrid, Spain. pp. 109-126.

Schwartz, A. A., 1976. New techniques for digital image enhancement. Proc. Caltech. Jet. Prop. Lab. Conf. Image Process. Tech. Pasadena, CA. pp. 2.1-2.12.

Sheffield, C., 1976. Digital Enhancement and analysis techniques in processing of earth resources data. Earth Observation Systems for Management and Environment Control. Plenum Press Inc., Washington, D. C. pp. 379-401.

Simpson, C. J., 1978. Landsat: developing techniques and applications in mineral and petroleum exploration. BMR Jour. of Austr. Geol. Geophys. 3: 181-191.

Smith. A. F. and R. N. Baker, 1975. Application of digitally enhanced Landsat data for geological mapping and analysis in southwestern Arizona. Wkshop. Env. Appl. Multispectral Imagery. Fort Belvoir, VA. pp. 48-71.

Soha, J. M., A. R. Gillespie, M. J. Abrams and D. P. Madina, 1976. Computer techniques for geological applications. Proc. Caltech. Jet. Prop. Lab. Conf. Image Process. Pasadena, CA. pp. 4.1-4.21.

Strome, W. M., S. S. Vishnubhatla and F. E. Guertin, 1975. Format Specifications for Canadian Landsat MSS System Corrected Computer Compatible Tape. Research Rpt. 75-3. Canada Centre for Remote Sensing, Ottawa, Ont. 64 pp.

Taranik, J. V., 1968. Principles of Computer Processing of Landsat Data for Geologic Applications. Open File Rpt. 78-117. United States Geological Survey. Souix Falls, S.D. 56 pp.

Taylor, M. M., 1978. Guide to Landsat Image Enhancement Programs on the CCRS Decsystem - 10/MAD Display. Tech. Rpt. 78-X-22. Defence and Civil Institute of Environmental Medicine. Toronto, Ont. 58 pp.

Thomas, I. L., 1979. Mapping New Zealand's moisture rich soils from Landsat. Proc. 13th Int. Symp. Rem. Sens. Env. Ann Arbor, MI. (In press).

Todd, W. J., 1977. Urban and regional land use change by using Landsat data. Jour. Research United States Geol. Sur. 5:529-534.

Tucker, C. J., 1978. A comparison of satellite sensor bands for vegetation monitoring. Photo. Eng. Rem. Sens. 44: 1369-1380.

Turner, R. E., W. A. Malila and R. F. Nalepka, 1971. Importance of atmospheric scattering in remote sensing. Proc. 7th Int. Symp. Rem. Sens. Env. Ann Arbor, MI., pp. 1651-1697.

Turner, R. E. and M. M. Spencer, 1972. Atmospheric model

for correction of spacecraft data. Proc. 8th Int. Symp. Rem. Sens. Env. Ann Arbor, MI. pp. 895-934.

Turner, R. M., 1973. Dynamics of Distribution and Density of Phreatophytes and other Arid-Land Plant Communities. Contract Rpt. 136096. United States Geological Survey. Washington, D. C., 22 pp.

Vanderbrug, G. J., 1977. Iterative enhancement of linear features. Computer Graphics and Image Processing, 6: 25-42.

Vincent, R. K., 1977. Geochemical mapping by spectral ratioing methods. Remote Sensing Applications for Mineral Exploration. Geospectra Corp. Washington, D. C. pp. 181-198.

Vishnubhatla, S. S., 1977. Radiometric Correction of Landsat I and Landsat II MSS Data. Tech. Rpt. 77-1, Canada Centre for Remote Sensing. Ottawa, Ont. 10 pp.

Vlcek, J., 1974. Difficulties in determining meaningful spectral signatures of forest tree canopies. ISP Commission VII Proc.: Symp. on Rem. Sens. and Photog. Interp. Banff, Abta. pp. 805 - 810.

Wallis, R., 1976. An approach to the space variant restoration and enhancement of images. Proc. Image Sci. Math. Symp. Sunnyvale, CA. pp. 107-111.

Webber, P. J., J. W. Richardson and J. T. Andrews, 1970. Post-glacial uplift and substrate age at Cape Henrietta-Maria, Southwestern Hudson Bay, Canada. Can. Jour. Earth Sci. 7: 317-325.

APPENDIX A

SPECIFICATIONS OF THE ERTS 100 RADIOMETER

(from Anon., 1974)

SPECTRAL BANDS – Four channels reproducing the ERTS MSS bandpasses (0.5 to 0.6 microns; 0.6 to 0.7 microns; 0.7 to 0.8 microns; and 0.8 to 1.1 microns). Glass absorption filters are used to correct the silicon detectors to simulate the ERTS photomultiplier response curves. Thin film filters procured to ERTS specifications are then added to precisely reproduce the ERTS bandpasses.

FIELD OF VIEW – Three modes of operation:

(1) 15 degree circular field of view for near terrain measurements;
(2) 1 degree square field of view to observe the 260 foot square resolution element of ERTS from aircraft altitude
(3) 2π steradian field of view for measuring downwelling (incident) radiation.

CALIBRATION ACCURACY – Calibrated using precision light sources and reflectance standards. An absolute accuracy of plus/minus 5% is maintained over the entire operational environmental range. Recalibration will not be required for periods of one year or more under typical use conditions.

OUTPUTS – Four independent low impedance (1000 ohm), high level (5 volts full scale) outputs. Case isolation provided. May be shorted to ground or each other without damage to instrument. Electrical bandpass of 0-80 Hz ensures high data rate capability with low noise operation.

CONTROLS – 1) Six position switch ("OFF", each of the four channels and "Battery Check" for display on the instrument meter)

2) Four separate selector switches - one for each channel for Gain X1, X5, X25 and X125.

SIGHT – Precision 1.5 power, erect image scope. Still and movie photography of the target area can be accomplished through this sight.

APPENDIX B

SUMMARY OF KOLMOGOROV-SMIRNOV TESTS

The results of the Kolmogorov-Smirnov two sample one-tailed tests are summarized in this appendix. There are nine groups of tests for each analysis in Chapter V. Three tables are presented for each group. They are:

I. CCT Pixel Digital Values. The coordinates for each pixel (n) are listed as columns x and y. Coordinate x is the horizontal coordinate and y is the vertical coordinate. Coordinates are listed for the Hook Point open water raw data table, the Hook Point and Churchill cover class tables, and the Hook Point and Churchill video filtering tables. No coordinates are given for the radiometer data. The corresponding digital values are listed in columns 4, 5, 6 and 7 for Band 4, Band 5, Band 6 and Band 7 MSS data respectively.

II. Digital Value Histograms. The CCT digital values are plotted in frequency histogram form, with frequency on the vertical axis and digital value on the horizontal axis. The band that each histogram represents is given at the bottom of each column of histograms and the cover class or data date that each histogram represents is given at the

left side of each row of histograms. Each histogram is labelled with an upper case letter.

III. Kolmogorov-Smirnov Summaries. The paired tests between the data are listed in a column with each pair tested indicated by two frequency histogram labels. The calculated D-MAX value appears in the second column. the test value (X^2) for large samples (from Conover (1971)) or the .1 significance level probability for small samples (from Conover (1971)) is also listed. The paired tests results are listed in the final column. Recall that the null hypothesis is that the two samples under investigation are not from different populations. Therefore, the tabular results are expressed as the probability that these two samples are drawn from the same population.

Appendix B.1

OPEN WATER RAW DATA-HOOK POINT

	June						July						Sept.					
n	x	y	4	5	6	7	x	y	4	5	6	7	x	y	4	5	6	7
1	1895	1415	32	24	13	5	1009	1245	41	27	25	6	1654	2243	29	18	8	1
2	1896	1416	34	25	15	5	1010	1245	42	29	25	6	1655	2243	29	20	10	1
3	1896	1416	34	25	17	5	1010	1246	43	31	26	6	1655	2244	29	21	10	1
4	1781	1065	35	26	17	5	895	1175	44	31	27	6	1540	2173	31	21	10	1
5	1781	1346	35	26	17	5	895	1176	45	32	28	7	1540	2174	35	22	13	1
6	1782	1346	36	26	18	5	896	1176	45	32	28	7	1541	2174	31	22	13	2
7	1782	1348	36	27	18	5	896	1178	45	32	28	7	1541	2176	31	22	13	2
8	1783	1348	36	27	18	5	897	1178	46	34	26	7	1542	2176	31	22	13	2
9	1784	1347	37	27	19	6	898	1177	46	34	26	8	1543	2175	31	22	13	2
10	1784	1348	37	27	19	6	898	1178	47	35	27	8	1543	2176	31	22	13	2
11	1785	1349	37	27	19	6	899	1179	47	36	27	8	1544	2177	31	23	11	2
12	1776	1349	38	28	19	6	890	1179	48	36	27	9	1535	2177	31	23	11	2
13	1777	1359	39	28	19	6	891	1180	49	35	29	9	1536	2178	31	24	10	3
14	1777	1351	38	29	20	7	892	1181	49	37	31	10	1537	2179	31	24	17	3
15	1817	1432	37	29	20	7	931	1262	51	38	30	10	1576	2260	31	24	15	3
16	1818	1432	37	30	21	7	932	1262	48	39	30	10	1577	2260	31	24	15	3
17	1818	1433	39	30	22	7	932	1263	47	35	30	11	1577	2261	33	23	14	3
18	1819	1432	38	30	23	7	933	1263	48	34	29	11	1578	2261	33	23	16	3
19	1819	1434	37	29	23	7	933	1264	46	33	28	9	1578	2262	33	23	16	3
20	1819	1435	37	29	25	7	933	1265	46	33	27	9	1578	2263	33	23	14	3
21	1820	1434	33	25	22	6	934	1264	45	33	26	9	1579	2262	32	23	14	2
22	1820	1435	33	26	21	6	934	1265	44	33	25	8	1579	2263	32	22	13	2
23	1821	1435	35	26	21	6	935	1265	44	33	26	8	1580	2263	32	22	13	2
24	1821	1436	35	26	18	6	935	1266	44	33	26	8	1580	2264	32	22	13	2
25	1854	1453	35	26	17	6	968	1283	45	32	25	8	1613	2281	32	21	13	1
26	1855	1454	35	27	16	6	969	1284	43	31	23	8	1614	2282	34	25	13	3
27	1856	1454	34	27	15	6	970	1284	42	30	28	7	1615	2282	34	25	13	3
28	1856	1455	34	27	14	5	970	1285	41	30	28	7	1615	2283	34	26	14	1
29	1857	1455	35	27	19	7	971	1285	40	30	28	6	1616	2283	28	21	8	3
30	1857	1456	35	27	19	7	971	1286	42	32	26	7	1616	2284	27	21	8	3
31	1857	1457	36	28	19	5	971	1287	43	32	27	7	1616	2285	29	21	9	2
32	1857	1470	36	28	19	6	971	1300	43	32	27	8	1616	2298	28	21	9	1
33	1858	1457	36	28	19	6	972	1287	43	28	27	8	1617	2285	30	20	6	1
34	1858	1458	36	28	19	6	972	1288	45	33	29	9	1617	2286	30	20	11	1
35	1858	1470	36	28	24	7	972	1300	45	33	29	9	1617	2298	30	19	9	1
36	1859	1459	36	28	24	7	973	1289	46	33	29	10	1618	2287	30	24	11	2
37	1859	1490	35	27	22	5	973	1290	46	33	30	10	1618	2289	30	23	11	2
38	1859	1499	37	27	21	7	973	1299	46	34	24	10	1618	2297	30	20	12	2
39	1878	1473	38	29	20	5	992	1303	44	34	24	8	1637	2301	30	19	7	1
40	1878	1474	36	29	20	5	992	1304	47	34	24	9	1637	2302	33	22	16	1
41	1879	1474	36	28	18	7	993	1304	48	34	24	9	1638	2302	33	23	15	2
42	1879	1412	37	26	17	6	993	1305	50	35	24	8	1638	2303	34	26	14	3

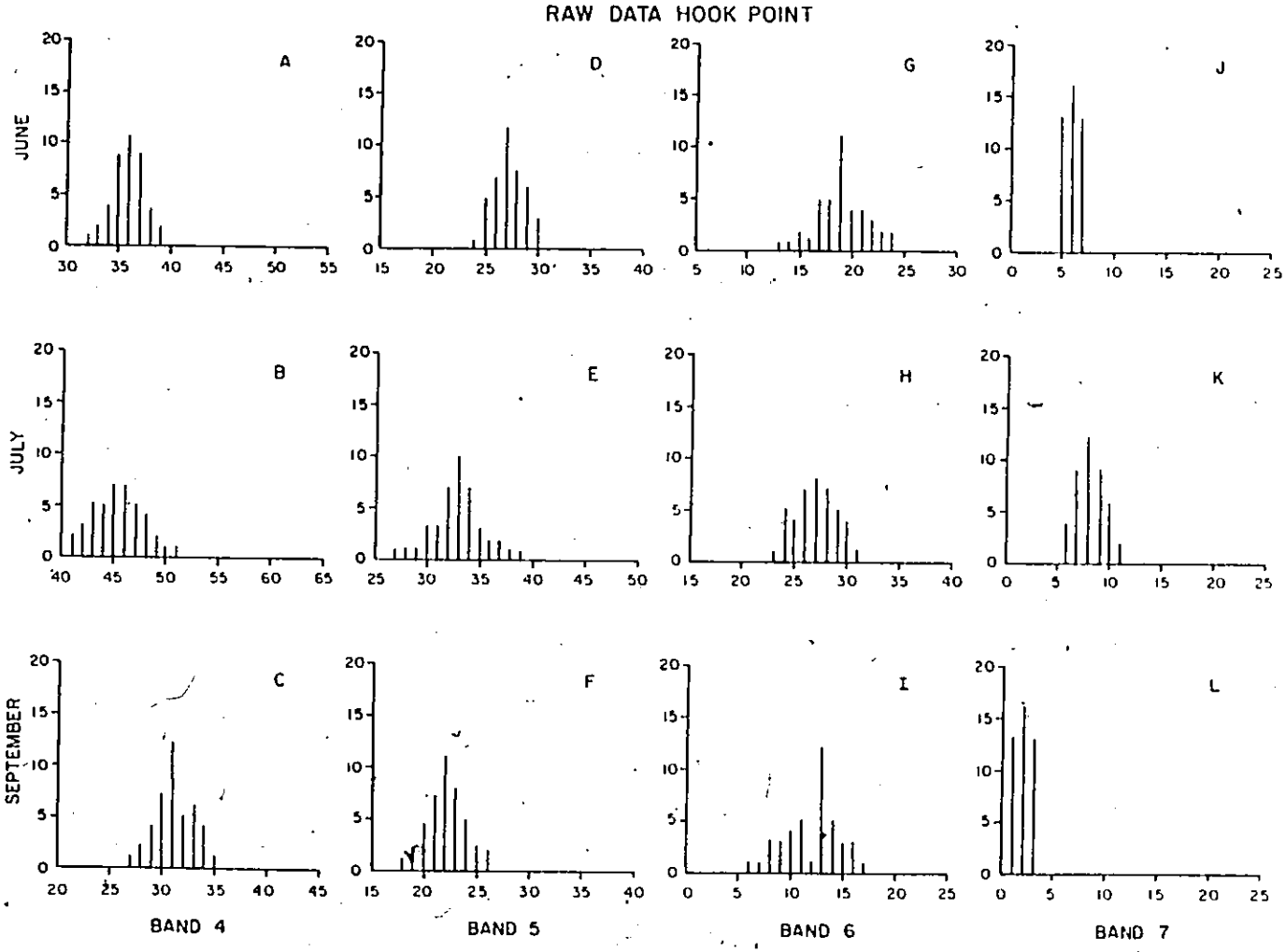
RAW DATA HOOK POINT
JUNE
JULY
SEPTEMBER
A
B
C
D
E
F
G
H
I
J
K
L
BAND 4
BAND 5
BAND 6
BAND 7

OPEN WATER RAW DATA-HOOK POINT

PAIR	D-MAX	X^2	Pr*
A - B	1	84	
B - C	.83	58	
A - C	1	84	
D - E	.86	62	
E - F	.88	65	
D - F	1	84	
G - H	.90	69	
H - I	1	84	
G - I	.83	58	
J - K	.69	40	
K - L	1	84	
J - L	1	84	

* Probability of both samples drawn from same population: shown only where Pr > .001.

Appendix B.2
OPEN WATER CORRECTED DATA-HOOK POINT

	JUNE				JULY				SEPTEMBER			
n	4	5	6	7	4	5	6	7	4	5	6	7
1	2	1	4	9	5	1	1	11	2	2	5	7
2	4	2	5	12	7	1	2	10	3	2	6	6
3	4	3	5	12	8	2	2	11	4	3	7	9
4	5	3	5	13	9	2	3	12	4	4	8	9
5	5	4	17	15	3	3	2	13	4	3	9	10
6	6	4	6	15	2	3	3	13	5	4	9	10
7	6	4	8	12	6	3	3	14	5	4	10	11
8	7	5	8	15	10	4	5	15	5	6	8	11
9	10	5	12	18	12	5	7	15	12	9	8	11
10	3	6	9	15	11	4	5	19	11	7	11	13
11	4	6	9	16	13	5	7	15	11	5	10	14
12	5	1	2	14	15	7	7	15	9	8	13	14
13	5	1	3	14	16	6	8	18	8	6	12	15
14	6	2	7	14	15	7	9	18	8	6	13	16
15	6	2	7	14	14	7	9	18	8	6	13	17
16	8	7	9	7	13	5	7	19	6	5	12	16
17	9	7	9	17	12	5	9	19	6	5	10	13
18	3	4	6	14	6	3	4	15	6	5	10	13
19	4	6	10	12	6	3	4	15	6	7	12	16
20	5	6	9	17	7	2	5	17	6	7	12	16
21	7	9	10	18	8	3	5	19	7	6	11	14
22	7	7	7	14	9	4	8	14	7	6	11	12
23	8	8	10	14	9	4	5	21	7	6	11	12
24	3	3	11	13	10	4	6	15	3	6	13	14
25	5	6	9	16	11	5	6	15	4	1	6	15
26	9	9	11	19	9	4	6	14	5	4	14	17
27	8	7	7	13	10	5	7	14	8	9	15	18
28	7	8	11	19	11	5	8	16	8	8	14	17
29	7	8	12	20	12	5	8	16	9	9	17	18
30	1	2	8	13	13	3	10	14	10	9	17	13
31	2	2	7	15	5	4	5	16	10	10	18	19
32	3	3	7	15	12	6	8	16	9	10	18	20
33	4	5	8	13	12	8	10	14	5	6	16	15
34	4	5	8	16	11	5	6	16	5	4	15	13
35	4	5	8	16	14	9	11	16	6	7	15	12
36	4	3	13	20	9	3	6	17	7	7	16	15
37	5	4	6	8	8	3	6	17	7	8	16	14
38	5	4	6	11	9	6	7	20	6	8	19	13
39	6	4	6	11	10	9	6	17	7	5	15	12
40	6	5	5	11	8	4	4	13	7	5	14	9
41	5	4	5	10	7	2	2	12	6	7	9	8
42	5	3	4	10	9	4	4	13	5	3	7	5

(same coordinates as Open Water Raw Data-Hook Point)

CORRECTED DATA-HOOK POINT

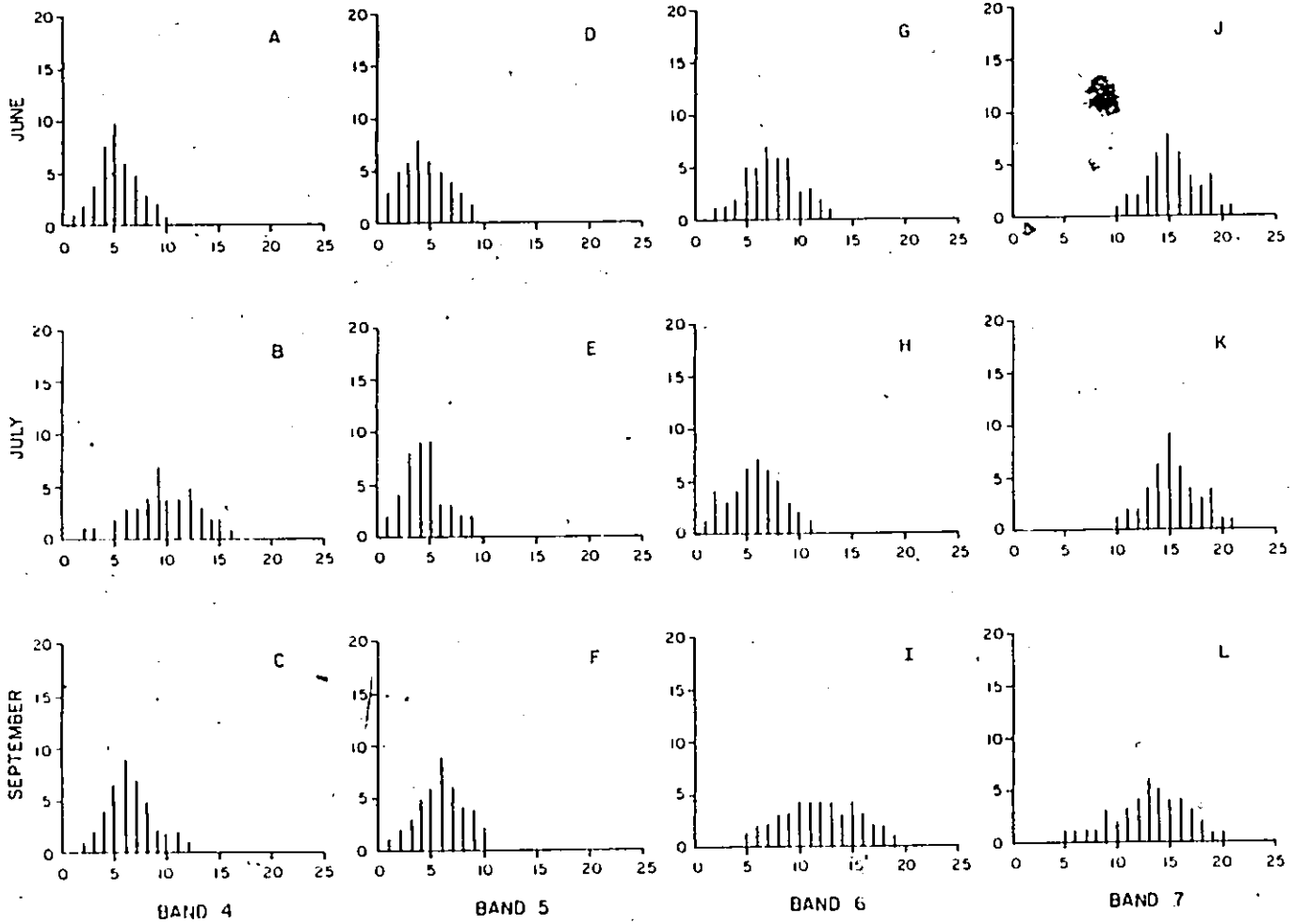

OPEN WATER CORRECTED DATA-HOOK POINT

PAIR	D-MAX	X^2	Pr*
A - B	.62	32.0	
B - C	.48	19.0	
A - C	.26	5.8	
D - E	.10	.76	.1 to .2
E - F	.36	11.0	
D - F	.26	5.8	
G - H	.26	5.8	
H - I	.67	37.0	
G - I	.53	23.0	
J - K	0	0	1.
K - L	.31	8.0	
J - L	.31	8.0	

* Probability of both samples drawn from same population shown only where Pr > .05.

Appendix B.3

COVER CLASSES-HOOK POINT

	A-THICKET						L-HEATH						T-FLATS						L-S FEN					
n	X	Y	4	5	6	7	X	Y	4	5	6	7	X	Y	4	5	6	7	X	Y	4	5	6	7
1	801	1202	10	5	21	34	898	1202	23	18	32	38	1084	1307	121	51	32	29	976	1253	25	16	39	55
2	802	1202	12	8	22	42	898	1203	25	20	35	39	1084	1308	123	52	38	31	977	1254	27	17	40	54
3	802	1203	11	6	21	35	899	1204	25	20	35	39	1084	1309	138	59	35	32	978	1255	26	16	39	56
4	803	1203	13	7	23	42	899	1204	25	21	34	40	1084	1310	136	59	37	34	978	1256	28	18	43	57
5	803	1204	15	9	24	42	899	1205	27	23	34	40	1084	1311	135	58	36	35	980	1260	27	17	40	58
6	804	1202	15	10	30	42	900	1206	27	23	37	41	1085	1307	134	58	33	33	985	1261	26	18	41	56
7	805	1203	15	10	24	43	910	1220	28	23	37	42	1085	1308	129	56	36	35	985	1262	26	18	42	58
8	900	1204	16	11	30	44	911	1221	29	22	36	42	1085	1309	129	56	36	35	990	1249	29	19	40	57
9	901	1205	17	12	30	41	912	1222	26	21	35	41	1085	1310	129	56	36	32	991	1250	27	17	42	56
10	902	1204	17	13	30	41	914	1223	26	21	35	41	1085	1311	128	56	38	31	992	1251	26	18	41	55
11	903	1205	18	14	31	45	915	1223	27	22	37	42	1086	1307	127	55	33	33	904	933	27	19	41	57
12	904	1206	11	7	24	41	916	1223	26	24	38	43	1086	1308	126	55	39	34	925	934	27	19	41	57
13	905	1207	18	19	30	45	917	1223	25	21	35	40	1086	1309	124	55	35	34	906	935	28	20	41	56
14	905	1208	12	10	23	45	898	1211	26	19	33	43	1086	1310	122	55	39	35	907	935	27	18	42	59
15	905	1209	13	11	22	36	898	1212	29	24	39	44	1110	1307	125	55	40	36	920	1220	28	19	41	59
16	905	1218	14	13	31	44	899	1211	24	19	36	40	1110	1308	126	56	39	37	915	1221	28	21	42	56
17	905	1219	18	20	37	44	899	1212	24	20	36	41	1110	1309	127	56	38	37	925	1221	28	20	43	57
18	905	1220	14	13	28	42	900	1200	27	22	36	42	1110	1310	128	54	38	38						
19	905	1221	13	8	28	47	900	1200	26	22	37	41	1111	1307	131	53	34	35						
20	906	1240	14	13	28	42	911	1200	21	25	38	41	1111	1308	131	54	37	35						
21	906	1241	13	13	29	44	912	1217	28	22	36	39	1111	1309	131	54	37	34						
22	907	1242	12	6	29	46							1111	1310	131	56	38	36						
23	907	1243	12	8	29	48							1111	1311	132	56	42	38						
24	907	1244	11	11	25	47							1112	1307	133	57	39	39						
25	907	1245	10	9	25	46							1112	1308	135	57	38	35						
26	908	1222	16	13	29	42							1112	1309	134	57	38	40						
27	908	1223	15	13	25	42							1112	1310	133	57	39	41						
28	908	1224	15	9	25	43							1115	1307	130	57	37	36						
29	908	1225	16	13	29	43							1115	1308	130	57	40	37						
30	908	1226	14	14	29	43							1114	1307	130	57	40	36						
31	907	1226	13	11	26	43							1114	1310	128	53	37	33						

A-THICKET

n	X	Y	4	5	6	7	X	Y	4	5	6	7
32	909	1230	17	12	26	39						
33	909	1231	18	15	27	38						
34	909	1232	15	12	26	38						
35	910	1233	16	15	27	38						
36	911	1247	15	14	28	39						
37	951	1243	15	14	36	39						
38	952	1244	16	15	35	39						
39	953	1245	13	12	26	38						
40	954	1246	17	16	34	40						
41	955	1210	15	15	33	40						
42	956	1211	14	12	27	40						
43	957	1212	14	12	26	41						
44	958	1213	19	18	33	43						
45	959	1214	16	12	27	37						
46	960	1215	16	14	27	37						
47	961	1216	16	14	28	44						
48	962	1217	19	15	32	37						
49	963	1218	19	14	28	40						
50	963	1219	17	16	28	40						
51	963	1220	20	18	32	41						
52	963	1221	20	17	27	36						
53	963	1222	21	17	31	41						
54	963	1223	17	16	31	41						

T-FLATS

X	Y	4	5	6	7	X	Y	4	5	6	7
1113	1307	130	58	35	30						
1113	1308	132	58	37	34						
1113	1309	137	60	41	39						
1113	1310	132	61	41	40						

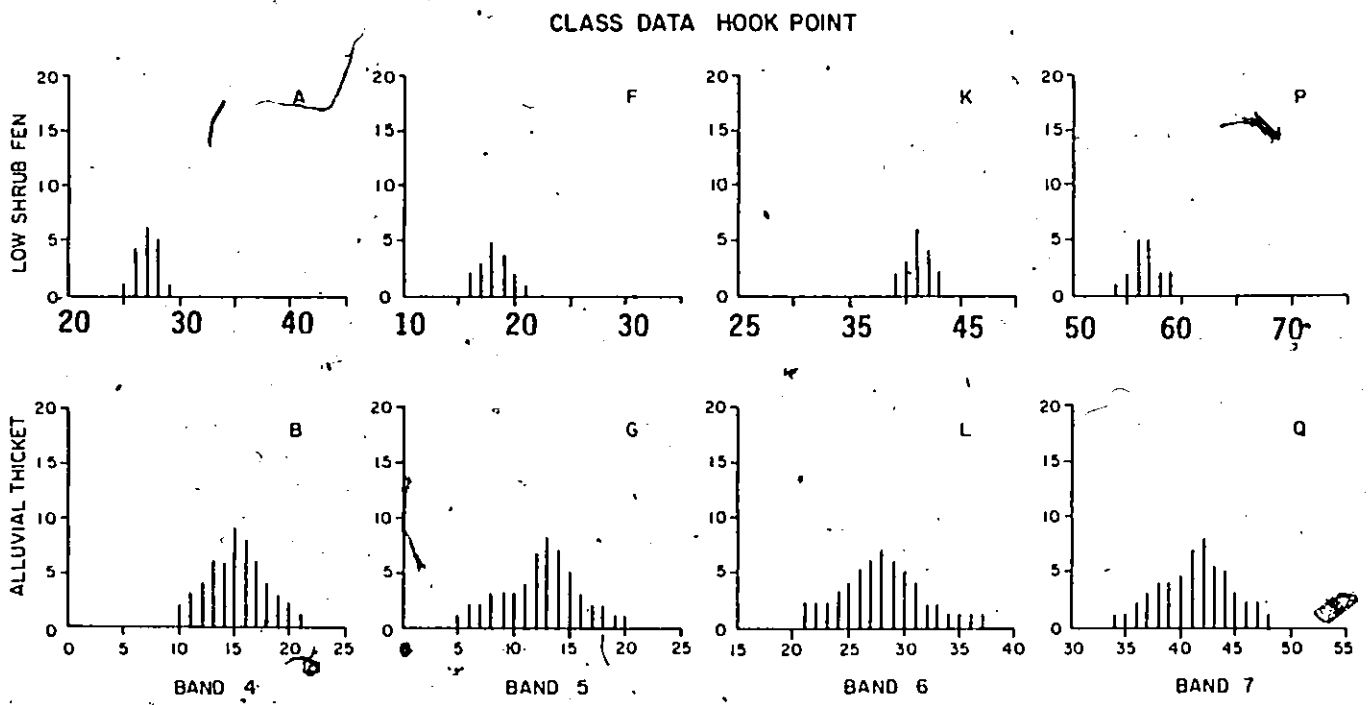
CLASS DATA HOOK POINT
LOW SHRUB FEN
ALLUVIAL THICKET
A
F
K
P
B
G
L
Q
BAND 4
BAND 5
BAND 6
BAND 7

CLASS DATA HOOK POINT

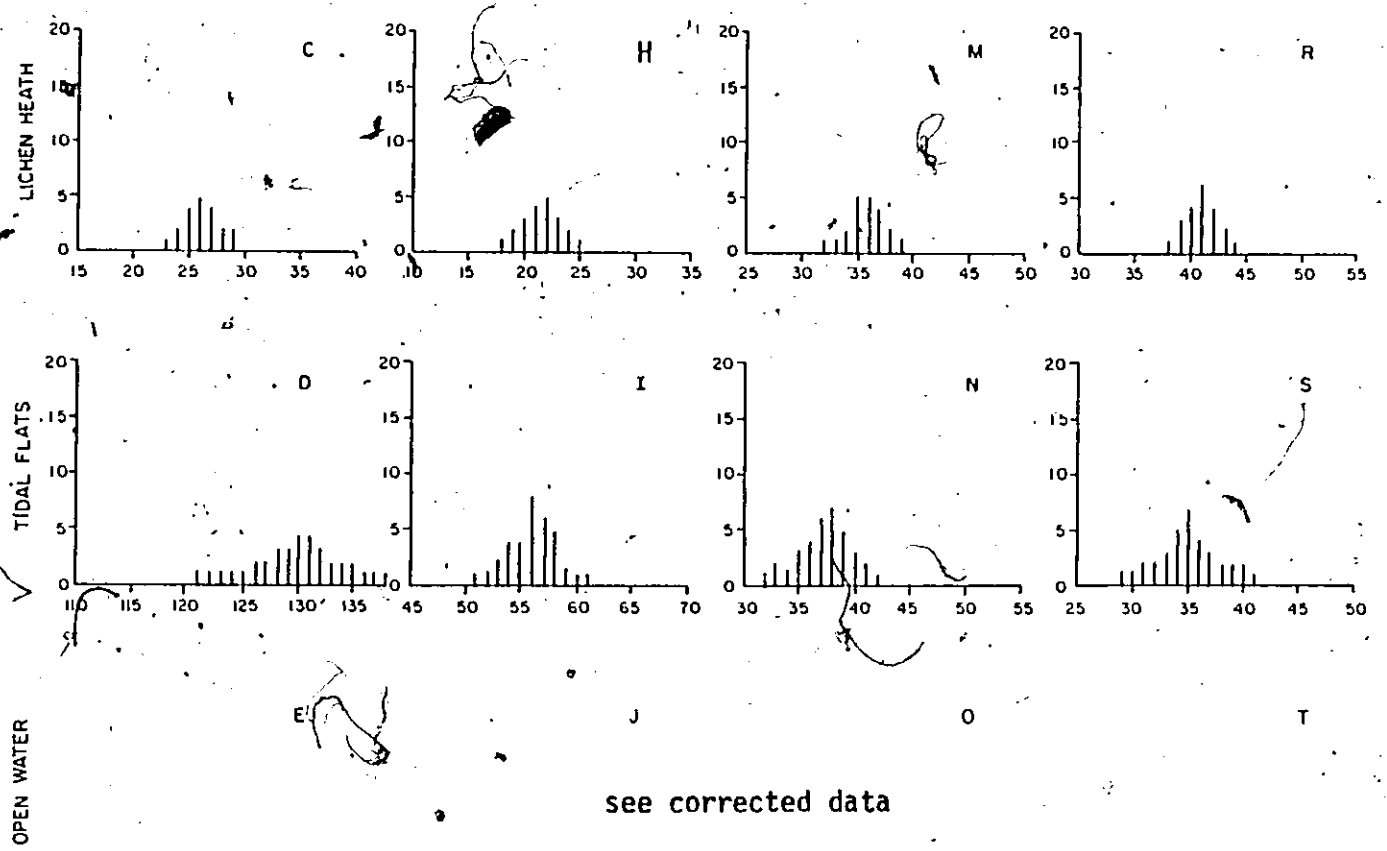

see corrected data

COVER CLASSES-HOOK POINT.

PAIR	D-MAX	X^2	Pr*
A - B	1	51.7	
A - C	.227	2.87	.2 to .3
A - D	1	45.8	
A - E	1	48.4	
B - C	1	60.4	
B - D	1	84.9	
B - E	.643	39.1	
C - D	1	52.5	
C - E	1	56.0	
D - E	1	76.4	
F - G	.833	35.9	
F - H	.717	19.3	
F - I	1	45.8	
F - J	1	48.4	
G - H	.926	51.8	
G - I	1	84.9	
G - J	.826	64.8	
H - I	1	52.5	
H - J	1	56.0	
I - J	1	76.4	
K - L	1	51.7	
K - M	1	37.5	
K - N	.769	27.1	
K - O	1	48.4	
L - M	.858	44.5	
L - N	.86	62.8	
L - O	1	94.5	
M - N	.343	6.2	
M - O	1	56.0	
N - O	1	76.4	
P - Q	1	51.7	
P - R	1	37.5	
P - S	1	45.8	
P - T	1	48.4	
Q - R	.216	2.8	.2 to .3
Q - S	.64	34.8	
Q - T	1	94.5	
R - S	.752	29.7	
R - T	1	56.0	
S - T	1	76.4	

* Probability of both samples drawn from same population: shown only where Pr > .05.

Appendix B.4

RADIOMETER DATA-HOOK POINT

	A-THICKET			T-FLATS			L-HEATH			L-S FEN		
n	4	5	6	4	5	6	4	5	6	4	5	6
1	5	4	14	55	25	30	9	10	6	14	10	17
2	5	4	14	56	26	30	10	10	7	16	12	19
3	4	3	13				10	10	7	15	11	18
4	6	5	14				10	10	7	15	11	18
5							11	10	8	15	11	18

RADIOMETER DATA HOOK POINT

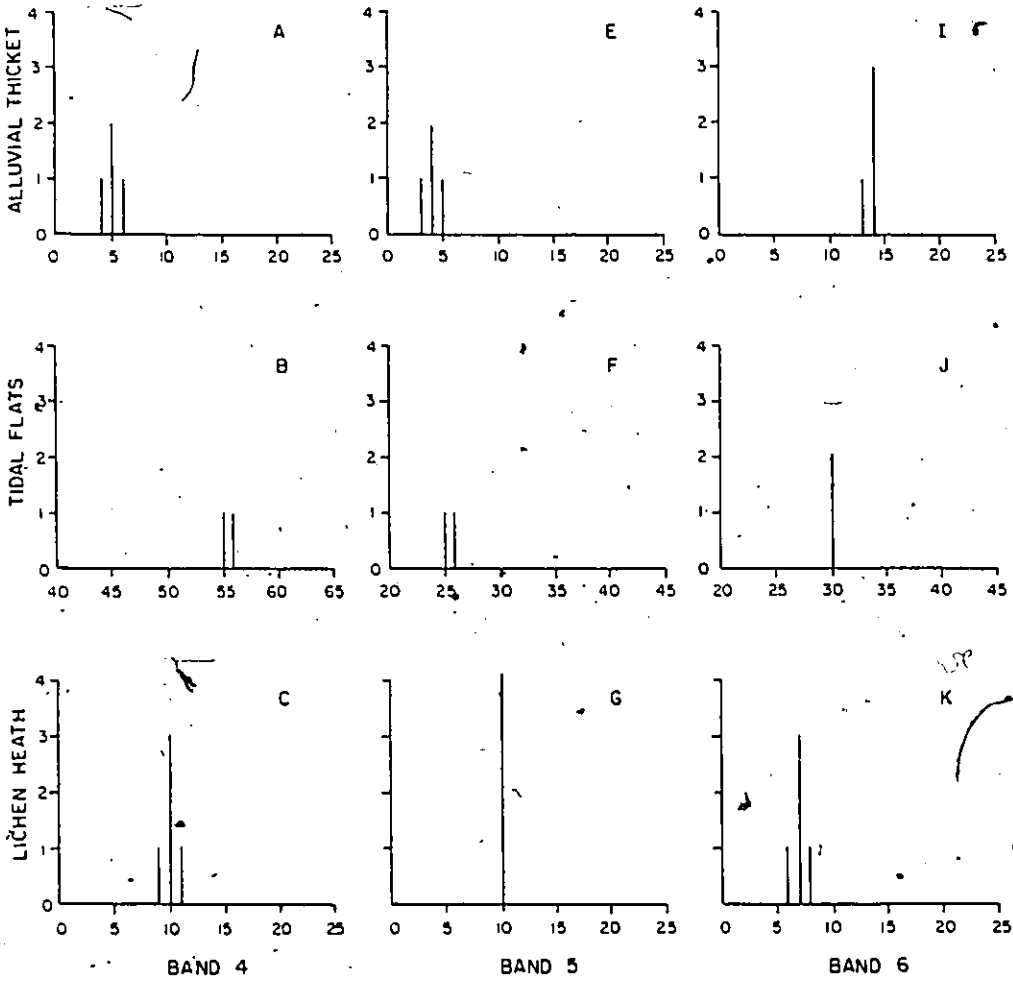

RADIOMETER DATA HOOK POINT

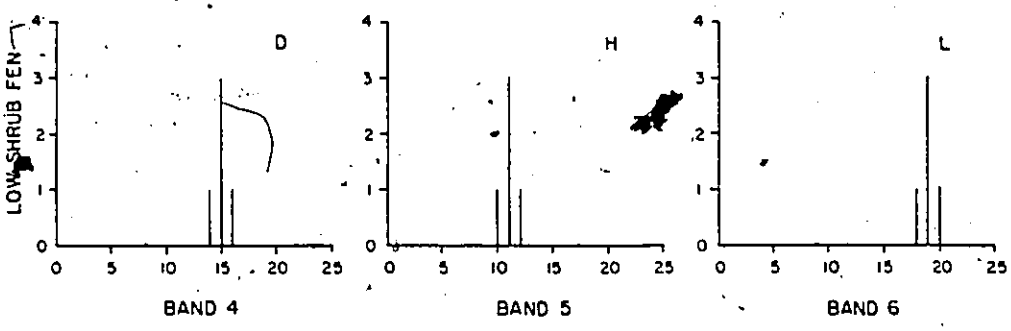

RADIOMETER DATA-HOOK POINT

PAIR	D-MAX	SIGNIFICANCE LEVEL Pr*
A - B	1	.75
A - C	1	.6
A - D	1	.6
B - C	1	.8
B - D	1	.8
C - D	1	.510
E - F	1	.75
E - G	1	.6
E - H	1	.6
F - G	1	.8
F - H	1	.8
G - H	.8	.510
I - J	1	.75
I - K	1	.6
I - L	1	.6
J - K	1	.8
J - L	1	.8
K - L	1	.510

* Probability of both samples drawn from same population: shown only where Pr > .1.

Appendix B.5

BAND RATIOING-HOOK POINT

TIDAL FLATS > 255

n	A-THICKET	L-HEATH	T-FLATS	L-S FEN	O-WATER
1	86	148		118	186
2	84	76		119	189
3	90	155		120	196
4	89	152		125	202
5	98	162		120	69
6	98	158		120	49
7	97	160		116	119
8	99	165		128	180
9	110	154		123	215
10	110	154		121	158
11	31	155		121	231
12	80	148		121	266
13	107	152		127	239
14	80	148		118	223
15	99	158		122	209
16	90	147		127	185
17	109	143		125	171
18	93	155			112
19	81	153			112
20	93	158			115
21	86	170			118
22	79				179
23	77				120
24	73				181
25	70				198
26	103				175
27	98				193

Cont'd.

n	A-THICKET	L-HEATH	T-FLATS	L-S FEN	O-WATER
28	96				186
29	101				202
30	92				247
31	87				90
32	114				202
33	121				229
34	106				186
35	111				234
36	104				145
37	104				130
38	109				125
39	95				160
40	112				167
41	102				159
42	97				187
43	95				
44	115				
45	113				
46	113				
47	99				
48	129				
49	122				
50	112				
51	124				
52	137				
53	129				
54	110				

BAND RATIOING-HOOK POINT

TIDAL FLATS > 225

(SAME COORDINATES AS COVER-CLASSES-HOOK POINT)

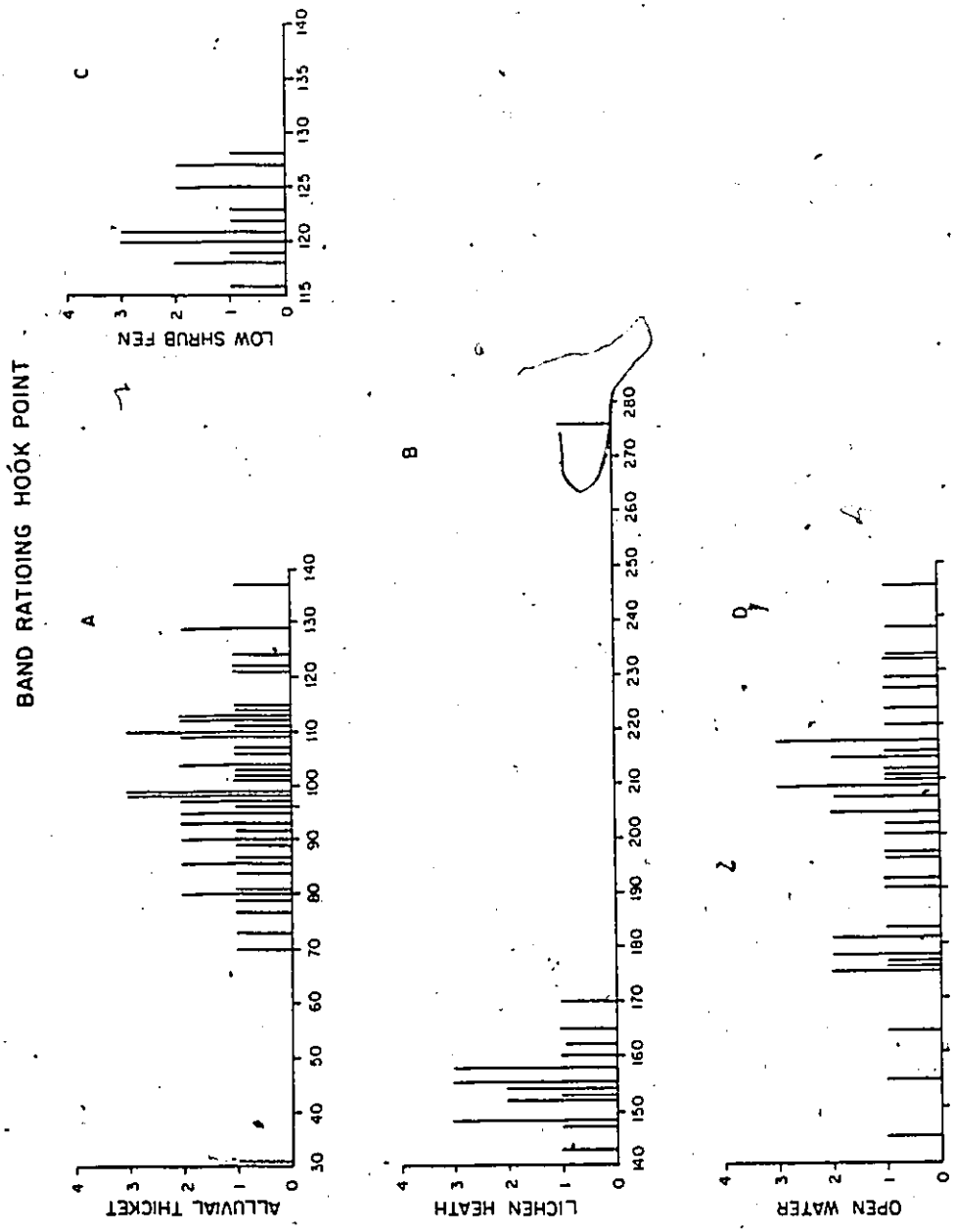
BAND RATIOING HOOK POINT
A
ALLUVIAL THICKET
B
LICHEN HEATH
C
LOW SHRUB FEN
OPEN WATER

BAND RATIOING-HOOK POINT

PAIR	D-MAX	X^2	Pr*
A - B	1	59.8	
A - C	.903	41.7	
A - D	1	59.8	
B - C	1	37.6	
B - D	.996	55.7	
C - D	.714	34.6	

* Probability of both samples drawn from same population: shown only where Pr > .001.

Appendix B.6

VIDEO FILTERING-HOOK POINT

	A-THICKET						L-HEATH						TIDAL FLATS						L-S FEN						OPEN WATER					
n	X	Y	4	5	6	7	X	Y	4	5	6	7	X	Y	4	5	6	7	X	Y	4	5	6	7	X	Y	4	5	6	7
1	670	1212	15	14	30	40	912	1226	26	22	36	41	1239	1352	128	56	39	36	911	968	26	17	42	58	911	840	9	4	6	16
2	629	1236	16	13	28	41	820	1103	27	23	36	42	1169	1335	129	57	37	35	919	826	25	16	42	56	948	942	10	4	5	15
3	580	842	16	13	30	42	990	1285	26	21	36	41	1247	1352	131	57	38	35	849	815	26	17	41	57	830	966	10	4	5	15
4	750	910	17	12	27	43	800	1218	25	20	36	40	1210	1357	130	57	37	35	440	976	26	17	42	58	740	997	9	4	6	15
5	880	914	16	13	28	42	892	1219	26	21	36	41	1067	1330	129	57	37	35	910	1201	24	16	40	56	830	921	8	4	5	16
6	816	983	16	13	26	41	715	1269	26	21	36	41	1190	1238	130	57	37	35	983	1117	24	18	43	57	500	864	10	3	4	18
7	610	984	17	14	29	41	903	1284	26	21	36	41	1131	1008	130	56	36	34	480	795	26	17	41	57	500	427	9	4	5	16
8	818	889	16	13	27	40	928	1250	26	20	36	41	1176	875	131	58	35	34	400	1190	25	18	41	57	940	362	9	4	5	16
9	940	1275	16	12	28	41																			937	808	9	4	4	15
10	934	1243	16	12	26	40																			1044	851	10	4	4	15
11	920	1246	16	14	29	41																			1080	657	8	4	6	17
12	540	644	16	15	31	41																			1046	607	11	4	6	18
13	520	865	15	11	25	41																			760	872	7	3	5	16
14																									336	900	12	3	5	16
15																									552	685	6	3	4	17
16																									521	868	6	3	4	17
17																									583	750	7	2	3	13
18																									514	864	8	4	5	16
19																									573	615	11	4	5	16
20																									588	721	11	6	7	15
21																									577	632	8	2	2	17
22																									503	829	12	4	5	17
23																									966	637	9	4	8	17
24																									950	817	9	7	7	14

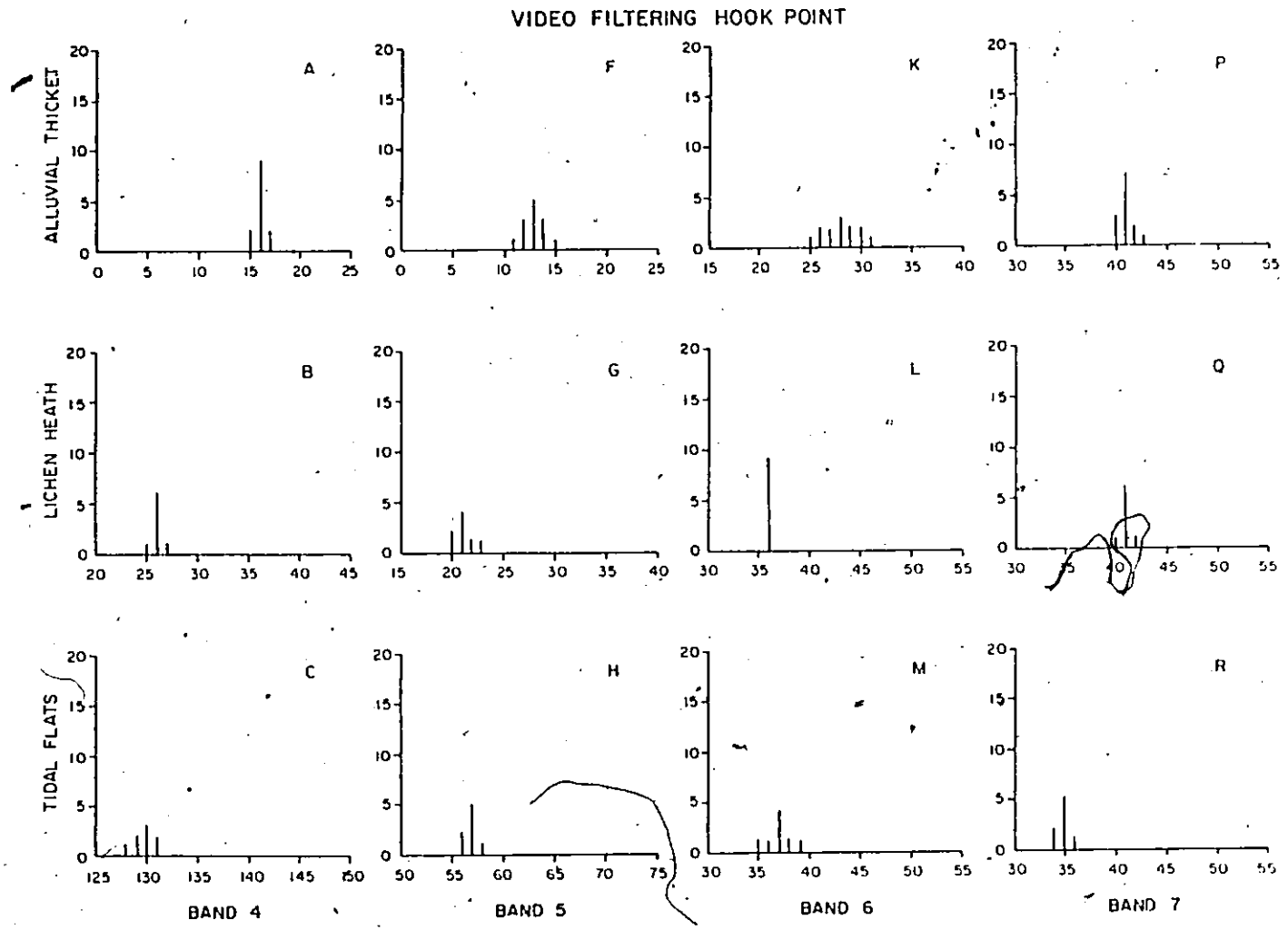
VIDEO FILTERING HOOK POINT
ALLUVIAL THICKET
LICHEN HEATH
TIDAL FLATS
A
F
K
P
B
G
L
Q
C
H
M
R
BAND 4
BAND 5
BAND 6
BAND 7

VIDEO FILTERING HOOK POINT

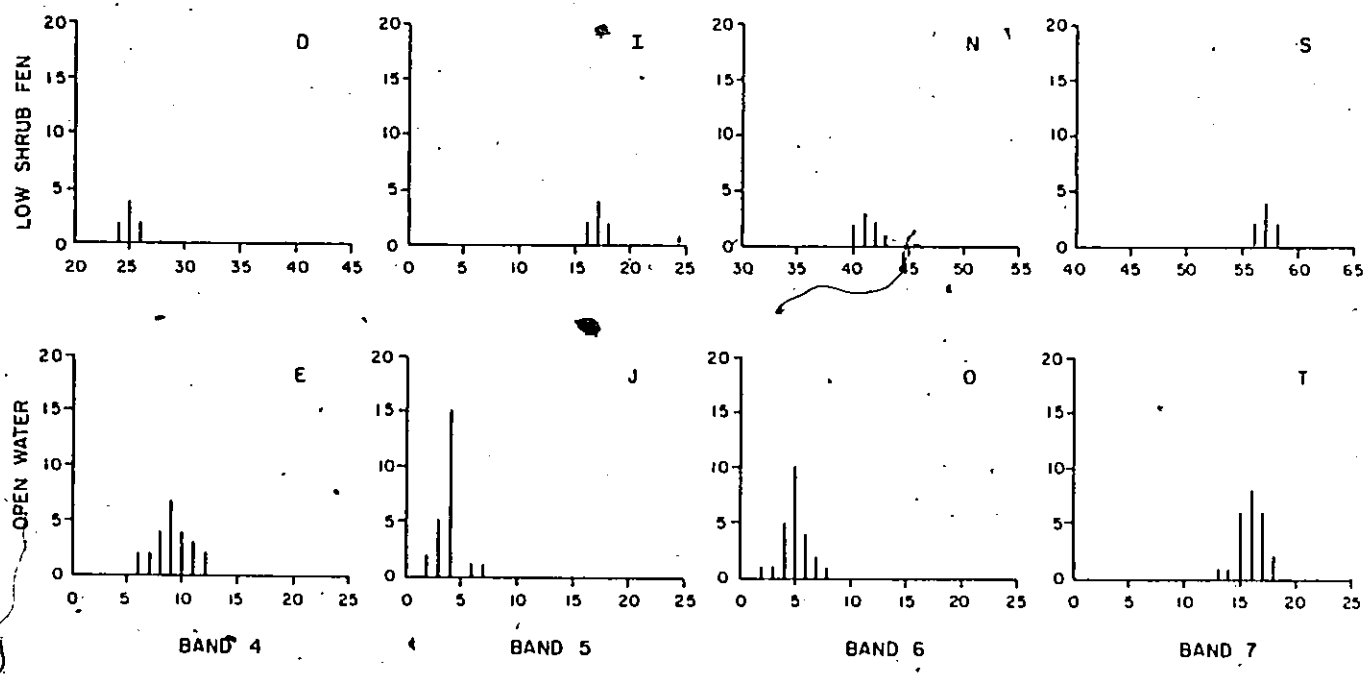

VIDEO FILTERING-HOOK POINT

PAIR	D-MAX	SIGNIFICANCE LEVEL	Pr*
A - B	1		.458
A - C	1		.458
A - D	1		.458
A - E	1	(X^2=33.7)	5.99
B - C	1		.358
B - D	.675		.358
B - E	1		.437
C - D	1		.358
C - E	1		.437
D - E	1		.437
F - G	1		.458
F - H	1		.458
F - I	1		.458
F - J	1	(X^2=33.7)	5.99
G - H	1		.358
G - I	1		.358
G - J	1		.437
H - I	1		.358
H - J	1		.437
I - J	1		.437
K - L	1		.458
K - M	1		.458
K - N	1		.458
K - O	1	(X^2=33.7)	5.99
L - M	.75		.358
L - N	1		.358
L - O	1		.437
M - N	1		.358
M - O	1		.437
N - O	1		.437
P - Q	.106		.458
P - R	1		.458
P - S	1		.458
P - T	1	(X^2=33.7)	5.99
Q - R	1		.358
Q - S	1		.358
Q - T	1		.437
R - S	1		.358
R - T	1		.437
S - T	1		.437

* Probability of both samples drawn from same population: shown only where Pr > .1.

Appendix B.7

COVER CLASSES - CHURCHILL

	O-WATER						U-SETTLEMENT						R-OUTCROP						L-WOODLAND						A-THICKET						L-HEATH					
n	x	y	4	5	6	7	x	y	4	5	6	7	x	y	4	5	6	7	x	y	4	5	6	7	x	y	4	5	6	7	x	y	4	5	6	7
1	2893	213	24	8	2	1	2900	230	40	32	32	55	2979	267	45	35	35	60	3013	257	26	23	45	64	3209	211	17	11	20	45	3196	229	20	13	25	46
2	2894	213	18	10	4	1	2900	231	41	40	31	55	2979	267	46	36	36	58	3013	257	24	21	45	65	3209	212	18	10	16	42	3197	229	22	17	28	47
3	2894	214	24	12	5	1	2900	232	47	34	35	58	2980	267	47	38	36	58	3014	257	24	21	45	65	3209	213	17	8	17	41	3197	230	32	19	29	50
4	2895	213	23	13	6	3	2900	233	45	36	35	58	2980	268	46	34	34	56	3014	257	22	23	44	64	3209	214	18	10	20	45	3197	231	22	17	28	49
5	2895	214	23	13	5	1	2910	241	40	36	36	59	2980	269	47	39	37	59	3014	259	26	23	46	66	3210	211	14	8	20	45	3197	232	23	18	30	50
6	2896	213	23	15	6	1	2910	242	47	37	38	59	2980	270	46	34	37	59	3014	260	28	24	43	63	3210	212	19	12	20	46	3140	228	22	18	30	50
7	2897	213	24	15	7	2	2910	243	43	35	36	59	2980	271	51	38	38	60	3015	257	27	24	46	65	3210	213	17	10	20	46	3140	229	20	17	28	49
8	2871	214	24	16	8	2	2911	231	48	37	37	58	2981	267	45	36	38	60	3015	258	23	22	47	66	3210	214	17	11	19	44	3140	230	21	16	29	51
9	2872	213	20	18	7	2	2912	232	47	37	37	58	2981	268	47	37	40	61	3015	259	23	22	46	66	3210	216	20	9	17	42	3140	231	22	18	28	56
10	2872	214	19	9	7	2	2912	233	43	35	36	60	2981	269	40	35	35	57	3015	260	27	25	43	66	3211	221	18	9	20	44	3137	221	23	18	29	52
11	2873	213	21	11	4	2	2912	234	42	34	36	61	2987	271	43	34	33	60	3021	257	26	23	45	64	3211	222	18	9	20	44	3137	222	24	20	31	53
12	2873	213	22	11	4	2	2913	235	41	33	34	59	2987	272	44	36	40	61	3021	258	24	22	44	64	3220	227	19	12	21	45	3148	301	21	14	26	47
13	2874	214	24	10	6	3	2913	237	42	38	39	61	2987	273	51	36	36	58	3022	258	29	24	44	65	3220	228	17	9	19	44	3148	302	21	15	28	50
14	2874	214	21	13	5	1	2913	239	43	38	39	61	2987	274	42	32	34	56	3022	259	25	22	45	65	3220	229	15	11	21	45	3148	303	22	16	28	50
15	2874	216	28	13	6	3	2914	241	45	36	35	62	2997	275	45	37	37	64	3023	257	27	23	45	65	3220	230	14	7	19	43	3148	304	21	15	27	48
16	2874	214	19	13	7	3	2914	242	49	37	36	62	2997	276	45	37	37	63	3023	258	25	22	46	65	3221	231	13	6	21	43	3148	305	22	17	27	48
17	2874	218	28	14	6	3	2915	242	49	37	36	60	2997	277	41	33	35	59	3023	259	25	23	47	66	3221	232	16	10	22	45	3156	201	21	16	27	48
18	2874	219	22	14	5	3	2915	243	46	38	35	59	3001	263	46	37	39	64							3221	233	19	11	19	43	3156	202	24	19	29	51
19	2874	220	27	14	6	1	2915	244	45	36	34	56	3002	264	42	33	34	56							3222	231	17	9	23	47	3156	203	21	16	26	50
20	2874	221	23	13	7	2	2931	231	44	34	34	57	3001	291	44	36	37	59							3222	232	15	7	18	44	3156	204	22	17	27	49
21	2888	213	26	13	8	1	2931	232	45	35	34	57	3001	292	45	36	37	63							3223	231	15	8	18	44	3156	205	23	17	27	49
22	2888	214	20	14	9	3	2931	233	45	35	35	63	3001	293	43	35	35	56							3223	232	16	9	18	47						
23	2888	215	21	14	6	3	2932	234	44	35	33	56	3001	294	48	38	36	58							3223	233	16	9	19	44						
24	2888	216	23	14	9	1	2932	235	43	35	35	63	3001	295	46	35	34	57							3223	234	16	10	22	46						
25	2888	217	20	15	6	1	2932	236	44	36	33	56	3002	297	47	40	40	61																		
26	2888	218	23	16	8	3	2935	245	46	38	38	59	3002	298	45	35	38	58																		
27	2889	213	22	13	8	3	2935	246	44	46	35	57	3002	299	48	39	39	59																		
28	2889	214	23	14	6	2	2935	247	49	40	39	60	3002	401	49	39	41	62																		
29	2889	215	23	11	3	1							3006	402	46	36	38	62																		
30	2889	216	24	9	2	1							3006	403	50	37	39	61																		
31	2990	213	24	10	3	2							3006	400	46	36	39	62																		
32	2990	214	25	12	4	2																														
33	2990	215	26	15	7	3																														
34	2990	216	22	12	5	3																														
35	2990	217	25	12	5	2																														
36	2990	218	22	17	7	2																														
37	2990	219	25	13	5	2																														

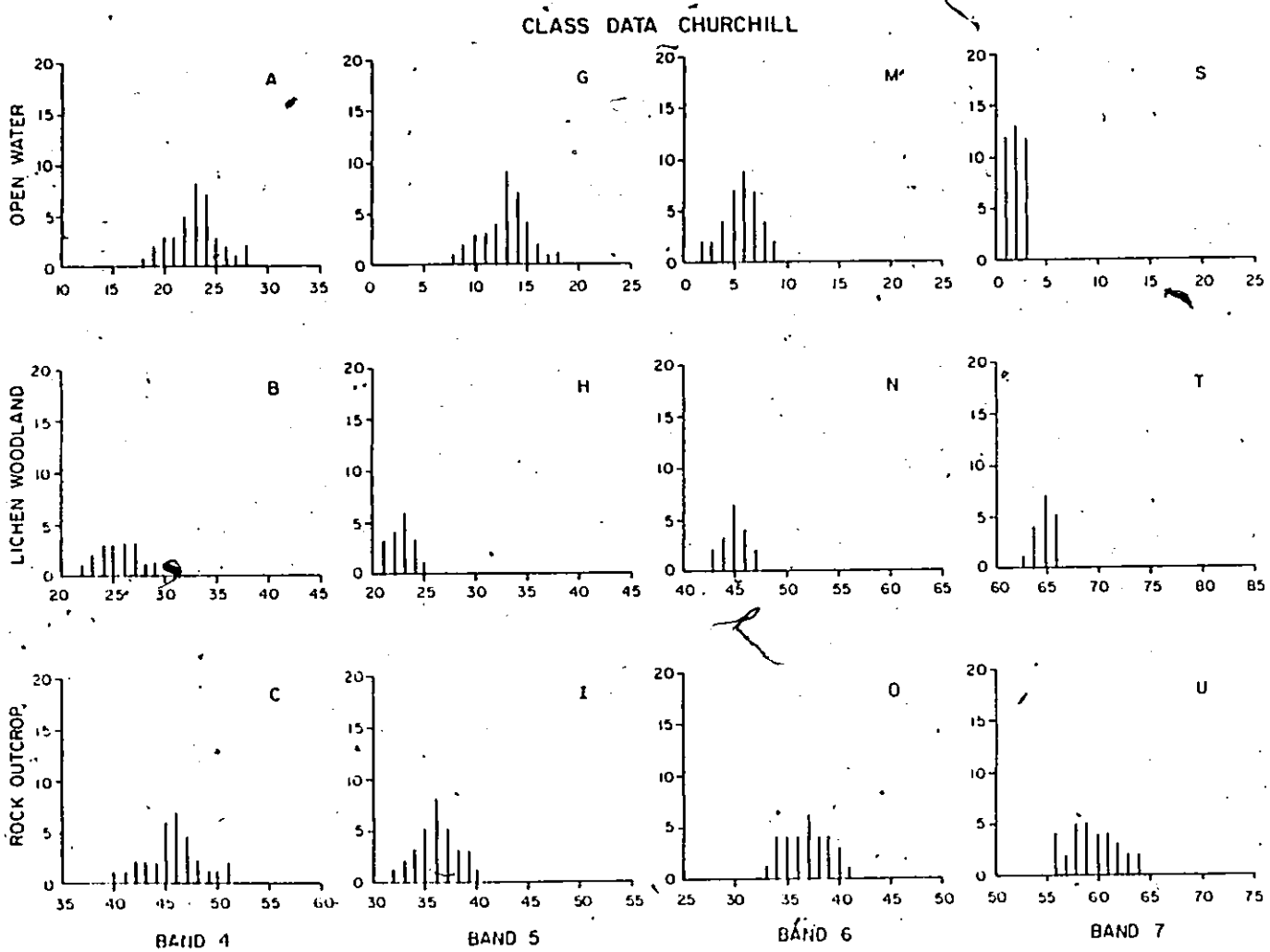
CLASS DATA CHURCHILL
OPEN WATER
LICHEN WOODLAND
ROCK OUTCROP
A
B
C
G
H
I
M
N
O
S
T
U
BAND 4
BAND 5
BAND 6
BAND 7

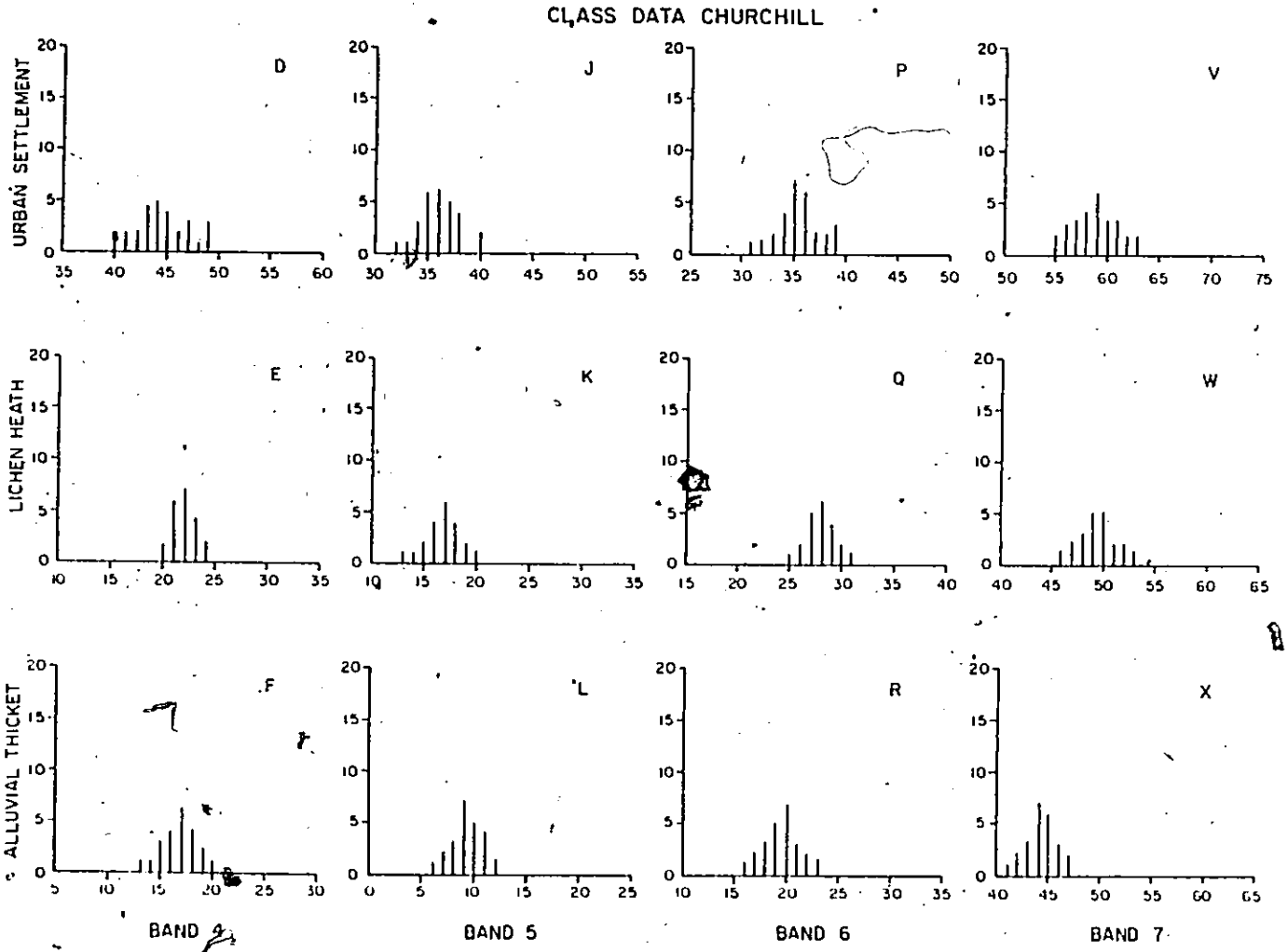
CLASS DATA CHURCHILL
URBAN SETTLEMENT
LICHEN HEATH
ALLUVIAL THICKET
D
J
P
V
E
K
Q
W
F
L
R
X
BAND 4
BAND 5
BAND 6
BAND 7

COVER CLASSES - CHURCHILL

PAIR	D-MAX	X^2	Pr*	PAIR	D-MAX	X^2	Pr*
A - B	.37	6.4		M - N	1	46.6	
A - C	1	67.5		M - 0	1	67.5	
A - D	1	63.7		M - P	1	63.7	
A - E	.33	.54	.7 to .8	M - Q	1	45.7	
A - F	.88	45.0		M - R	1	52.8	
B - C	1	43.9		N - 0	1	43.9	
B - D	1	42.3		N - P	1	42.3	
B - E	.67	16.9		N - Q	1	37.6	
B - F	1	39.8		N - R	1	39.8	
C - D	.267	4.4	.1 to .2	0 - P	.25	3.6	.1 to .2
C - E	1	50.1		0 - Q	1	50.1	
C - F	1	54.1		0 - R	1	54.1	
D - E	1	48.0		P - Q	.97	45.2	
D - F	1	57.1		P - R	1	57.1	
E - F	.96	41.3		Q - R	1	48.8	
G - H	1	46.6		S - T	1	46.6	
G - I	1	67.5		S - U	1	67.5	
G - J	1	63.7		S - V	1	63.7	
G - K	.67	20.5		S - W	1	45.7	
G - L	.69	27.7		S - X	1	52.8	
H - I	1	43.9		T - U	.87	33.2	
H - J	1	42.3		T - V	.95	38.1	
H - K	1	37.6		T - W	1	37.6	
H - L	1	39.8		T - X	1	39.8	
I - J	.058	.20	.7 to .8	U - V	.11	.71	.7
I - K	1	50.1		U - W	1	50.1	
I - L	1	54.1		U - X	1	54.1	
J - K	1	48.0		V - W	1	48.0	
J - L	1	57.1		V - X	1	57.1	
K - L	1	48.8		W - X	.9	36.0	

* Probability of both samples drawn from same population: shown only where Pr > .05.

Appendix B.8

BAND RATIOING CHURCHILL

OPEN WATER >255

n	0-WATER	U-SETTLEMENT	R-OUTCROP	L-WOODLAND	A-THICKET	L-HEATH
1		159	162	119	111	119
2		161	168	110	118	124
3		170	170	110	116	123
4		165	172	107	114	121
5		152	168	114	102	124
6		168	166	120	116	120
7		159	176	116	110	115
8		173	162	107	112	116
9		170	165	107	125	117
10		157	172	116	116	120
11		172	177	119	116	122
12		154	158	111	117	121
13		153	179	121	112	117
14		162	162	112	105	120
15		156	156	116	104	119
16		159	157	121	101	122
17		154	154	111	108	119
18		171	176		120	122
19		169	162		109	119
20		164	164		106	124
21		170	157		106	117
22		157	164		106	121
23		167	173		109	123
24		153	170		107	
25		167	165			
26		166	165			
27		164	171			
28		171	167			
29			161			
30			171			
31			161			

(SAME CORDINATES AS
COVER CLASSES - CHURCHILL)

BAND RATIOING CHURCHILL

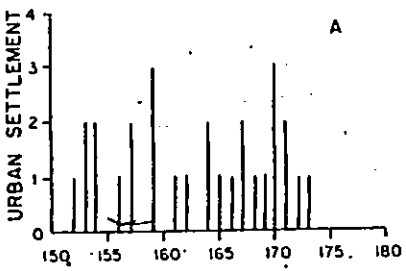

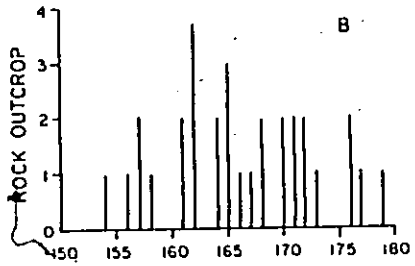

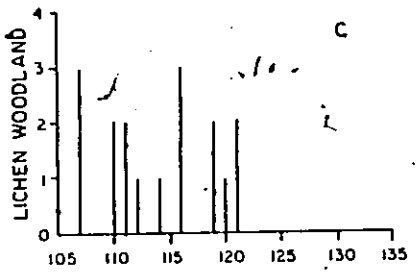

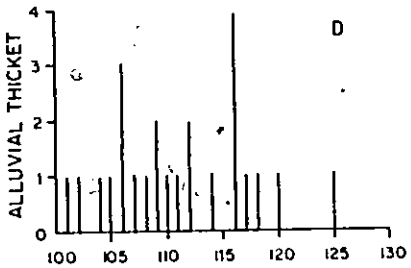

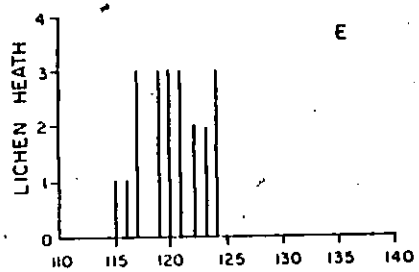

BAND RATIOING - CHURCHILL

PAIR	D-MAX	X^2	Pr*
A - B	.227	2.98	.2 to .3
A - C	1	42.3	
A - D	1	59.7	
A - E	1	48.0	
B - C	1	43.4	
B - D	1	53.3	
B - E	1	49.4	
C - D	.292	3.39	.1 to .2
C - E	.67	16.9	
D - E	.732	24.0	

* Probability of both samples drawn from same population: shown only where Pr > .001.

Appendix B.9

VIDEO FILTERING CHURCHILL

	O-WATER						U-SETTLEMENT						R-OUTCROP						L-WOODLAND						A-THICKET						L-HEATH					
n	x	y	4	5	6	7	x	y	4	5	6	7	x	y	4	5	6	7	x	y	4	5	6	7	x	y	4	5	6	6	x	y	4	5	6	7
1	2879	175	12	3	2	2	2993	252	44	36	37	57	3038	206	43	35	34	56	3080	364	24	21	45	65	3246	298	19	10	16	40	3157	289	23	16	28	49
2	3023	140	12	2	2	2	2997	337	44	37	38	61	3024	226	44	35	35	57	2077	281	25	23	45	65	3251	224	19	11	20	42	3134	283	23	16	28	49
3	2862	137	11	7	2	2	2943	200	46	36	38	58	3018	298	44	35	35	57	2062	356	25	24	45	66	3371	289	19	11	19	42	3136	297	23	16	27	49
4	3005	159	12	9	2	2	2964	238	44	35	35	59	3083	277	44	35	35	57	2080	329	25	23	45	65	3389	272	19	12	21	41						
5	3063	138	13	5	2	2	2857	207	44	36	37	59	3093	217	44	35	36	57	2209	340	27	24	45	64	3444	294	20	12	18	43						
6	3053	248	14	6	2	2	2990	267	44	36	37	59							3020	523	23	23	45	65	3382	207	21	13	22	44						
7	3024	229	13	5	2	2	2923	294	44	36	37	60							2181	381	24	24	45	64	3369	231	18	10	17	40						
8	2846	248	14	6	2	2	2915	231	43	36	36	56							2732	382	23	20	44	64	3361	260	19	11	19	42						
9	2892	287	13	5	2	1													3089	579	24	20	45	65	3345	215	19	11	19	42						
10	2846	329	13	5	2	2													3070	440	24	23	45	65	3318	289	18	11	19	43						
11	3077	389	10	8	2	2													3078	387	22	20	46	66												
12	3017	377	13	5	2	2													2241	384	23	25	45	65												
13	3195	180	14	5	2	2																														
14	2932	161	15	5	2	2																														
15	3149	190	16	4	2	2																														
16	2960	348	16	2	2	2																														
17	3085	278	15	7	2	2																														
18	2982	297	12	5	3	3																														
19	3016	236	13	5	2	2																														
20	2992	234	14	5	2	2																														
21	3146	275	10	4	2	2																														
22	3066	350	11	3	2	2																														

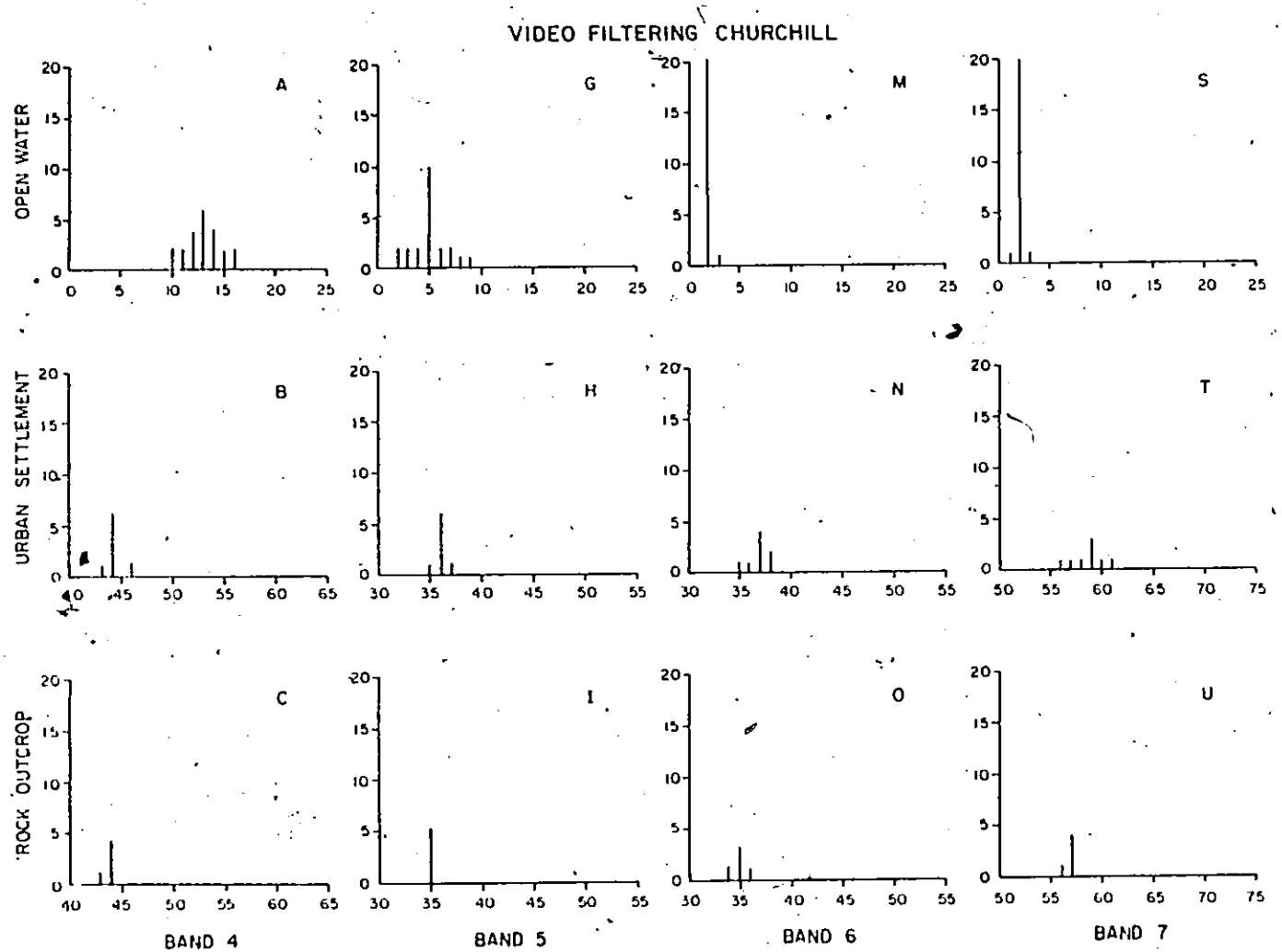
VIDEO FILTERING CHURCHILL
OPEN WATER
URBAN SETTLEMENT
ROCK OUTCROP
A
G
M
S
B
H
N
T
C
I
O
U
BAND 4
BAND 5
BAND 6
BAND 7

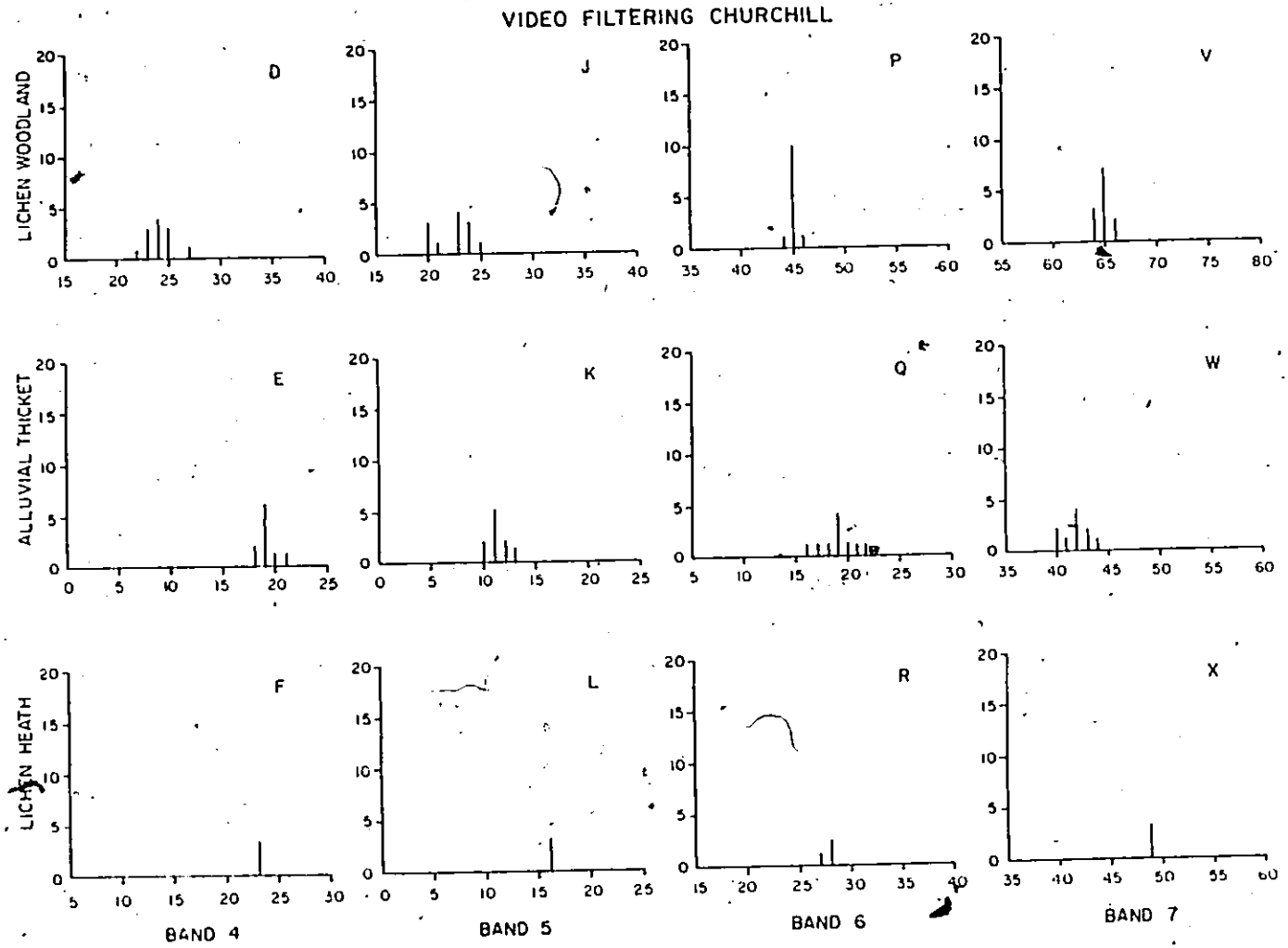
VIDEO FILTERING CHURCHILL
LICHEN WOODLAND
ALLUVIAL THICKET
LICHEN HEATH
D
J
P
V
E
K
Q
W
F
L
R
X
BAND 4
BAND 5
BAND 6
BAND 7

VIDEO FILTERING - CHURCHILL

PAIR	D-MAX	SIGNIFICANCE LEVEL	Pr*	PAIR	D-MAX	SIGNIFICANCE LEVEL	Pr*
A - B	1	.437		M - N	1	.437	
A - C	1	.562		M - O	1	.562	
A - D	1	.366		M - P	1	.366	
A - E	1	.40		M - Q	1	.40	
A - F	1	.583		M - R	1	.583	
B - C	.125	.625	**	N - O	.75	.625	
B - D	1	.458		N - P	1	.428	
B - E	1	.475		N - Q	1	.475	
B - F	1	.625		N - R	1	.625	
C - D	1	.583		O - P	1	.583	
C - E	1	.55		O - Q	1	.55	
C - F	1	.75		O - R	1	.75	
D - E	1	.40		P - Q	1	.40	
D - F	.67	.583		P - R	1	.583	
E - F	1	.60		Q - R	1	.60	
G - H	1	.437		S - T	1	.437	
G - I	1	.562		S - U	1	.562	
G - J	1	.366		S - V	1	.366	
G - K	1	.40		S - W	1	.40	
G - L	1	.583		S - X	1	.583	
H - I	.875	.625		T - U	.75	.625	
H - J	1	.458		T - V	1	.458	
H - K	1	.475		T - W	1	.475	
H - L	1	.625		T - X	1	.625	
I - J	1	.583		U - V	1	.583	
I - K	1	.55		U - W	1	.55	
I - L	1	.75		U - X	1	.75	
J - K	1	.40		V - W	1	.40	
J - L	1	.583		V - X	1	.583	
K - L	1	.60		W - X	1	.60	

* Probability of both samples drawn from same population: shown only where Pr > .1.